Investigation on the Transient Added Mass of Sheet Ice

by

© Craig Titus Martin

A thesis submitted to the

School of Graduate Studies

in partial fulfilment of the

requirements for the degree of

Master of Engineering

Department of Engineering and Applied Science

Memorial University of Newfoundland

May 2019

St. John's Newfoundland

Abstract

This experimental study investigates the transient added mass of model ice floes accelerated horizontally along the free surface. The models were accelerated by one of two means: (1) a mass and pulley system to apply a step-wise force, and (2) a spring-powered cannon to apply an impulsive impact force. The kinematics of the models were obtained using high-speed image tracking and an accelerometer sensor. For the step force experiment, four ice shapes consisting of a disk and three irregular circumscribed polygons were tested at three levels of applied load. Equivalent added mass was calculated by applying Newton's Second Law. For the impulsive impact experiment, only the disk was tested using three impact velocities. Conservation of Momentum was used to estimate the mass of the fluid accelerated with the model. Frequency domain calculations were also completed using panel-method based software for comparison of the results.

Acknowledgments

First and foremost, I would like to express my gratitude to my supervisors, Dr. Heather Peng, and Dr. Claude Daley for their support and guidance throughout my time at Memorial University. I would like to thank the GEM Project group for their generous financial support which made this research possible.

Special thanks to Matt Curtis for offering his expertise in the lab and his advice on data acquisition and high-speed image capture, as well as to Dr. Lorenzo Moro for his guidance on signal processing.

I would also like to take this opportunity to extend my sincere thanks to Dr. Rocky Taylor and Dr. Aleksey Marchenko for providing me with the chance to study at the University Centre in Svalbard during my studies and experience ice mechanics in nature.

I would like to acknowledge the support of all the friends I have made along the way, especially Tobias Brueckner and Anke Krutof who never failed to provide helpful advice or exciting outdoor adventures. Lastly, I would like to thank my mother and father, Sue and Paul, as well as my sister, Sarah, for their love and nurturing support.

Contents

List of Tables

List of Figures

Chapter 1

Introduction

The frequency dependence of hydrodynamic added mass has been extensively researched through methods relying on the use of harmonic excitation. However, limited research is available for cases of non-harmonic, transient excitation forces. This is a topic of interest for better predicting the energy absorbed by the surrounding water during ice-structure interactions, thus leading to more accurate ice loading predictions.

The intent of the work is to complete a series of fundamental experiments to examine the transient hydrodynamic added mass of an ice mass due to an external force applied to the body. For simplification, only the effects on a single body are considered and the interaction effects are neglected. Two types of external forces were investigated and categorized as: (1) a step-wise force and (2) an impulsive impact force, which are illustrated as unit functions in Figure 1.1.

A mass and pulley system was used to apply a known instantaneous step-wise force to the ice model. An impulsive impact force was generated using a spring-powered

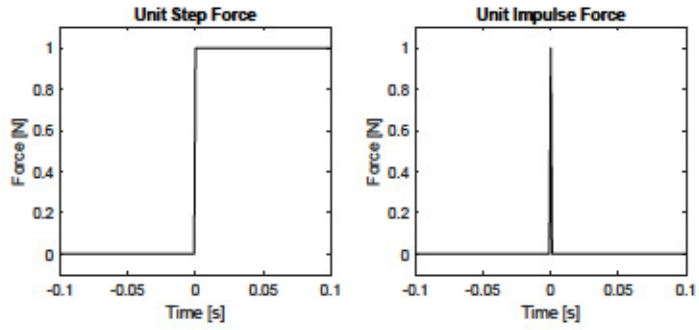

Figure 1.1: Unit Step and Unit Impulse Force Plots

cannon which shot a ball bearing that collided with the ice model. Four different ice floe geometries were tested while the magnitude of the forces was varied.

During the preliminary testing, a high-speed camera was used to record the trajectory of the ice models and analyze the kinematics. The MatLab™ Image Processing Toolbox was used to track the model displacement which could then be used to determine velocity and acceleration. Due to large amounts of noise within the high-speed video data, the tests were repeated with the addition of an accelerometer sensor mounted to the ice models.

Using the kinematic data from the step force experiment, equivalent added mass was determined by applying Newton's Second Law which was based on the methodology used by Motora et al. (1969) for experiments involving ship collisions.

The impulsive impact experiment was inspired by Popov's ship-ice collision model (Popov et al., 1968), where a method for determining the effective mass of a perfectly inelastic collision is considered by applying conservation of momentum. This method relies on the assumption that a certain amount of momentum will be transferred to the adjoining water mass surrounding the floating body.

To compare the results of the experiments with classical frequency-domain added mass calculations, a numerical study using the panel-method based software WAMIT® was also completed.

1.1 Literature Review and Theory

The concept of added mass was first introduced by Bessel (1828) who investigated the motion of a pendulum in fluid. Bessel observed a longer period of oscillation in fluid compared to a vacuum which suggests that the fluid causes an increase of the effective mass of the system.

Since then, countless studies have been completed on oscillating bodies in fluid, due to the convenient side-effect that it reduces the memory effects of the fluid. On the other hand, limited work was completed on non-oscillatory bodies. It was not until several years later when Basset (1888), Boussinesq (1885), and Oseen (1927) attempted to describe the rectilinear motion of a sphere released in fluid, which was based on the Navier-Stokes equations. This work formed the basis of a more recent study on the hydrodynamics of submerged ice collisions completed by Chander (2015). Chander's work verified the proximity effect on added mass during an underwater ice impact by releasing a submerged sphere underneath a model ship hull. The trajectory of the sphere was obtained using a high-speed camera, and the resultant impact force was measured using a load cell on the hull. Numerical simulations of the experiment with and without the hydrodynamic effects were compared to the results of the experiment, and they found that "the submerged impact force values were higher than the impact force without fluid effects" (Chander, 2015). Chander

suggests that the increase in the impact forces is due to the momentum carried by the fluid. Specifically, Chander found the added mass coefficient to be approximately 0.5 at a distance of equal to the diameter of the sphere and then increases to a maximum value at the point of impact. The maximum values obtained at the point of impact were in the range of 1.5 to 3 times the mass of the body.

Bird (1984) completed a series of tests to examine the forces on a submerged horizontal cylinder accelerated in a fluid. The total measured force is separated into three parts: the virtual force, determined by the acceleration; the conventional pseudo-steady state drag force, obtained from the velocity; and the history force which consists of any of the remaining force. The total force F_T on the cylinder was measured using strain gauges and is given as:

$$F_T = F_V + F_D + F_H \tag{1.1}$$

F_V Virtual Force

F_D Pseudo Steady-State Drag Force

F_H History Force

Where the virtual force can be defined as;

$$_V = (m + m_A)a \tag{1.2}$$

and the pseudo steady-state drag force is given as:

$$F_D = -C_D \frac{1}{2} \rho L D |V| V \tag{1.3}$$

Where C_D is the drag coefficient, ρ is the fluid density, V is the velocity of the cylinder, and L and D are the length and diameter of the cylinder respectively.

In Bird's tests, the total forces on a submerged circular cylinder were measured for the following cases:

- Acceleration from rest to constant velocity.
- Deceleration to rest from constant velocity.
- Acceleration from a low velocity to a higher constant velocity.
- Reversal of motion from a constant forward velocity to a constant reverse velocity.

Results from the experimental investigations of Bird (1984) show that the history force is smaller in magnitude than the added mass force for displacements less than 0.5 times the diameter.

In more recent work, the rectilinear motion of submerged bodies has commonly been performed using a mass and pulley system to apply a known force on a body. In the case of Chan and Kang (2011), a mass and pulley system outfitted with an optical encoder was used to determine the added mass and damping coefficients of a bio-mimicking fish robot.

A similar, yet larger scale mass and pulley system was setup by Zhang et al. (2013) to investigate the influence of water on ship collisions with fixed structures. Their experiment consisted of a ship model which collided with a pressure sensor mounted above the waterline to compare the impact loads of a vessel inside and outside of water. Zhang et al. concluded that the impact forces decreased due to the influence

of water, and proposed that collision energy is dissipated by the fluid's damping effects.

Previously, Motora et al. (1969) also completed a series of model tests and theoretical calculations to produce more accurate estimates of the energy absorbed during ship-ship collisions. In the past, Minorsky (1959) proposed a constant added mass coefficient of 0.4 for sway which has been widely used for modeling ship-ship and ship-ice collisions.

The theoretical calculations of Motora et al. (1969) were based on the frequency-dependent equation of transverse motion given in terms of apparent mass $m^*(\omega)$ and damping $c(\omega)$:

$$m^*(\omega)\ddot{x}(t) + c(\omega)\dot{x}(t) = f(t) \tag{1.4}$$

Through applying Fourier transforms to the equation of motion, a time-series equivalent added mass coefficient is calculated from the frequency dependent added mass and damping coefficients obtained from the strip theory method. Motora et al. (1969) compare the theoretical results against experimental results of model scale tests of ship's motion in sway. The authors propose the use of "an equivalent added mass i.e., supposing an exact solution of the acceleration (a) of the collided ship acted by a prescribed force (f)" (Motora et al., 1969). From Equation 1.5, three equivalent added masses, $\bar{m}_y''$, $\bar{m}_y'$, and $\bar{m}_y$ are formulated with respect to acceleration, velocity, and absorbed energy respectively.

$$f = (m + \bar{m}''_y)a \tag{1.5}$$

Therefore, the equivalent added mass ($\bar{m}''_y$) for the acceleration $a(t)$ is:

$$m + \bar{m}''_y = \frac{f(t)}{a(t)} \tag{1.6}$$

Where, m is the mass of the body and $f(t)$ is the applied force. Similarly, the equivalent added mass for the velocity $v(t)$ is given as:

$$m + \bar{m}'_y = \frac{\int_0^t f(\tau)d\tau}{v(t)} \tag{1.7}$$

Finally, another equivalent added mass provides the exact value of absorbed energy as follows:

$$m + \bar{m}_y = \frac{\int_0^t f(\tau)v(\tau)d\tau}{\frac{1}{2}v^2(t)} \tag{1.8}$$

The experimental setup used by Motora et al. to validate these calculations consisted of a ship model outfitted with an accelerometer on a friction-less guide. Much like the previously discussed experiments, a step-wise force was applied using mass and pulley system.

The key takeaway from these experiments is that the equivalent added mass varies throughout the collision process. In the case of sway, their results suggest that equiv-

alent added mass varies between 0.4 and 1.4 times the mass of the given ship model. The assumption of constant added mass is only justifiable if the collision is very short. The authors propose that "if the duration of the collision is very short, then the [equivalent added mass] is practically equal to the [infinite frequency added mass]" (Motora et al., 1969).

J. Petersen and Pedersen (1981) and Petersen (1982) later expanded on the work of Motora et al. by applying the above formulations to a two-dimensional ship collision model. The horizontal motions in surge, sway, and yaw were considered for a ship-ship collision occurring at an angle slightly off from 90-degrees. Results of Petersen (1982) provide equivalent added mass values for sway of 0.2-1.25 times the mass of the ship; and values for yaw of 0.02-0.08 times the moment of inertia of the ship. The added mass in surge was assumed to be 0.05 times the mass of the ship which was based on earlier works of Motora (1960) who suggested values between 0.02-0.07 times the mass of the ship.

Song et al. (2016) compared the constant added mass (CAM) and fluid-structure interaction (FSI) methods used for modeling ship-ship and ship-ice collision. In contrast to the CAM approach, the FSI method explicitly models the surrounding fluid flow. Numerical simulations and laboratory experiments were completed for a collision between a steel structure and a fresh water ice mass. Song et al. (2016) found that the CAM method indicated higher the peak contact forces than the FSI due to the lack of hydrodynamic interaction effects between the ice mass and the structure. The FSI method was found to provide better agreement with the experimental results, however required significantly more computational power in comparison to the CAM method.

Popov et al. (1968) developed a theoretical model to calculate the magnitude of stresses during ship-ice collisions based on the laws of momentum and energy balances. Within this work, Popov et al. (1968) represents a three-dimensional impact between a solid-body ship structure and circular ice floe as a one-dimensional impact occurring along the normal. In this transformation, an equivalent mass and velocity are determined from which the impact momentum can be calculated. The impact momentum (S) of the ice floe is given in terms of the ice mass (m), coefficients of the adjoining water mass (λ), and the resulting ice floe velocity (v) after impact.

$$m(1+\lambda)v = S \tag{1.9}$$

Regarding the ice floe, Popov et al. (1968) assumed values for the adjoining water mass coefficient based on theoretical values for an oblate ellipsoid, where the floe thickness is negligible compared to its expanse. The coefficients are assumed to be 0.0 in surge and 1.0 in pitch and heave.

The work of Popov et al. (1968) was later expanded on by Daley (1999) with the incorporation of pressure-area effects. It is this updated model that forms the foundation of the GPU-Event-Mechanics (GEM) simulation approach which was completed as part of the STepS2 research project (Daley et al., 2014).

To summarize, Table 1.1 provides a summary of the different notions of transient added mass and their coefficients from the literature.

Table 1.1: Summary of transient added mass values from literature.

Author	Impact	Value
Minorsky (1959)	Ship-Ship	Constant Added Mass Coefficient of 0.4 in sway.
Motora (1960)	Ship-Ship	Equivalent Added Mass Coefficient of 0.02-0.07 in surge.
Motora et al. (1969)	Ship-Ship	Equivalent Added Mass Coefficient of 0.4-1.4 in sway.
Popov et al. (1968)	Ship-Ice	Adjoining Water Mass Coefficient (ice) of 0.0 in surge and 1.0 in pitch and heave.
Chander (2015)	Ship-Ice	Added Mass Coefficient of 0.5 to 1.5-3.0 at the point of impact.

Chapter 2

Methodology

From the past literature, three separate notions of added mass have emerged. Firstly, there is the classical hydrodynamic added mass (m_a) often associated with oscillating bodies in ideal fluid and defined in terms of a frequency-dependent coefficient ($C_a(\omega)$). Second, the equivalent added mass coefficient ($\tilde{C}_a$), proposed by Motora et al. (1969), is calculated in the time domain and is transient in nature. Finally, Popov et al. (1968) provides an adjoining water mass coefficient (λ) which arises from applying laws of momentum to a collision. There is currently no published data available which focuses on the non-oscillatory transient added mass that compares these approaches.

Two experimental methods for investigating the added mass of sheet ice were developed based on the work of Motora et al. (1969) and Popov et al. (1968) described in Chapter 1. These methods consist of a Step Force Experiment and a Impulsive Impact Experiment which will be discussed in the following sections. Additionally, a numerical study was completed using the panel-method based software, WAMIT®, to investigate the hydrodynamic added mass of an oscillating disk and is presented

in Chapter 5.

2.0.1 Step Force Experiment

The step force experiment employs a mass and pulley system to apply a prescribed step-wise force to the ice model. The purpose of this experiment is to examine the equivalent added mass of the geometries under a constant applied force. The equivalent added mass (Δm) is calculated by applying Newton's Second Law, where the applied force (f) and ice mass (m) is known, and acceleration a is measured.

$$f = (m + \Delta m)a \tag{2.1}$$

In the case of the mass and pulley system, the applied force is assumed to be equal to the weight of a prescribed mass hung perpendicular to the floor. The applied weight could easily be changed to investigate the behavior of the floe under different levels of applied load. The friction within the pulleys was assumed to be negligible compared to the applied loads.

2.0.2 Impulsive Impact Experiment

Unlike the step force experiment, the intent of the impulsive impact experiment is to investigate what happens when an instantaneous force is applied then suddenly disappears. This could be related to a glancing impact of a ship hull with an ice floe. Based on the work of Popov et al. (1968), the proposed approach for determining the adjoining water mass applies conservation of momentum to a perfectly inelastic

collision to determine the mass of fluid that is accelerated with the body.

Momentum is the mass (m) of an object multiplied by its velocity (v). Conservation of momentum states that the total momentum of a system remains constant when there are no external forces acting on the system. Considering a collision between masses m_1 and m_2, the total momentum will be equal before and after the collision, which can be written as:

$$m_1 v_{1i} + m_2 v_{2i} = m_1 v_{1f} + m_2 v_{2f} \tag{2.2}$$

In a perfectly inelastic collision, shown in Figure 2.1, where a projectile of mass (m_1) becomes embedded within a stationary mass (m_2), where $v_{2i} = 0$, Equation 2.2 can be rewritten as follows:

$$m_1 v_{1i} + m_2(0) = (m_1 + m_2) v_{12f} \tag{2.3}$$

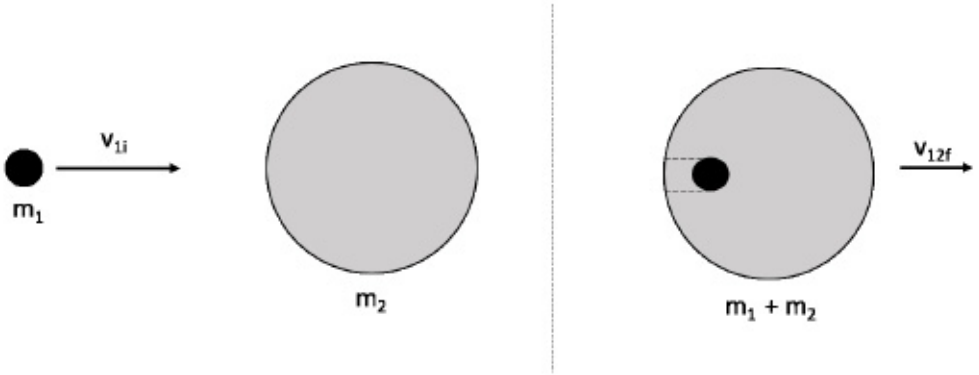

Figure 2.1: Momentum Problem

In the case where the second mass (m_2) is floating, the surrounding fluid will cause a loss of momentum within the system. The momentum of the water surrounding m_2 can be defined by an adjoining water mass (m_w) with a velocity (v_w).

$$m_1 v_{1i} = (m_1 + m_2) v_{12f} + m_w v_w \tag{2.4}$$

Where $m_w v_w$ represents the momentum transferred to the water mass following the collision.

In order to estimate the adjoining water mass based on the kinematics of the ice floe, it is assumed that the mean velocity of the water is equal to the final velocity of the coupled masses m_1 and m_2 (i.e., $v_{12f} = v_w$).

If the mass and velocity of the bodies are known, the mass of the adjoining water mass can be found using Equation 2.5.

$$m_w = \frac{m_1 v_{1i}}{v_{12f}} - (m_1 + m_2) \tag{2.5}$$

The adjoining water mass coefficient (λ) can then be calculated using Equation 2.6.

$$\lambda = \frac{m_w}{(m_1 + m_2)} \tag{2.6}$$

Chapter 3

Experimental Setup

A series of experiments investigating the added mass due to a step force and impulsive loads were completed within the trim tank located in the Fluids and Hydraulics Laboratory at Memorial University of Newfoundland. A multi-purpose "A"-Frame structure was constructed to house a pulley system for the step-force experiment, as well as support the high-speed camera, lighting system, and cables.

3.1 Mass and Pulley System

A pulley system was constructed using a low-stretch fishing line to connect a vertically hanging mass to the floating ice model fed through a series of two pulleys. Ball bearing pulleys were selected in order to minimize the effects of friction on the system.

A light-weight thread connected to the opposing side of the ice model was fixed to the side of the tank which restricted the model from being pulled forward by the hanging weight. This state of equilibrium was broken by burning the thread using a small torch. This created a nearly instantaneous step-wise force which caused

Figure 3.1: Low-Friction Pulley

the model to accelerate in the forward direction. Burning the string prevented any unwanted pulling on the string while it was being cut. A diagram of the setup is presented in Figure 3.2.

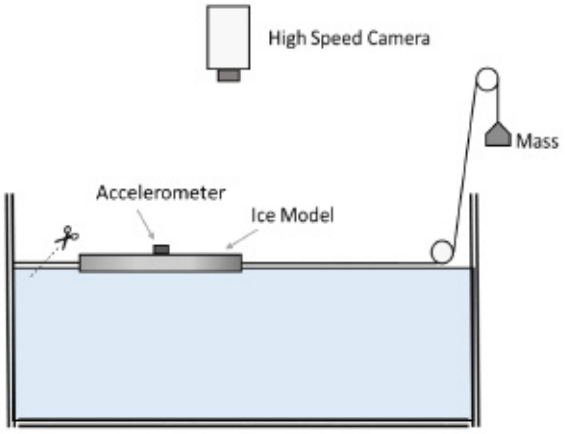

Figure 3.2: Step-Force Pulley Experiment Design Diagram

The high-speed camera and lighting system were mounted perpendicular to the water surface in order to track the position of the floe. Tracking points were placed on the ice models to identify its position within each frame. An accelerometer sensor was also mounted to the ice model to measure acceleration directly. A photo of the

setup is presented in Figure 3.3.

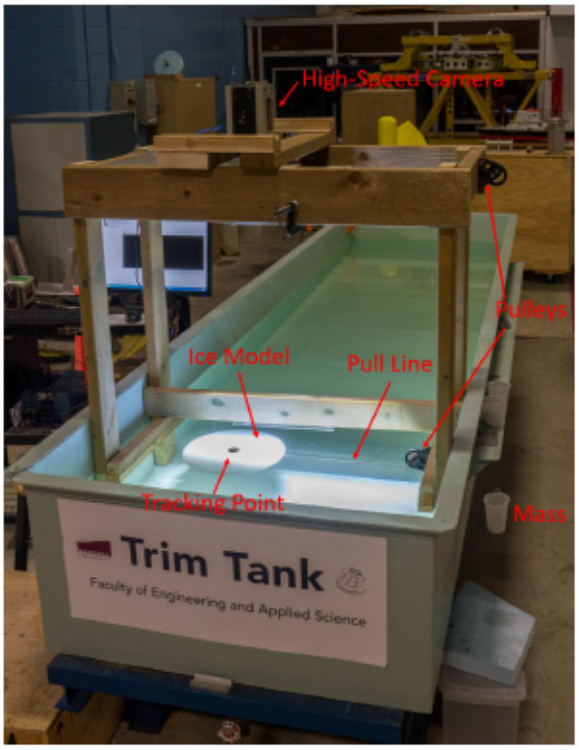

Figure 3.3: Step-Force Pulley Experiment Setup

3.1.1 Mass Selection

In order to maintain a basis for comparison across the different ice model geometries, the applied mass was selected based on a percentage of the total mass of the ice floe. Several preliminary trial runs were conducted and indicated the ideal testing range for the given setup was between 3% and 5% of the ice mass. In cases where the applied mass was greater than 5%, the models would accelerate at a rate high enough to cause water to over-top the leading edge of the floe. The weight of the water on the

leading edge caused the front of the floe to pitch downward and become submerged. In cases where the applied mass was less than 3%, friction in the pulleys and the cutting of the line appeared to have an increasing effect on the data. In consequence, three levels of applied masses equivalent to 3%, 4%, and 5% of the model ice masses were selected for testing.

3.2 Projectile Launcher

The impulsive impact experiment relies on creating a perfectly inelastic collision between a projectile and the ice floe model. This was achieved using a projectile launcher which launched a ball into a foam catcher that was fixed on top of the ice model as shown in Figure 3.4. The same high-speed camera and lighting setup used in the step force experiment was used for these tests.

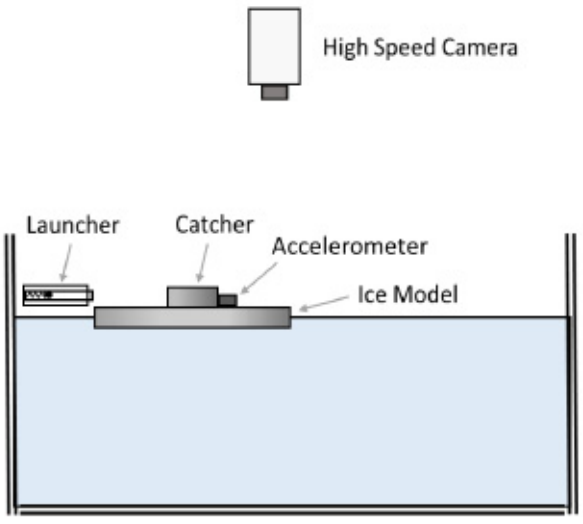

Figure 3.4: Impulsive Impact Experiment Design Diagram

Many different types of projectile launchers were considered when designing the impulsive impact experiment. The following selection criteria were defined for the optimal launcher:

- Capable of producing repeatable projectile velocities.
- Provide enough accuracy to hit the target.
- Produce sufficient momentum to move the model ice floe.
- Must be safe to operate in the lab.
- Ability to generate different amounts of momentum (either by varying projectile velocity or mass).

A spring-powered cannon was chosen as it fulfilled all the above criteria. Instead of designing a purpose-built spring cannon, PASCO™'s Mini Launcher shown in Figure 3.5 was chosen for this experiment. This launcher is typically used in Physics labs to teach projectile motion and provides good repeatability and shooting flexibility.

The PASCO™ Mini Launcher launches a 16mm diameter steel ball with a mass of 16.3g at three repeatable velocities. A series of test launches recorded with the high-speed camera showed that, when fired horizontally, the average initial velocities for each setting were 3.45, 4.48, and 5.81 m/s respectively.

A standard laboratory support stand and rod were used to mount the launcher. The launcher was aimed to launch the steel ball parallel to the water surface and into a foam catcher mounted at the center of ice model. The ball was painted matte black to provide higher contrast within the high-speed video which helped facilitate object tracking.

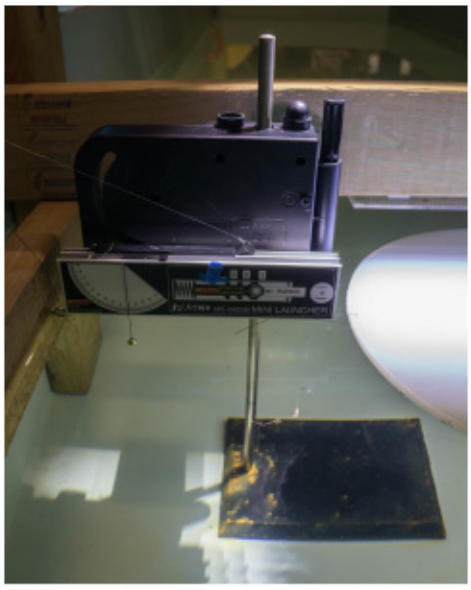

Figure 3.5: PASCO™ Mini Launcher

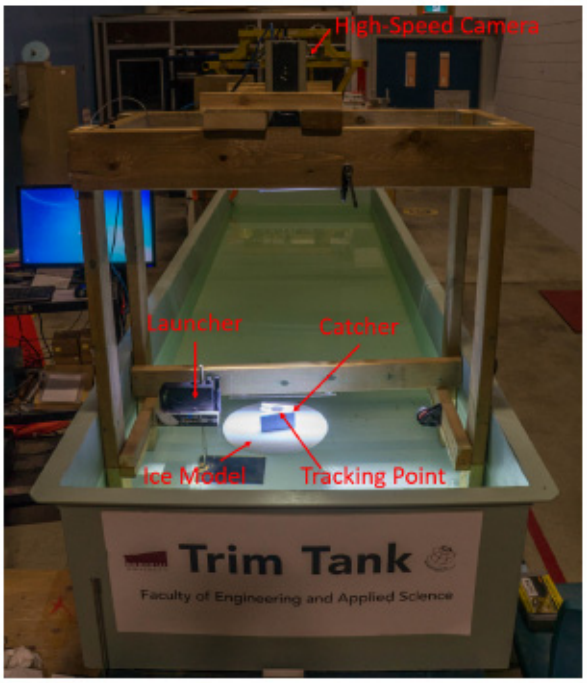

Figure 3.6: Impulsive Impact Experiment Setup

In order to ensure the model was stationary before each run, the model was fixed to the sides of the tank using the low-stretch fishing line and lightweight string as shown in Figure 3.7. The low-stretch fishing line was first fixed on the opposite side to the launcher. The thread was then pulled taut and held in place by placing the thread between the rim of the tank and the edge of a small 2g mass. This provided just enough friction to hold the model in place before the launcher was triggered. The force of the impact was used to free the thread as it was assumed that the force required to free the thread was negligible compared to the impact force.

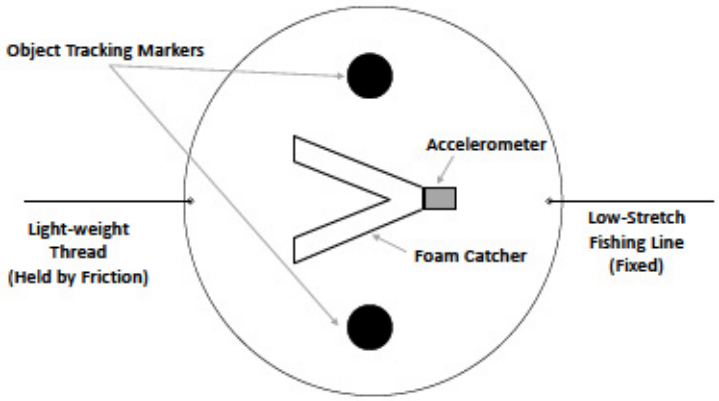

Figure 3.7: Ice Floe Model Diagram for Impulsive Impact Experiment

3.3 Ice Models

The use of real ice was not practical for these tests so polypropylene sheets were used to fabricate four ice models of varying geometries. Polypropylene was selected due to its rigidity and density that is similar to ice. A summary of the properties of the four models is presented in Table 3.1 and drawings of the models are presented in Figure 3.8. When designing the ice models, the diameter of the circumscribed circle of the irregular polygons were kept equal to the diameter of the disk.

Table 3.1: Models

Model	Diameter [mm]	Depth [mm]	Area [cm2]	Mass [kg]
Disk	300	19	707	0.812
5-Sided Polygon	300	19	524	0.602
4-Sided Polygon	300	19	426	0.488
3-Sided Polygon	300	19	284	0.324

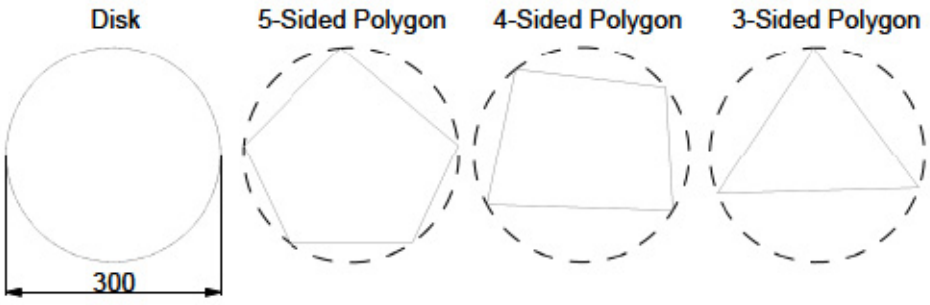

Figure 3.8: Top-view of Ice Models

3.4 High-Speed Camera

A high-speed camera capable of measuring the displacement of the ice floe and projectile was needed in order to determine their velocity and acceleration. A Mega Speed™ MS 55K camera was paired with a Tameron 28-75 F/2.8 lens for high-speed video capture. The following settings were used for all the high-speed recordings:

Table 3.2: High Speed Camera Settings

Frame Rate:	1000 FPS
Resolution:	1280x800
Exposure:	833 μsec
Aperture:	F/4
Focal Length:	28mm

Direct Current (DC) lights were required to avoid flickering in the frames of the high-speed video. Two LED light fixtures powered by a DC power supply were mounted next to the camera.

The dimensions of the video frames were calibrated according to markings of known length placed within the frame. Each frame was analyzed using the MatLab™ Image Processing Toolbox using the image detection algorithm discussed in Chapter 4.

3.5 Accelerometer Sensor

A voltage mode Piezoelectric Accelerometer was introduced to the setup in order to measure the acceleration of the model directly. When the accelerometer is accelerated

the quartz crystals within the sensing element deform which alters the electric field across the crystals. Voltage is applied to the sensor via a special low noise cable connected to a power supply coupler. The change in voltage due to the acceleration is recorded with a data acquisition unit (DAQ) which is connected to a computer. The signal flow from the accelerometer is summarized in Figure 3.9.

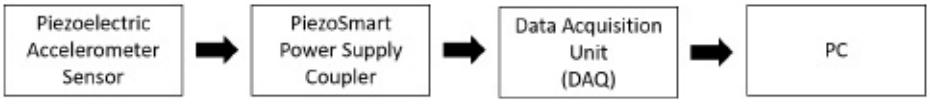

Figure 3.9: Accelerometer Signal Flow Chart

The specifications for the selected voltage mode accelerometer is presented in Table 3.3.

Table 3.3: Accelerometer Specifications

Brand:	Kistler
Model:	8704B100
Measuring Range:	$+/-$ 100 g
Sensitivity:	50.43 mV/g
Resonant Frequency:	54.0 kHz

3.6 Design of Experiments

The statistical method of Design of Experiments (DOE) was used to perform the step force and impulsive impact experiments. Through applying a full factorial design, the DOE method allows for consideration of all possible combinations of input values in order to characterize the main effects and interactions of the response variables. For the step force experiment, a multi-level categoric (or general factorial) design was selected to investigate the effects and interaction of shape and applied load on the response of the ice floe model. Two responses were considered including the acceleration and equivalent added mass of floe. A summary of the factors is provided in Table 3.4.

Table 3.4: Factors of Step Force Experiment

Factor	Name	Type	Levels
A	Percent of Ice Mass	Categoric	3
B	Ice Floe Shape	Categoric	4

In the case of the step force experiment, four shapes were tested at three different load levels. Initially, two replicates were completed for each combination of shape and load using the high-speed camera and accelerometer consisting of 24 runs. After analyzing this data, it was determined that additional runs were required to obtain a better understanding of the variability of the results. In consequence, the design was augmented to include three additional replicates for each level combination, providing an additional 36 data series. The final experimental design consists of a total of 60

runs, divided into two separate blocks, containing the first and second set of runs respectively.

For the impulsive impact experiment, only the disk-shaped floe could be tested due to equipment availability and time restraints. As a result, a general one-factor multi-level categoric design was selected. The factor under consideration was the projectile launcher setting which consisted of three levels. Two replicates were successfully completed for each level providing a total of six runs.

For both experiments, the method of Analysis of Variance (ANOVA) was used for the calculation of the main effects and interaction effect. The ANOVA test determines whether the experimental results are significant by evaluating the average response of each factor. By performing replicate runs, ANOVA also provides an estimation of the experimental error. Results of the ANOVA analysis are presented in Chapter 7.

Chapter 4

Signal Processing

4.1 Image Tracking

A high-speed camera was used to record both the step-force experiment and the impulsive impact experiment. To simplify the task of tracking ice models of irregular and variable shapes, circular markers where used to track the models. The MatLab™ Image Processing Toolbox was used to develop a script for identifying the location of circular markers within each frame.

In the case of the step-force experiment, circular matte black adhesive markers were placed on top of the models. The center of the circular markers were aligned with the center of gravity of each model. The high contrast between the black markers and light backdrop made it easier to isolate the marker from the surroundings using image detection techniques. Tracking the position of the circular makers meant that the center of gravity of the model could be determined for each frame of the high-speed footage.

A similar approach was used for impulsive impact experiment, where steel ball was painted with a matte black finish to create higher contrast within the frame. The initial velocity of the projectile, v_{1i}, is determined using the footage just before impact; while the final combined velocity of the projectile and model, v_{12f}, was determined once the projectile has been embedded in the foam catcher. It was possible to differentiate the projectile from the circular markers on the floe based on the size of the objects.

4.1.1 Circular Object Tracking Algorithm

The MatLab™ script containing the image detection algorithm described in this section is presented in Appendix A.

The first step of the algorithm is to import image file. The high-speed camera outputs frames as individual bitmap gray-scale images. Each frame is imported and processed one at a time to reduce memory usage. The images are cropped to contain only the area of interest to help further reduce computational time.

Images taken with the high-speed camera tend to be quite noisy which can make the edges of the object's boundary appear soft. The contrast is adjusted using the 'imadjust' function which can be found within Image Processing Toolbox. Adjusting the contrast helps make the boundary appear more defined and increases the chances that the object will be successfully detected.

Once the adjustments are complete, the 'imfindcircles' function is used to identify the location of circular objects within a specified range of radii using Circular Hough Transform (CHT). The CHT algorithm is a robust method for identifying imperfect

shapes in noisy and irregularly lit images such as the example provided in Figure 4.1.

The algorithm works by first locating any edges in the image using the desired edge detection technique, as illustrated in Figure 4.2. Next, circles of the specified radii are drawn around each point along the edge as shown in Figure 4.3.

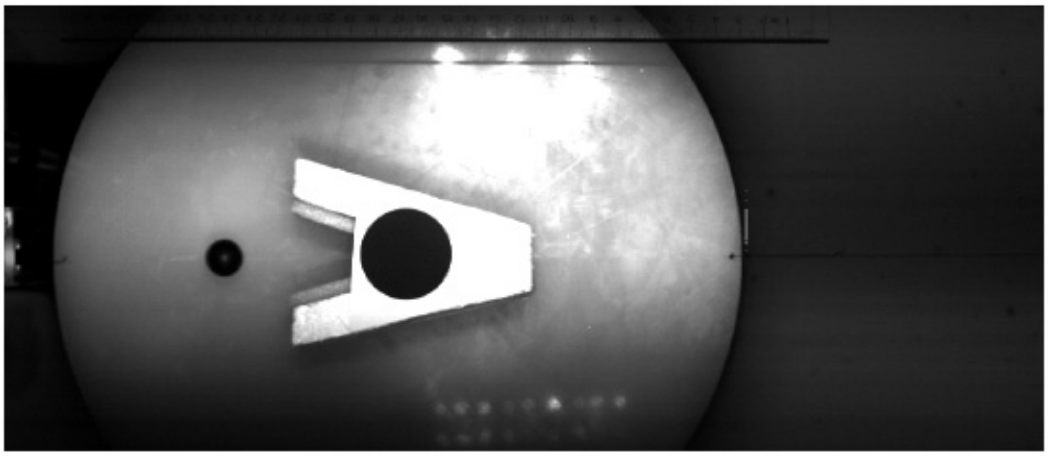

Figure 4.1: Sample frame just prior to projectile impact

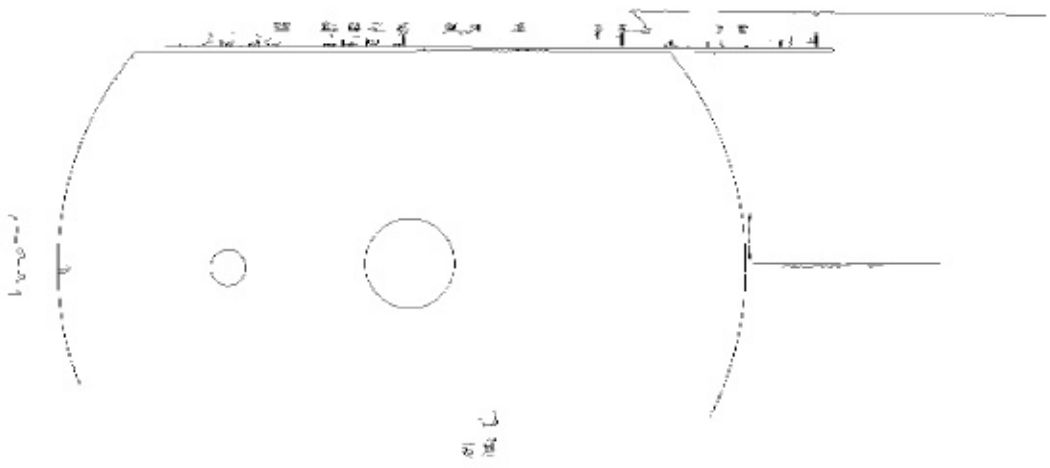

Figure 4.2: Sample edge detection image

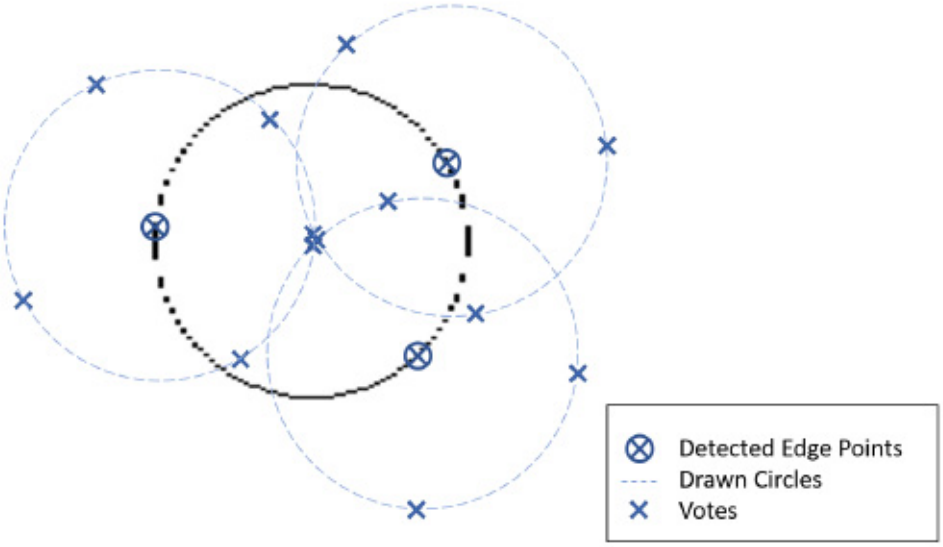

Figure 4.3: Illustration of the voting procedure for the CHT algorithm

The points along the circumference of the newly drawn circles are stored in an 'accumulator' matrix which contains information on the number of circles that pass through a given coordinate. Locations within this matrix containing a local maximum, correspond to the center of a circle in the image (Pedersen, 2007). The position and radius of the identified circle is given in terms of pixels. Figure 4.4 shows an outline of the detected objects.

4.1.2 Filtering and Derivatives of Object Tracking Data

A separate MatLab™ script, provided in Appendix B, handles the interpolation of missing data, data filtering, and calculation of the time derivatives (i.e., velocity and acceleration).

There were rare instances where the object tracking algorithm failed to detect

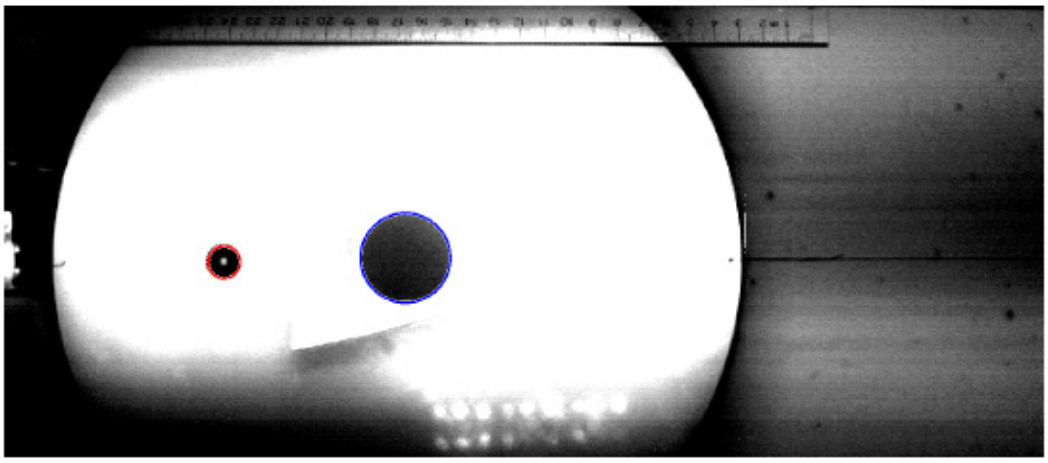

Figure 4.4: Detected Circles: Projectile (Red); Center of Ice Model (Blue)

any objects in the image. In this case, 1-D linear interpolation was applied to the displacement-time series to fill the missing values.

Differentiation of the displacement-time data made it clear that the original signal contained random noise. The relatively high frequency of the noise indicates it was likely due to the high sampling rate of the camera. In consequence, an infinite impulse response (IIR) filter was applied to the displacement-time signal in the form of a low pass Butterworth filter. The low pass filter removes the unwanted high-frequency noise from the signal.

An IIR filter was chosen over finite impulse response (FIR) filters such as a moving average filter because FIR filters tend to round off the output signal. By nature of the moving average filter, it causes the velocity and acceleration curve to extend into the region where the body should be stationary.

The displacement-time signal was filtered with a low pass Butterworth filter designed using MatLab™'s Signal Processing Toolbox. A passband from 0 to 20 Hz was defined in order to remove as much noise as possible without overly degrading

the signal. The first and second time-derivatives were calculated from the original filtered signal to obtain the velocity and acceleration time series.

4.2 Accelerometer Data

Acceleration measurements from the accelerometer sensor were recorded using LabView™ software at a sampling rate of 1000 Hertz. At the beginning of each run, acceleration of the model at rest was measured in order to zero the sensor readings during post-processing. An average of the acceleration measurements during this period was subtracted from the data series to zero the acceleration.

4.2.1 Filtering and Integration of Accelerometer Data

The MatLab™ script also contained in Appendix B was used to calculate the first and second integral of the acceleration with respect to time using the trapezoidal method. By the nature of integration, little to no filtering is needed to achieve smooth velocity and displacement curves.

4.3 Equivalent Added Mass Calculations

4.3.1 Step Force Experiment

In the step force experiment, the equivalent added mass can be calculated using Newton's second law, where $F = (m + \Delta m)a$. In this case, acceleration is measured while the applied force can be estimated based on the weight of the mass calculated

assuming an gravitational acceleration of $9.80655 m/s^2$. This leaves the equivalent added mass as the only unknown.

To form a basis of comparison across multiple runs and complete a statistical analysis of the responses, the equivalent added mass was calculated for two acceleration measurements obtained from the kinematic data: (1) the average acceleration, and (2) the maximum acceleration. To illustrate, a sample time series of velocity and acceleration data are presented in Figure 4.5. The average acceleration was obtained from the slope of the velocity curve, while the maximum acceleration is taken directly as the maximum measured acceleration.

4.3.2 Impulsive Impact Experiment

As discussed previously, conservation of momentum is applied by comparing the momentum of the system just before the collision and after the collision has finished. With the ice mass stationary prior to the collision, the initial momentum is simply calculated based on the mass and velocity of the projectile. Due to the transient nature of the collision, special care is needed for determining when the collision is over. In this case, the acceleration versus time plots were used to identify the time (t_s) at which the transient was over and the acceleration had settled. The velocity at this time could then be used for calculating the momentum and adjoining water mass. The sample data series presented in Figure 4.6, illustrates the selection of the above data points. It is noted that the filtering applied to the raw accelerometer data reduces the peak value for acceleration. As a result, the raw data was used for the momentum calculations as it provided practically identical results for velocity.

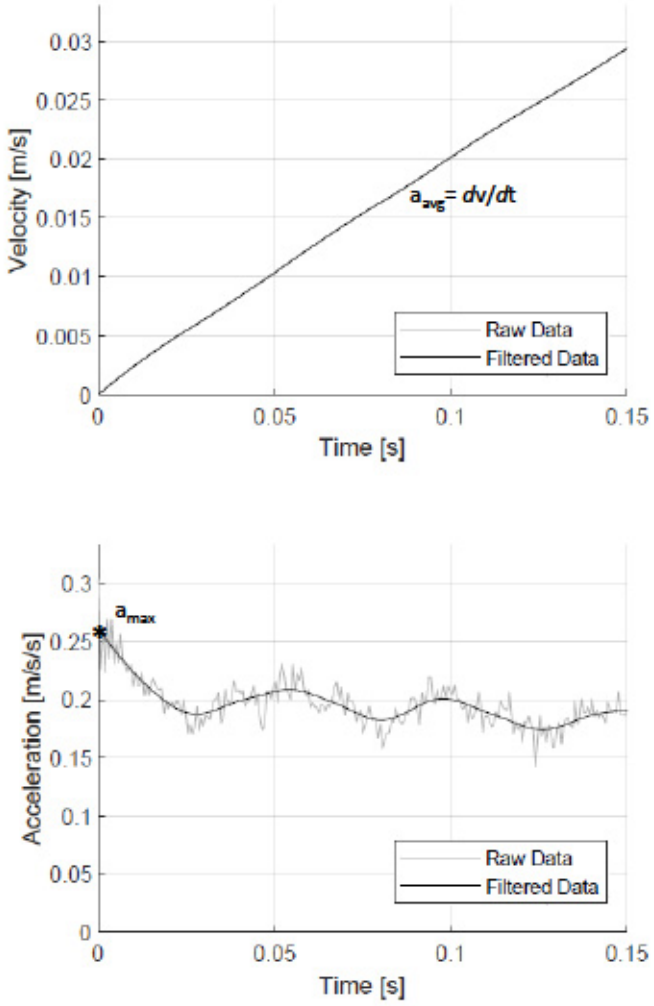

Figure 4.5: Sample Data Series for Step Force Experiment

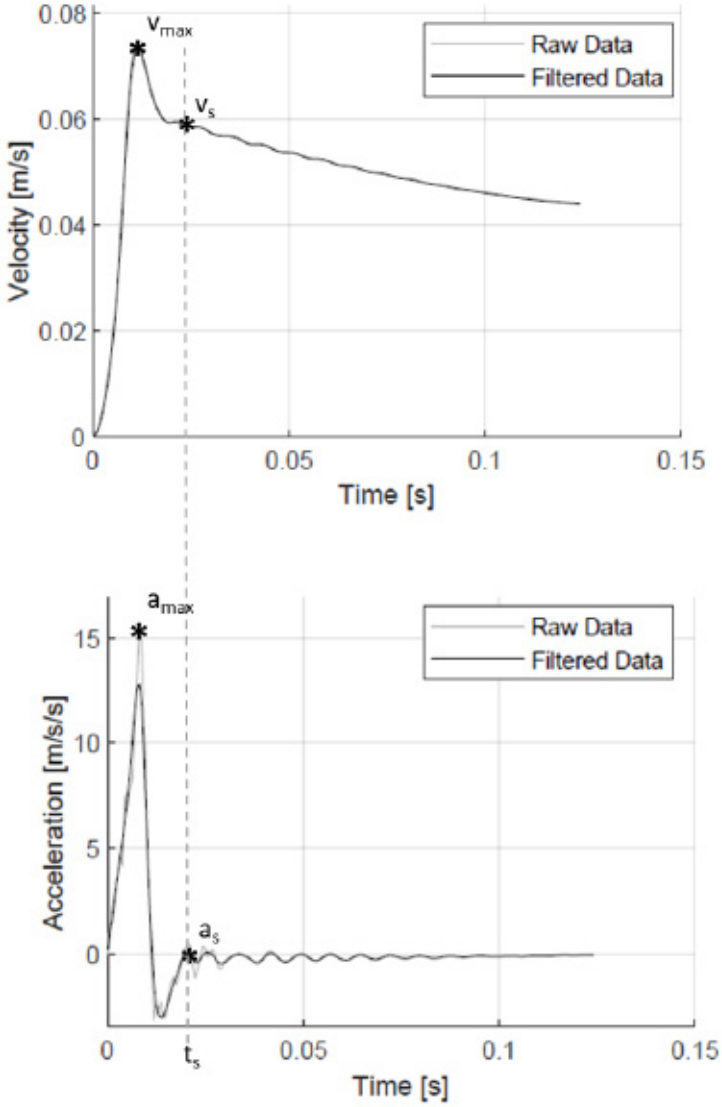

Figure 4.6: Sample Data Series for Impulsive Impact Experiment

Chapter 5

Numerical Analysis

5.1 WAMIT® Model

Analysis of cylindrical geometries was completed using the panel-method based software, WAMIT®, in an attempt to identify any relationship between the numerical and experimental results. Cylindrically shaped bodies were selected to directly compare the experimental results of the disk-shaped floe and to validate the numerical results against analytical models taken from literature.

The WAMIT® software is based on potential flow theory and performs linear analysis of surface wave interaction based on frequency-domain calculations. The frequency dependent added mass calculations are not directly comparable to the experimental time domain results; however, it has been suggested by Motora et al. (1969) that, "if the duration of the collision is very short, then the [equivalent added mass] is practically equal to the [infinite frequency added mass]".

5.2 Methodology

To validate the numerical analysis and gain confidence in the results, published analytical data was used as a baseline. From the research, there are no published analytical models for predicting the added mass of a thin disk in the horizontal plane. Alternatively, Wendel (1950) provides tabulated results for the added mass coefficient of a submerged horizontal cylinder in the transverse direction according to its length-to-diameter ratio (L/D). The smallest L/D ratio available is 1.2, which is considerably longer than the disk-shaped floe. A deeply submerged cylinder of $L/D = 1.2$ was used as the baseline for the validation of the numerical added mass calculations.

Once the numerical model was validated against the published analytical results, it was confirmed that the same cylinder, rotated vertically, would produce the same added mass values is sway. From there, the effect of reducing the L/D ratio was investigated by maintaining a constant diameter while reducing the length. The ratios considered were $L/D = 0.6, 0.1, 0.04$ (where 0.04 is the ratio of the disk-shaped floe). Next, the effect of submergence depth was investigated by bringing the disk-shaped model to the surface. Table 5.1 provides a summary of the runs according to L/D and distance from the free surface.

Table 5.1: L/D ratio and submergence depth of a vertical cylinder ($D = 0.300m$)

L/D	Submergence Depth [m]
1.2	-15.0
0.6	-15.0
0.1	-15.0
0.04	-15.0
0.04	-0.25
0.04	-0.10
0.04	-0.05
0.04	0.0

5.3 Geometry Files

The geometries were modeled within the 3D modeling software Rhino 5 and exported as an Initial Graphics Exchange Specification (IGES) file to be imported into Aero-Hydro's MultiSurf software. The mesh generated from the geometry within MultiSurf was then exported as a geometric data file which consisted of a list of panels compatible with the WAMIT® software. The radii of gyration and vertical center of gravity, used in the force control file, was calculated using intrinsic Rhino functions.

A mesh convergence study was completed based on 10mm, 7.5mm, and 5mm mesh sizing. Mesh convergence was achieved within a 1% difference for the added mass response of the 7.5mm and 5mm mesh sizes.

5.4 Model Assumptions

For this analysis, the fluid is assumed to be ideal, and the water depth is infinite. As such, it should be noted that the effect of viscosity is not considered in this analysis, and therefore there is no sheer flow present. Although only the added mass in the horizontal plane is of interest, all six degrees of motion were considered in the evaluation of the radiation problem. The iterative solver was used to evaluate the solution for the linear systems solving for the radiation and diffraction velocity potentials. The diffraction potential was solved from the diffraction problem instead of the scattering problem as this significantly reduces the CPU time and storage requirements.

5.5 Results

The numerical model was validated based on the tabulated results from Wendel (1950) for a ratio of $L/D = 1.2$. The L/D was incrementally decreased until the ratio of the disk shape floe was achieved. The relationship between added mass coefficient in sway and L/D from Wendel (1950) was extended with the results of the numerical analysis and is presented in Figure 5.1.

Further evaluation of the disk-shaped floe geometry was completed where the distance from the free surface was incrementally decreased until reaching the surface. The relationship between the added mass coefficient for sway and wave frequency (ω) is presented in Figure 5.2. For submergence depths deeper than 0.25m, the added mass is practically independent of the wave frequency. The frequency dependence of

the added mass coefficient increases as the body approaches the free surface. At the free surface, the infinite-frequency added mass coefficient was calculated to be close to 0%, while the zero-frequency added mass was approximately 13%.

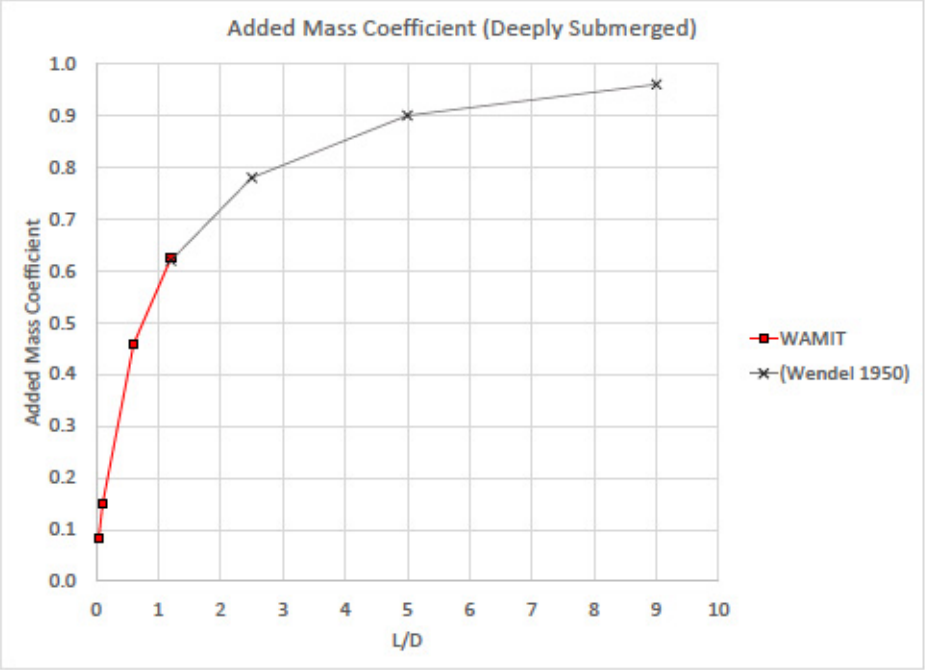

Figure 5.1: Sway Added Mass Coefficient of a Cylinder versus L/D

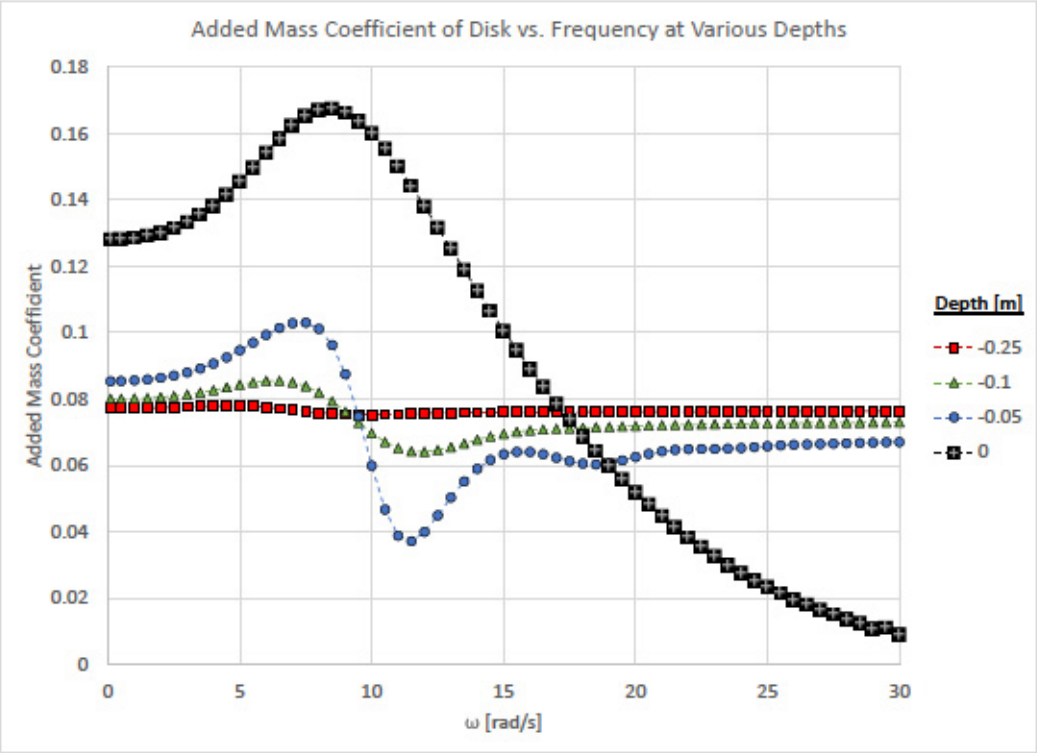

Figure 5.2: Sway Added Mass Coefficient of a Disk versus Frequency (ω)

Chapter 6

Experimental Results

6.1 Step Force Experiment

Tests were completed using four ice models consisting of a disk and a 3-, 4-, and 5-sided irregular circumscribed polygon. For each ice model, three levels of applied load equivalent to 3%, 4%, and 5% of the model's total mass were tested. The kinematic plots for each test are presented in Appendix C, which contains a side-by-side comparison of the accelerometer and high-speed camera data where available. Overall, good agreement between the two measurement techniques was achieved, however, the accelerometer data was considered more reliable for the time period of interest during the initial acceleration. Compared to the high-speed data, the accelerometer data required less filtering and provided better resolution of the step increase of acceleration.

To compare the results across multiple runs and complete a statistical analysis of the responses, the maximum acceleration, and average acceleration, obtained from

the slope of the velocity curve for each run, were recorded in tabular format and are presented in Appendix D. Plots summarizing the maximum acceleration and average acceleration versus the percent of ice mass are presented in Figure 6.1 and Figure 6.2 respectively. Statistical calculations were also carried out for the least significant difference bars about the predicted means of each factor combination.

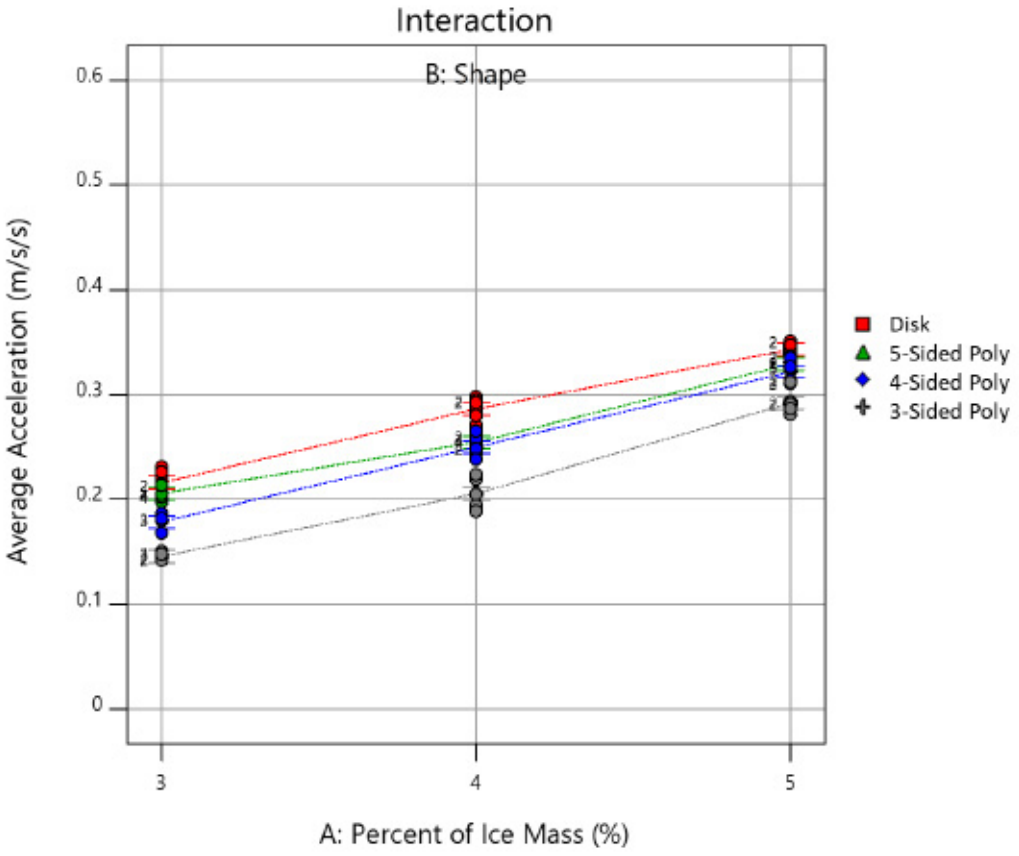

Figure 6.1: Average Acceleration versus Percent of Ice Mass

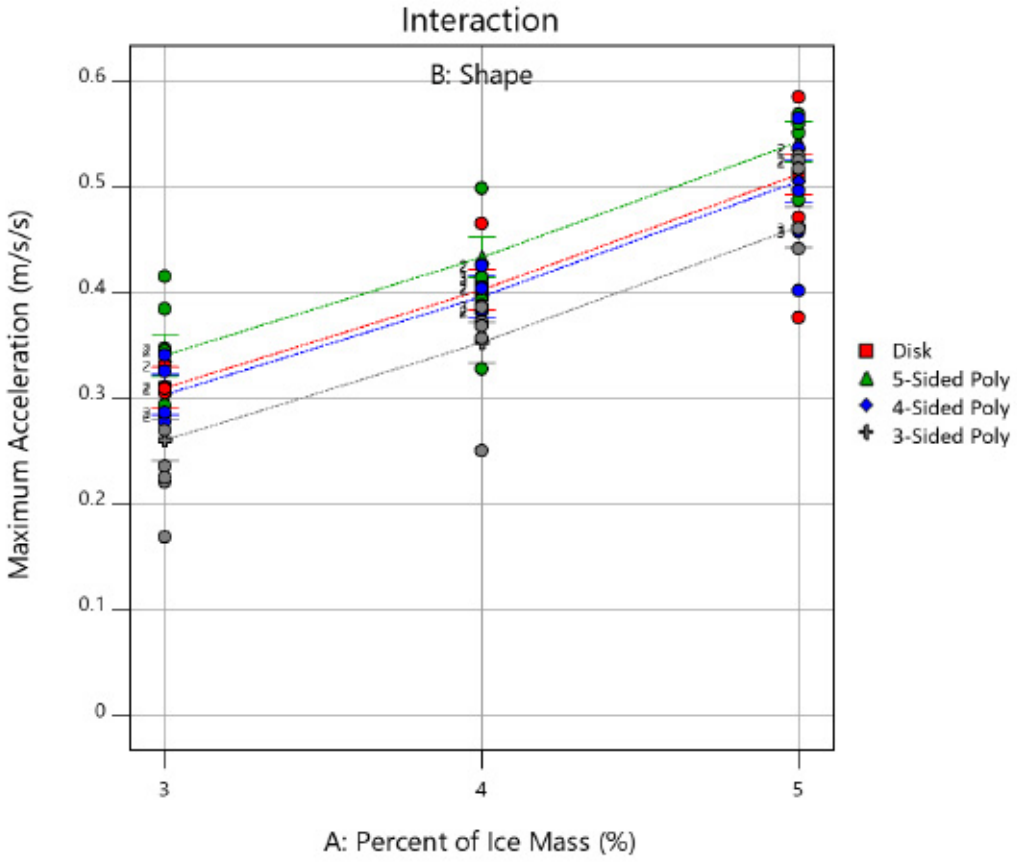

Figure 6.2: Max Acceleration versus Percent of Ice Mass

6.2 Impulsive Impact Experiment

The impulsive impact experiment was performed on the disk model using each of the three settings on the projectile launcher. Two replicates were completed for each of the launcher's settings providing a total of 6 runs. The kinematic plots of each run is provided in Appendix E, which provides a side-by-side comparison of the accelerometer and high-speed camera data. The projectile velocity just prior to impact was estimated using image tracking. The maximum velocity of ice floe model was found using the accelerometer and high-speed camera data. The steady state velocity after the transient was also estimated using the accelerometer data. The projectile velocity, as well as the maximum and steady state ice floe velocities are presented in Table 6.1.

Table 6.1: Acceleration and Velocity Measurements of the Disk

Launcher Setting [Clicks]	Projectile Velocity [m/s]	Max. Accel. (Accelerometer) [m/s^2]	Max. Vel. (Camera) [m/s]	Max. Vel. (Accelerometer) [m/s]	Steady Vel. (Accelerometer) [m/s]
1	3.465	15.34	0.0591	0.0735	0.0594
1	3.443	16.79	0.0669	0.0732	0.0571
2	4.468	31.69	0.0887	0.1030	0.0741
2	4.486	28.28	0.0870	0.0924	0.0747
3	5.755	41.28	0.1070	0.1249	0.0987
3	5.876	51.31	0.1054	0.1460	0.1003

The relationship between the initial projectile velocities and the resulting ice floe velocities is presented in Figure 6.3. A linear trend line which passes through the origin was fitted to the steady-state and maximum velocity data series.

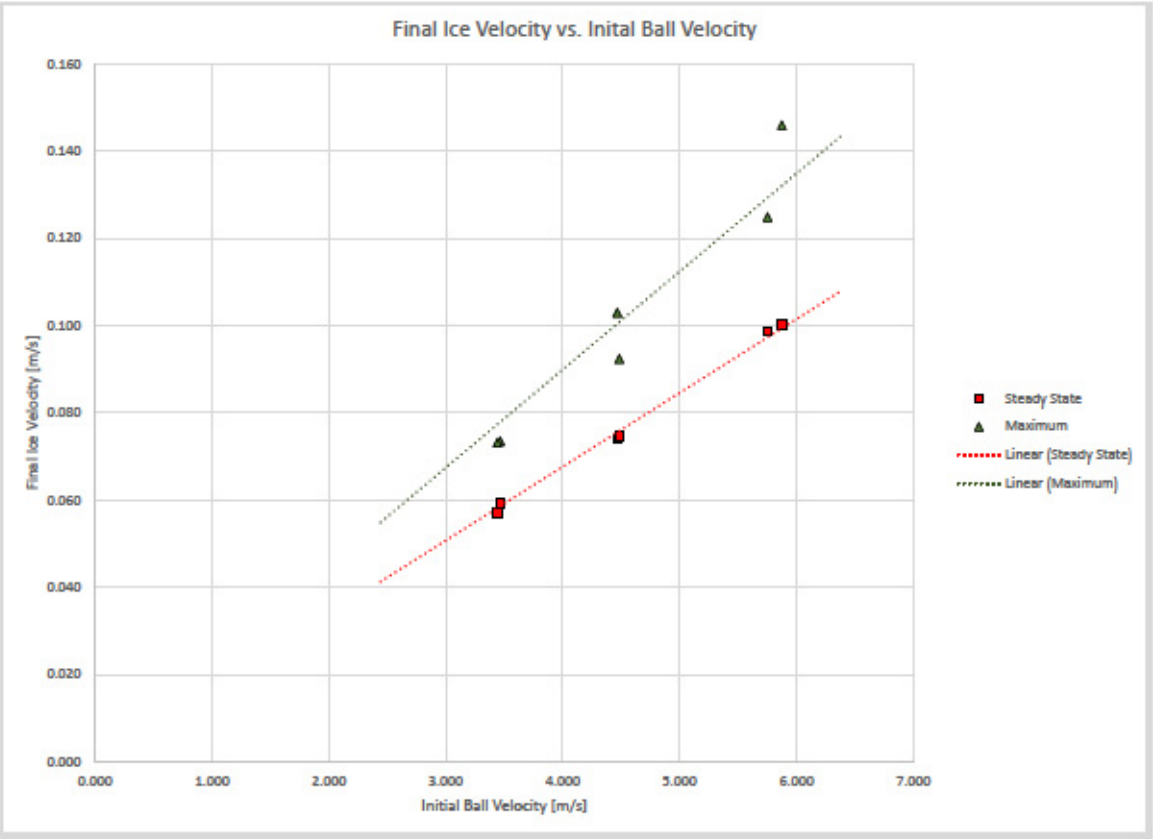

Figure 6.3: Velocity of the Ice versus Projectile Velocity

Chapter 7

Discussion

7.1 Step Force Experiment

The relationship between the applied force and resulting acceleration can be directly related to the apparent mass of the object by Newton's Second Law. The apparent mass is calculated by dividing the applied force by the acceleration. The equivalent added mass is then found by subtracting the mass of the model. These calculations were carried out using average acceleration and estimated applied force from each run to perform statistical analysis. The relationship between equivalent added mass and the estimated applied force is presented in Figure 7.1.

Alternatively, in the case of Figure 7.2, the apparent mass can also be calculated as the inverse of the slope for the line of best fit that passes through zero. The equivalent added mass is then calculated by subtracting the measured mass of the ice model.

From Figure 7.2, calculations were carried out using the graphical approach, and

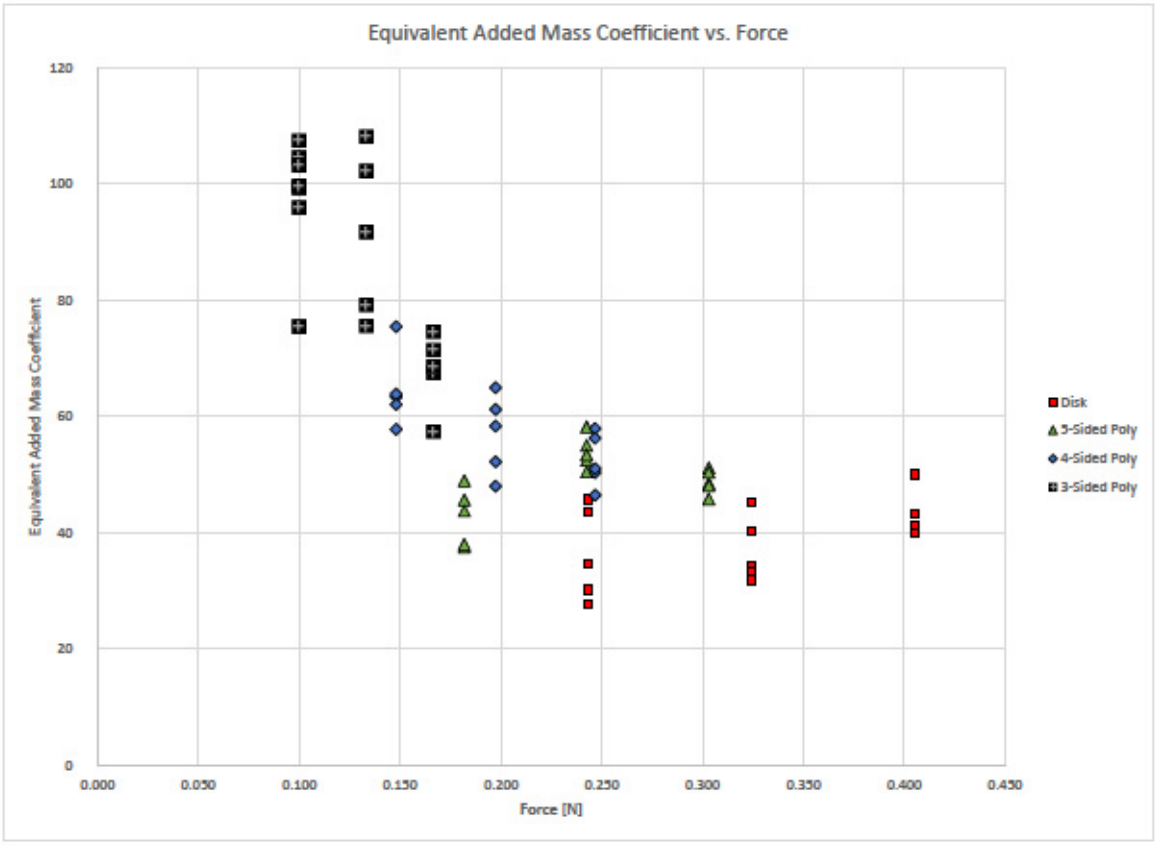

Figure 7.1: Equivalent Added Mass versus Estimated Applied Force

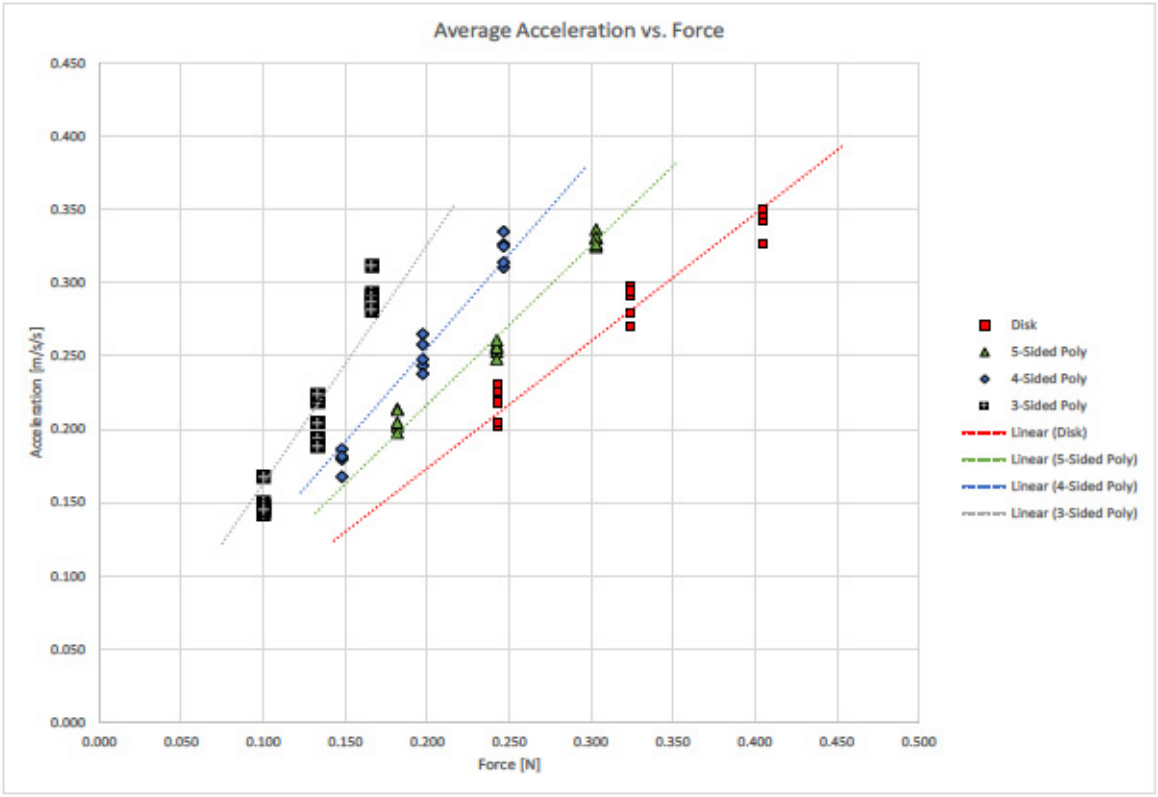

Figure 7.2: Acceleration versus Estimated Force

the results are presented in Table 7.1.

Table 7.1: Results from Graphical Method of Calculating Added Mass

Shape	Ice Mass [kg]	Slope (a/F) [1/kg]	Apparent Mass [kg]	Δm [kg]	$\tilde{C}_a$
Disk	0.826	0.867	1.153	0.327	40%
5-Sided	0.618	1.085	0.922	0.304	49%
4-Sided	0.503	1.277	0.783	0.280	56%
3-Sided	0.340	1.629	0.614	0.274	81%

Statistical analysis was completed using the Analysis of Variance (ANOVA) method for determining the main effects and interaction effect. This was done by evaluating the average response of each factor to determine whether it produced a significant response. Since replicate runs were conducted, ANOVA was also used to provide an estimation of the experimental error.

The two factors: A-Percent of Ice Mass, and B-Shape, were considered in modeling the Average Acceleration and Equivalent Added Mass. The ANOVA tables for Average Acceleration and Equivalent Added Mass are presented in Table 7.2 and Table 7.3 respectively. Assuming a level of significance of 0.05, it can be seen that the model and all its effects are significant. In both cases, the lack of fit is shown to be insignificant.

Regarding the acceleration, the ANOVA model suggests that the percent of the ice mass has the largest influence on the resulting acceleration. This is likely a result of the applied mass being chosen relative to the mass of each shape.

Table 7.2: Analysis of Variance for Average Acceleration

Source	Sum of Squares	df	Mean Square	F-value	p-value
Block	0.0003	1	0.0003		
Model	0.2207	11	0.0201	222.62	<0.0001
A-Percent of Ice Mass	0.1824	2	0.0912	1011.72	<0.0001
B-Shape	0.0364	3	0.0121	134.54	<0.0001
AB	0.0020	6	0.0003	3.63	0.0048
Residual	0.0042	47	0.0001		
Lack of Fit	0.0011	11	0.0001	1.19	0.3287
Pure Error	0.0031	36	0.0001		
Cor Total	0.2252	59			

Table 7.3: Analysis of Variance for Equivalent Added Mass

Source	Sum of Squares	df	Mean Square	F-value	p-value
Block	0.0095	1	0.0095		
Model	2.3201	11	0.2106	49.67	<0.0001
A-Percent of Ice Mass	0.0776	2	0.0388	9.15	0.0004
B-Shape	1.9410	3	0.6466	152.52	<0.0001
AB	0.2987	6	0.0498	11.74	<0.0001
Residual	0.1993	47	0.0042		
Lack of Fit	0.0459	11	0.0042	0.9803	0.4814
Pure Error	0.1533	36	0.0043		
Cor Total	2.5203	59			

The opposite is true for the equivalent added mass model, which indicates that the shape of the ice floe is the most influential factor. When comparing the different shapes in Figure 7.3, an increase in added mass can be observed as the floes become less round. This could be explained by the irregularity of the floe and presence of corners which could generate disturbances within the flow field, thus increasing the amount of fluid accelerated with the model.

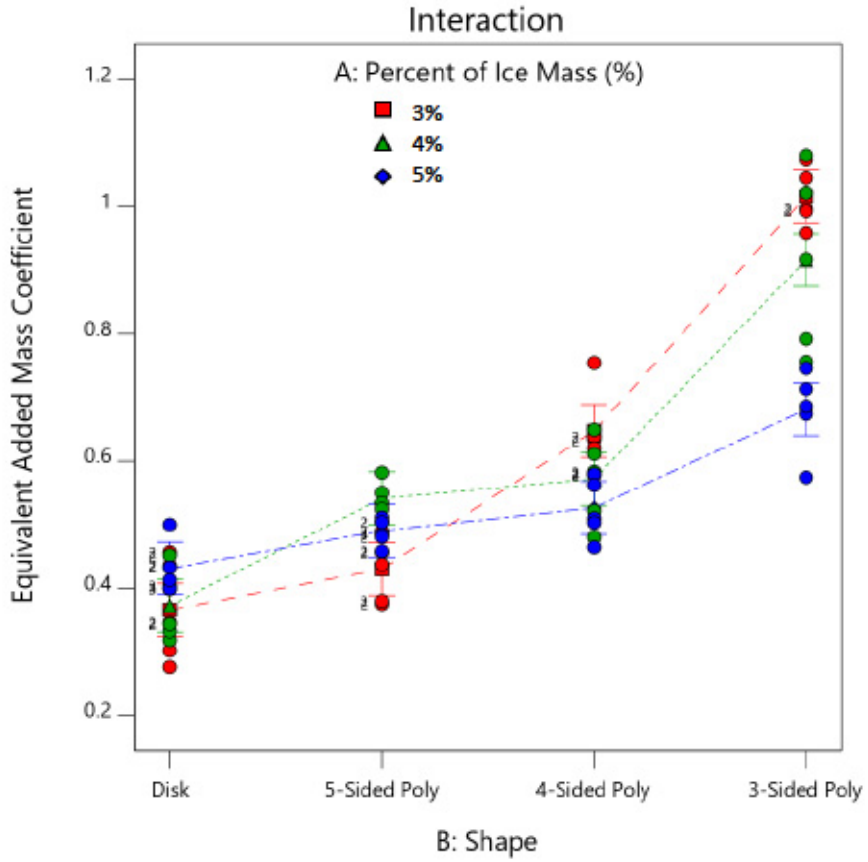

Figure 7.3: Equivalent Added Mass versus Ice Floe Shape

It is also noted that the variability between loading conditions appears to increase as the floes become less round. It is likely not a result of friction within the system

because this would provide a systematic error that would consistently overestimate the added mass. Instead, it is more likely that this variability is due to irregularities of the shape. It is possible that as the shape becomes less round, they become more susceptible to initial conditions which could cause greater variability. Other notable sources of variability between runs could include:

- Movement of model prior to release. Although water surface and model was allowed to settle before each run, it is possible movement was still present.
- Leaking and evaporation could have caused slight changes in water level throughout the testing period. The water level was regularly adjusted to align with the underside of the pulley to avoid pull in vertical directions.
- The cable connecting the accelerometer was hung in a way to minimize any force on the model, however, it was not possible to completely prevent this. A lighter-weight model would be more susceptible to the cable's influence.
- Water over-topping the front edge of the model causing the front of the model to pitch downward.
- Model rotation may occur due to irregular floe shapes.
- Vortices formed at the sharp corners affect the flow field development.

To further investigate the random error between nominally identical runs, the standard deviation was calculated for each factor combination and is presented in Table 7.4.

Table 7.4: Random Error of Equivalent Added Mass

Shape	Percent of Ice Mass	Mean of $\tilde{C}_a$	Standard Deviation
Disk	3%	36%	8.0%
	4%	37%	5.6%
	5%	43%	4.2%
5-Poly	3%	43%	4.9%
	4%	54%	2.9%
	5%	49%	2.1%
4-Poly	3%	64%	6.6%
	4%	57%	6.8%
	5%	52%	4.7%
3-Poly	3%	101%	4.6%
	4%	91%	14.1%
	5%	68%	6.5%

It would likely be possible to reduce the variability between runs by restricting the model's degrees of freedom to surge by placing the model on frictionless tracks similar to Motora et al. (1969). Doing so would reduce the effects of rotation and over-topping, however, may lead to unnatural behavior of the floe. Another option for reducing the sensitivity to the initial conditions may be to increase the scale of the experiment. If thickness and weight were increased, the model's sensitivity to the cable's influence, changes in water level, and over-topping phenomena might be reduced.

7.1.1 Relating Irregular Floes to a Disk

A method for estimating the added mass of an arbitrary irregular circumscribed polynomial was developed based on the notion that the entrained fluid around the model may be related to the mass of its circumscribed disk. As shown in Figure 3.8 previously, the polygon ice models were designed to fit within a 300mm diameter circumscribed circle. The equivalent added mass coefficient ($\tilde{C}_{a,disk}$) was normalized according to a circumscribed disk using Equation 7.1. In this case, m_{disk} is equal to the measured mass of the disk ice model. The relationship between the normalized added mass coefficient and the estimated force is presented in Figure 7.4.

$$\tilde{C}_{a,disk} = \frac{\Delta m}{m_{disk}} \tag{7.1}$$

From Figure 7.4, the set of values for the normalized added mass coefficient has an average value of 37% with a standard deviation of 6%. This is important because

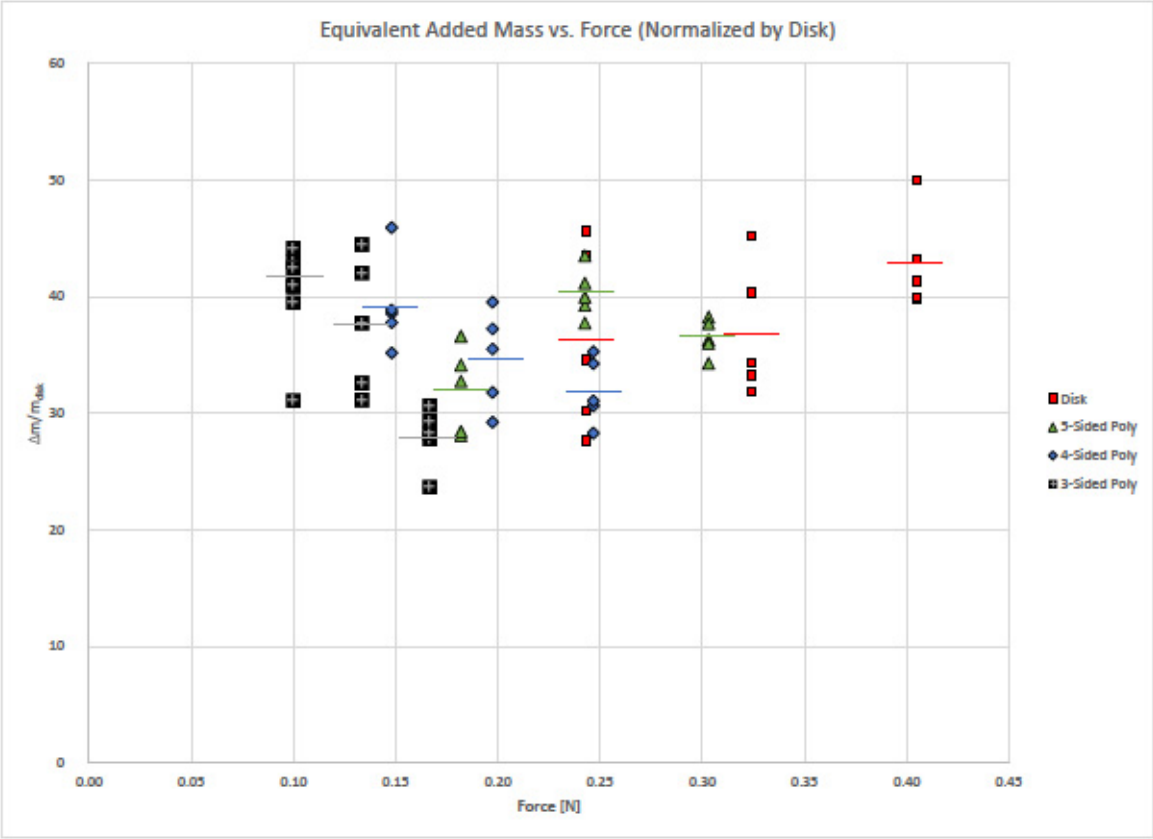

Figure 7.4: Added mass normalized according to a circumscribed disk

this approach may provide a means to efficiently estimate the equivalent added mass of randomly generated circumscribed floes within simulations such as GEM.

7.2 Impulse Experiment

Principles of conservation of momentum were applied to the selected velocities to determine the values for adjoining water mass which is presented in Table 7.5.

Table 7.5: Adjoining Water Mass for the Impulsive Impact Experiment on a Disk

Launcher Setting [Clicks]	$\Delta m_{w,Vmax}$ [kg]	$m_{w,s}$ [kg]	λ_{Vmax}	λ_s
1	-0.0851	0.0991	-10%	12%
1	-0.0871	0.1302	-10%	15%
2	-0.1470	0.1302	-17%	15%
2	-0.0622	0.1264	-7%	15%
3	-0.1028	0.0983	-12%	11%
3	-0.1983	0.1024	-23%	12%

The calculations for the maximum velocity provide unexpected negative mass values, which suggest that the fluid is forcing the body at this instance. A possible cause of this is that the ball has not completely settled in the catcher and has not yet matched the velocity of the ice model. It is also possible that elasticity within the foam catcher, or in the connection between the foam catcher and ice model, could have led to this unexpected result. Based on this result, it seems practical to instead consider

the steady-state velocity at which point the projectile is seemingly settled and the total momentum has been transferred. After the transient has settled, the adjoining water mass coefficient has an average value of 13% across all the runs. It can be noted that regardless of what final velocity was selected, the resulting coefficient appears to be independent of the projectile velocity. However, when examining the maximum accelerations presented in Table 6.1, it can be seen that the resulting acceleration is dependent on the projectile velocity.

Several challenges arose during testing which affected the quality of the data and ultimately limited the number of usable runs. Firstly, observation of the high-speed data revealed multiple impacts occurred from the projectile bouncing between the walls of the foam catcher. Accelerometer measurements presented within Appendix E reveal multiple peaks within the acceleration curve which support this observation. Furthermore, many runs had to be discarded because the foam catcher failed to catch the ball. The high-speed video showed this was often due to poor aim which prevented the ball from getting properly wedged into the 'v'-shaped catcher. The accelerometer cable also provided issues which resulted in additional discarded runs. Unlike the step force experiment, this experiment proved to be more susceptible to small forces from the cable which sometimes caused the ice model to move or rotate. Special care was given to adjust the cable before each run to try and minimize the cable's influence, however in some instances it was unavoidable.

7.3 Comparison of Results

The disk-shaped ice floe model provides a point of comparison between the two experimental studies and numerical results. Based on the results of the experiments, there does not appear to be any relationship between equivalent added mass and adjoining water mass. However, it is interesting to note the similarity between the adjoining water mass coefficient and the zero-frequency added mass coefficient that were found to be approximately 13%. This is particularly surprising because in the past it was suggested that equivalent added mass could be approximated by the infinite-frequency added mass.

Chapter 8

Conclusions and Recommendations

8.1 Step Force Experiment

A mass and pulley setup was used to apply a step-wise increase in force to model ice floes to examine the effect of the floe shape and the magnitude of the applied load on the equivalent added mass. The kinematics of four shapes, consisting of a disk and three circumscribed irregular polygons, were evaluated for three levels of applied load. As would be expected, the results suggest that the magnitude of acceleration is most influenced by the applied load which increases with higher loads. Calculations of equivalent added mass reveal that it is most sensitive to the body's geometry. Observation of the data suggests that the added mass coefficient increases as the floe becomes less round or more irregular.

Values for equivalent added mass were found to be in the range of 0.25 to 1.10 times the mass of the floe. These results fall within the same range found by Motora et al. (1969) and Petersen (1982) for the case of a ship collision in sway.

The relationship between a disk and irregular circumscribed polygons was explored by normalizing the equivalent added mass according to the mass of its circumscribed disk. Results show that the normalized coefficient was 0.25-0.50 times the mass of its circumscribed disk. Relating the irregular polygonal shapes to a disk may provide a unique opportunity for efficiently estimating equivalent added mass within computer simulations. Further work is needed to validate this normalized coefficient, especially with regards to the initial orientation of the model. All tests were repeated in the same orientation, therefore future studies should investigate whether the orientation will effect the proposed normalized coefficient.

There is still much experimental work needed to begin to fully understand the added mass of a body undergoing a step increase in applied force. The completed experiments failed to fully understand the effect of the applied load because the load was varied according to the mass of the model being tested. It is recommended that future tests apply forces which are consistent across all shapes to allow for better comparison between the models. One possibility may be to design various shapes with a constant mass and then apply consistent loads—this way the relationship between the ice floe mass and the weight mass can be maintained. Alternatively, it may be possible to define a range of forces which do not cause excessive amounts of over-topping or friction effects.

8.2 Impulsive Impact Experiment

A spring cannon was used to create an impulsive force on the ice floe model. By capturing the ball with the foam catcher, it was possible to create a perfectly inelastic

collision. Based on the assumption that an unknown amount of water mass would be accelerated with the floe, it was possible to apply conservation of momentum to estimate the adjoining water mass.

From the experimental trials, six tests completed using the disk-shaped floe at three impact velocities were analyzed using the high-speed camera and accelerometer data. As expected, observations show that an increase in projectile impact velocity causes an increase in the resultant acceleration of the floe. The analysis also reveals that the projectile velocity has little effect on the adjoining water mass. The results of these test suggest that the adjoining water mass is approximately 13% of the mass of the disk. When compared to frequency-domain calculations for added mass, the results suggest that the value for adjoining water mass is equal to the zero-frequency added mass.

Several problems arose during laboratory testing which limited the number of usable runs including issues with the experimental setup and equipment availability. It is suggested that alternate catching mechanisms be considered to improve the repeatability of the tests. Furthermore, the quality of the tests could be improved by increasing the scale of the models in an effort to negate the effects of the accelerometer cable during the tests.

It is recommended that further impulsive impact experiments be conducted to verify the relationship between adjoining water mass and the zero-frequency added mass. In doing so, the initial orientation of the model could also be varied to investigate its effect. Alternative methods might also be explored to better estimate the velocity of water entrained by the floe. One method might be to estimate the mean velocity of water based on the velocity profile of the surrounding fluid. It may also

be of interest to explore the use of other computational fluid dynamics models such as the finite element method to directly model the fluid volume. Alternatively, turbulence models may be used to conduct a simulation of unsteady flow. Although not directly related to added mass, special consideration should be given to the effect of viscosity which will create sheer flow within the fluid that is not captured in potential flow theory models such as WAMIT®. Due to the plate-like geometry of the floe, a relatively large portion of the underwater area will be subjected to sheer flow when accelerated in the horizontal direction.

Beyond this work, the obvious next step would be to try to better understand the changes in added mass as a ship's hull approaches and impacts the floe. This problem is far more complex due to the three-dimensional nature of the hull form which can cause rotational motion as well as lead to proximity effects. The relative velocity of the bodies will likely be of considerable importance. In particular, the presence of a ship's bow wave may have a significant impact on the relative velocity of the floe at the point of collision. Ultimately, having a better understanding of the hydrodynamic effects of ice collisions will help produce better load predictions leading to improved structural designs and increased safety.

Bibliography

Basset, A. B. (1888). On the motion of a sphere in a viscous liquid. *Philosophical Transactions of the Royal Society of London Mathematical, Physical and Engineering Sciences*, 179:43–63.

Bessel, F. (1828). *Investigations on the length of the seconds pendulum.* Berlin.

Bird, A. R. (1984). *Measured fluid forces on an accelerated-decelerated circular cylinder.* PhD thesis, Northwestern University, Evanston, Illinois.

Boussinesq, J. (1885). Sur la resistance d'une sphere solide.

Chan, W. L. and Kang, T. (2011). Simultaneous determination of drag coefficient and added mass. *IEEE Journal of Oceanic Engineering*, 36(3):422–430.

Chander, S. (2015). Experimental and numerical hydrodynamic study of submerged ice collision. Master's thesis, Memorial University of Newfoundland, St. John's, Newfoundland.

Daley, C. (1999). Energy based ice collision forces. In *Proc. of the 15th International Conference on Port and Ocean Engineering under Arctic Conditions*, Helsinki, Finland. POAC '99.

Daley, C., Alawneh, S., Peters, D., and Colbourne, B. (2014). Gpu-event-mechanics evaluation of ice impact load statistics.

J. Petersen, M. and Pedersen, P. (1981). Collisions between ships and offshore platforms. 4.

Minorsky, V. (1959). An analysis of ship collisions with reference to protection of nuclear power plants. *Journal of Ship Research*, pages 1–4.

Motora, S. (1960). On the measurement of added mass and added moment of inertia of ships in steering motion.

Motora, S., Fujino, M., Sugiura, M., and Sugita, M. (1969). Equivalent added mass of ship in collision. *J.S.N.A. Japan*, 126(10):138–148.

Oseen, C. W. (1927). Neuere methoden und ergebnisse in der hydrodynamik. *Leipzig Akademische Verlagsgesellschaft mb H.*

Pedersen, S. J. K. (2007). *Aalborg University, Vision, Graphics, and Interactive Systems*, 123.

Petersen, M. J. (1982). Dynamics of ship collisions. *Ocean Engineering*, 9(4):295–329.

Popov, Y., Faddeev, O., Kheisin, D., and Yakovlev, A. (1968). *Strength of Ships Sailing in Ice.* Defense Technical Information Center.

Song, M., Kim, E., Amdahl, J., Ma, J., and Huang, Y. (2016). A comparative analysis of the fluid-structure interaction method and the constant added mass method for ice structure collisions. *Marine Structures*, 49:58–75.

Wendel, K. (1950). *Hydrodynamic Masses and Hydrodynamic Moments of Inertia*, volume 44 of *The David W. Taylor Model Basin*. Defense Technical Information Center. Translation.

Zhang, H., Wu, W., Tan, Z., and Cheng, Z. (2013). Experiment research of the influence of water on ship collision.

Appendix A

Image Analysis MatLab™ Script

```
%% High Speed Image Tracking ---------------------------------------%%
% Author: Craig Martin
% Description:
%  Uses functionality from the Image Processing Toolbox to identify cicular
%  objects within a frame. Positions of tracking point and projectile are
%  determined for each frame of the high speed video. Positions are output
%  to a track file containing position in terms of pixels.
%%-----------------------------------------------------------------------%%
clear all; clc; close all;

for RunIdx = 1:5 %List of Run Index Numbers
    clearvars -except RunIdx detect_fail detect_fail_prj
    %% User Input
    disp_fig = 1;   % 1 - Display Figures, 0 - Hide Figures
    dir = 'E:\Accel\';
    frame_delta = 1;
    vert_crop = 300; % Crop frame vertically
    horz_crop = 50;  % Crop frame horizontally
    % Tuning Factors : Ice Tracking Points
    Rmin_ice = 40; % imciclefind min radius
    Rmax_ice = 70; % imcirclefind max radius
    CFsens = 0.89; % imcirclefind sensitivity
    cntrst_lo_in = 0.07; % Low contrast limit adjustment
    cntrst_hi_in = 0.25; % High contrast limit adjustment
```

```
% Tuning Factors : Projectile
Rmin_prj = 15; % imciclefind min radius for projectile
Rmax_prj = 45; % imcirclefind max radius for projectile
cntrst_lo_in_prj = 0.0;  % Low contrast limit adjustment
cntrst_hi_in_prj = 0.08; % High contrast limit adjustment

%% Read Run Index File
exp = 1;
run_data = read_runfile_cam(exp);
run_name = char(run_data{2}(RunIdx));
frame_start = run_data{8}(RunIdx);
frame_finish = run_data{9}(RunIdx);
fps = run_data{5}(RunIdx);  % Frames per second
subdir = [run_name '\'];
prj_start = run_data{10}(RunIdx);  %Frame which projectile enters
prj_finish = run_data{11}(RunIdx); %Frame which projectile leaves

%% Image Detection Code
detect_fail(RunIdx) = 0;    %Initialize counter for detection failures
detect_fail_prj(RunIdx) = 0;%Initialize counter for detection failures
num_frames = frame_finish - frame_start;
if (disp_fig==1 && num_frames>10); disp_fig = 0; end
tic
for i = 1:frame_delta:num_frames+1
```

```
frame_id = i+frame_start-1;
% Read Image File:
img = imread(fullfile(dir, subdir, sprintf('File%07d.bmp',frame_id)));
% Adjust Contrast:
img_prj = imadjust(img,[cntrst_lo_in_prj,cntrst_hi_in_prj],[]);
img = imadjust(img,[cntrst_lo_in,cntrst_hi_in],[]);
%% Detect Projectile:
if (frame_id >= prj_start && frame_id <= prj_finish)
    [centers_prj,radii_prj] = imfindcircles(img_prj, ...
                                        [Rmin_prj Rmax_prj], ...
                                        'ObjectPolarity','Dark',...
                                        'Sensitivity',CFsens);
    % Display detected circles in frame:
    if disp_fig == 1; figure,imshow(img),title('Proj_Circle'); end
    if disp_fig == 1; viscircles(centers_prj,radii_prj,...
                                            'EdgeColor','r'); end
    % Sort Circles by Size:
    if length(radii_prj) == 1
        centroid_prj(i,1:2) = centers_prj(1,:);
    else
        centroid_prj(i,1:2) = nan;
        detect_fail_prj(RunIdx) = detect_fail_prj(RunIdx) + 1;
    end
else
```

```
        centroid_prj(i,1:2) = 0.0;
    end
    %% Detect Ice Model:
    [centers,radii] = imfindcircles(img,[Rmin_ice Rmax_ice], ...
                                    'ObjectPolarity','Dark', ...
                                    'Sensitivity',CFsens);
    % Display detected circles in frame:
    if disp_fig == 1; figure,imshow(img),title('Circle'); end
    if disp_fig == 1; viscircles(centers,radii,'EdgeColor','b'); end
    % Sort Circles by Size:
    [r_m,r_n] = size(radii);
    if r_m > 1 && r_m < 3
        centroid(i,1:2) = centers(1,:);
        centroid(i,3:4) = centers(2,:);
    else
        centroid(i,1:4) = nan;
        detect_fail(RunIdx) = detect_fail(RunIdx) + 1;
    end
end

%% Cmd Output
run_time = toc;
out = sprintf('Run: %s \n Time: %d \n Ice Fail: %d \n Prj Fail: %d',...
              run_name,run_time,detect_fail(RunIdx),...
```

```
                detect_fail_prj(RunIdx));
    disp(out);

    %% Generate Time Series
    t = ((0:frame_delta:num_frames) ./ fps)';

    %% CSV Output
    csvwrite(strcat(run_name,'_track.csv'), [t, centroid(:,:)]);
    csvwrite(strcat(run_name,'_proj.csv') , [t, centroid_prj(:,:)]);
end
```

Appendix B

Signal Processing and Plotting MatLab™ Script

```
%% Data Plotter for High Speed Image Tracking & Accelerometer ---------%%
% Author: Craig Martin
% Description:
%    This script handles the signal processing of the high-speed image
%    tracking data and accelerometer data. An automated selection process
%    allows user to specify what experiment, shape, load level and
%    iteration is plotted. Results are output to a .eps file.
%%-------------------------------------------------------------------%%
clear; clc; close all;
%% User Input
    timewindow = [0.0 0.15]; % Range of time to plot
    exp = 1;       % Experiment: 0 - Force <or> 1 - Impulse
    ShapeIdx = -1; % List of shape indices (Use -1 to evaluate all)
    LevelIdx = -1; % List of Load level indices (Use -1 to evaluate all)
    Iteration = -1;% List of iteration numbers (Use -1 to evaluate all)
    PLOTS_ON = 1;  % Switch to turn plotting on(1)/off(0)


%% Create List of Run Indices:
  if exp == 0 %Step Force
    Run_Data = read_runfile(0);
    [m,~] = size(Run_Data);
    if ShapeIdx < 0
        ShapeIdx = [1 5 4 3]; %DO NOT EDIT
    end
```

```
  if LevelIdx < 0
      LevelIdx = [3 4 5]; %DO NOT EDIT
  end
  if Iteration < 0
      Iteration = [1 2 3 4 5 6 7]; %DO NOT EDIT
  end
else %Impulse
  Run_Data = read_runfile(1);
  [m,~] = size(Run_Data);
  if ShapeIdx < 0
      ShapeIdx = [1]; %DO NOT EDIT
  end
  if LevelIdx < 0
      LevelIdx = [1 2 3]; %DO NOT EDIT
  end
  if Iteration < 0
      Iteration = [1 2]; %DO NOT EDIT
  end
end
[row1,~] = find(Run_Data{12}==ShapeIdx);
[row2,~] = find(Run_Data{7}==LevelIdx);
[row3,~] = find(Run_Data{3}==Iteration);
% Run List
RunList = intersect(row1,row2);
```

```
  RunList = intersect(RunList,row3);
  A_peak = zeros(length(RunList),6);

for I = 1:length(RunList)
    clearvars -except leg RunList I exp timewindow A_peak PLOTS_ON
    % Determine Run Index Number:
    RunIdx = RunList(I);
    %% Read Data File
    run_data = read_runfile(exp);
    run_name = char(run_data{2}(RunIdx));   %Run identifier
    itr = run_data{3}(RunIdx);              %Run iteration
    shape = char(run_data{4}(RunIdx));      %Shape of ice model
    m_ice = run_data{6}(RunIdx);    %Mass of ice model [kg]
    per_clk = run_data{7}(RunIdx);  %Percentage of ice mass or # of clicks
    span = 100;
    m = 3;
    n = 0;
    % Check Data Files Exist
    if exp == 0 % Step Force
        % High-Speed Camera Data
        fname_cam = strcat('FRC_cam\', run_name,'_track.csv');
        if exist(fname_cam,'file')
            exist_cam = 1;
            n = n+1;
```

```
    else
        exist_cam = 0;
    end
    % Accelerometer Data
    fname_acc = strcat('FRC_acc\', run_name,'.xlsx');
    if exist(fname_acc,'file')
        exist_acc = 1;
        n = n+1;
    else
        exist_acc = 0;
    end
else % Impulse
    % High-Speed Camera Data:
    fname_cam = strcat('IMP_cam\', run_name,'_track.csv');
    if exist(fname_cam,'file')
        exist_cam = 1;
        n = n+1;
    else
        exist_cam = 0;
    end
    % Accelerometer Data:
    fname_acc = strcat('IMP_acc\', run_name,'.xlsx');
    if exist(fname_acc,'file')
        exist_acc = 1;
```

```
            n = n+1;
        else
            exist_acc = 0;
        end
    end

%% Calculate High-Speed Camera Kinematics
if exist_cam
    [t_cam,s_cam] = read_cam(exp,RunIdx); % Read Data File
    [kin_raw_cam,kin_filt_cam] = cam_kin(t_cam,s_cam,exp);
    t_cam = kin_raw_cam(:,1);
    % Extract Acceleration Values of Interest:
    A_peak(I,1) = max(kin_filt_cam(1:150,4));
    A_peak(I,2) = lin_slope(kin_filt_cam(1:span,1),kin_filt_cam(1:span,3));
end

%% Calculate Accelerometer Kinematics
if exist_acc
    [t_acc,a_acc] = read_acc(exp,RunIdx); % Read Data File
    [kin_raw_acc,kin_filt_acc] = acc_kin(t_acc,a_acc,exp);
    % Extract Acceleration Values of Interest:
    A_peak(I,3) = kin_raw_acc(1,4);
    A_peak(I,4) = kin_filt_acc(1,4);
    A_peak(I,5) = lin_slope(kin_filt_acc(1:span,1),kin_filt_acc(1:span,3));
```

```
end

%% Plotting:
if PLOTS_ON
  gray = [0.7 0.7 0.7];
  subplot_fig = figure;
  if exist_acc
      if exist_cam
          sp = [1,3,5];
      else
          sp = [1,2,3];
      end
      sp1 = subplot(m,n,sp(1));
          hold on;
          plot(t_acc,kin_raw_acc(:,2),'color',gray);
          plot(t_acc,kin_filt_acc(:,2),'k');
          xlim(timewindow);
          grid on;
          ylabel('Displacement [m]');
          xlabel('Time [s]');
          title('Accelerometer');
          legend( ...
              'Raw Data', ...
              'Filtered Data', ...
```

```
            'Location', 'northwest');
    sp2 = subplot(m,n,sp(2));
        hold on;
        plot(t_acc,kin_raw_acc(:,3),'color',gray);
        plot(t_acc,kin_filt_acc(:,3),'k');
        xlim(timewindow);
        grid on;
        ylabel('Velocity [m/s]');
        xlabel('Time [s]');
    sp3 = subplot(m,n,sp(3));
        hold on;
        plot(t_acc,kin_raw_acc(:,4),'color',gray);
        plot(t_acc,kin_filt_acc(:,4),'k');
        %plot(t_lin,A_lin);
        xlim(timewindow);
        grid on;
        ylabel('Acceleration [m/s/s]');
        xlabel('Time [s]');
end
if exist_cam
    if exist_acc
        sp = [2,4,6];
    else
        sp = [1,2,3];
```

```
end
sp4 = subplot(m,n,sp(1));
    hold on;
    plot(t_cam,kin_raw_cam(:,2),'color',gray);
    plot(t_cam,kin_filt_cam(:,2),'k');
    xlim(timewindow);
    grid on;
    ylabel('Displacement [m]');
    xlabel('Time [s]');
    title('High-Speed Camera');
    legend( ...
        'Raw Data', ...
        'Filtered Data', ...
        'Location', 'northwest');
sp5 = subplot(m,n,sp(2));
    hold on;
    plot(t_cam,kin_raw_cam(:,3),'color',gray);
    plot(t_cam,kin_filt_cam(:,3),'k');
    xlim(timewindow);
    grid on;
    ylabel('Velocity [m/s]');
    xlabel('Time [s]');

sp6 = subplot(m,n,sp(3),'align');
```

```
        hold on;
        plot(t_cam,kin_filt_cam(:,4),'color',gray);
        plot(t_cam,kin_filt_cam(:,4),'k');
        xlim(timewindow);
        grid on;
        ylabel('Acceleration [m/s/s]');
        xlabel('Time [s]');
        %sp6.Position = [0.5703 0.1377 0.3347 0.1881];
end
%Set Plot Limits
if exp == 0 % Step Force
    if exist_acc
        s_lim = ylim(sp1) .* 1.1;
        s_lim = [0 s_lim(2)];
        v_lim = ylim(sp2) .* 1.1;
        v_lim = [0 v_lim(2)];
        a_lim = ylim(sp3) .* 1.1;
        a_lim = [0 a_lim(2)];
        ylim(sp1,s_lim);
        ylim(sp2,v_lim);
        ylim(sp3,a_lim);
    end
    if exist_acc && exist_cam
        ylim(sp4,s_lim);
```

```
        ylim(sp5,v_lim);
        ylim(sp6,a_lim);
    end
else % Impulse
    if exist_acc
        s_lim = ylim(sp1) .* 1.1;
        v_lim = ylim(sp2) .* 1.1;
        a_lim = ylim(sp3) .* 1.1;
        ylim(sp1,s_lim);
        ylim(sp2,v_lim);
        ylim(sp3,a_lim);
    end
    if exist_acc && exist_cam
        ylim(sp4,s_lim);
        ylim(sp5,v_lim);
        ylim(sp6,a_lim);
    end
end
% Set Plot Titles
if exp == 0 % Step Force
    fig_title = ['Step-Force Kinematics of a ', shape, ': ', ...
                num2str(per_clk), '\% of Ice Mass (Run ', ...
                num2str(itr), ')'];
else % Impulse
```

```
        if per_clk > 1; clicks = ' clicks';
        else; clicks = ' click'; end
        fig_title = ['Impusle-Momentum Kinematics of a ', shape, ': ', ...
                     num2str(per_clk), clicks, ' (Run ', num2str(itr), ')'];
    end
    % Print Plots to .EPS File
    set(gcf, 'Position', [850, 50, 825, 900]);
    set(gcf,'paperpositionmode','auto')
    print(run_name, '-depsc');
  end
end
```

```
function [t_cam,s_cam] = read_cam(exp,run)
%% Read High Speed Camera Data---------------------------------------%%
% Author: Craig Martin
% Description: Reads the run information database as well as
% the position data file obtained from image tracking. Handles
% interpolation of missing values caused by detection failures of
% tracking algorthim. Scales position data according to pixel measurements
% and calculates the position of the center of the ice floe.
% Input: exp - Type of Experiement (0 - Step Force, 1 - Impulse),
%        run - run number.
%%-----------------------------------------------------------------------%%
    % Read Run Information
    run_data = read_runfile_cam(exp);
    run_name = char(run_data{2}(run)); %Run identifier
    fps = run_data{5}(run); %Frames per second
    pp10cm_x = run_data{13}(run); %Pixels per 10cm in x-direction
    pp10cm_y = run_data{12}(run); %Pixels per 10cm in y-direction
    shape = char(run_data{4}(run)); %Shape of ice floe
    per_clk = run_data{7}(run); %Percentage of ice mass or number of clicks
    % Read Run Data File
    if exp == 0
        folder_cam = 'FRC_cam\';
    else
        folder_cam = 'IMP_cam\';
```

```
end
fname = strcat(folder_cam, run_name,'_track.csv');
if exist(fname,'file') %Check if File Exists
    data = csvread(fname);
    [~,m] = size(data);
    num_pt = (m - 1)/2; % Number of Tracking points
    t = data(:,1);
    for pt = 1 : num_pt
        x(:,pt) = data(:,(pt.*2));
        y(:,pt) = data(:,(pt.*2)+1);
        x(:,pt) = interp_nan(x(:,pt),t); %linear interp of missing val.
        y(:,pt) = interp_nan(y(:,pt),t); %linear interp of missing val.
    end
    % Scale X,Y data
    ppm_x = pp10cm_x * 10; % Pixels per meter in x-direction
    x = x ./ ppm_x;
    ppm_y = pp10cm_y * 10; % Pixels per meter in y-direction
    y = y ./ ppm_y;
    % Calculate Center of Points (xc,yc)
    xc = sum(x,2)./num_pt;
    yc = sum(y,2)./num_pt;
    % Calculate Displacement
    for i = 1:length(xc)-1
        S(i) = sqrt((xc(i+1) - xc(1))^2 + (yc(i+1) - yc(1))^2);
```

```
        end
        t_cam = t;
        s_cam = [0 S]';
    else
        t_cam = [0:0.001:0.25]';
        s_cam = zeros(size(t_cam));
    end
end
```

```
function [t_acc,a_acc] = read_acc(exp,run)
%% Read Accelerometer Sensor Data-------------------------------------%%
% Author: Craig Martin
% Description: Reads the run information database as well as
% the accleration data file obtained from accelerometer. Accelerometer data
% is zeroed according to an average of obtained from the tare region.
% Input: exp - Type of Experiement (0 - Step Force, 1 - Impulse),
%        run - run number.
%%------------------------------------------------------------------------%%
    % Read Run Information
    run_data = read_runfile(exp);
    run_name = char(run_data{2}(run)); %Run identifier
    shape = char(run_data{4}(run)); %Shape of ice model
    m_ice = run_data{6}(run); %Mass of ice model
    per_clk = run_data{7}(run); %Percentage of ice mass or number of clicks
    sample = run_data{5}(run); %Sampling Rate of Sensor [Hz]
    tare_i = run_data{8}(run); %Start of tare region
    tare_f = run_data{9}(run); %End of tare region
    crop_i = run_data{10}(run); %Start of region to crop
    crop_f = run_data{11}(run); %End of region to crop
    % Read Run Data File
    if exp == 0
        folder_acc = 'FRC_acc\';
    else
```

```
        folder_acc = 'IMP_acc\';
    end
    fname = strcat(folder_acc, run_name,'.xlsx');
    if exist(fname,'file') %Check if File Exists
        data_acc = xlsread(fname);
        t_acc = data_acc(11:end,1);
        a_acc = data_acc(11:end,2);
        % Crop / Zero Data
        tare_val = mean(a_acc(tare_i:tare_f));
        a_acc = a_acc(crop_i:crop_f) - tare_val;
        t_acc = t_acc(crop_i:crop_f) - t_acc(crop_i);
        a_acc = a_acc .* 9.80665;
    else
        t_acc = [0:0.001:0.25]';
        a_acc = zeros(size(t_acc));
    end
end
```

```
function [kin_raw,kin_filt] = cam_kin(t,s,exp)
%% Kinematic Calculations for High Speed Camera Data-------------------%%
% Author: Craig Martin
% Description: Calculates velocity and acceleration from high speed
%  postion data using the central difference method to calculate the
%  gradient. Calculations are performed for raw data and
%  data filtered using a polynomial fit.
% Input: t - time series, a - acceleration series, exp - Type of
%  Experiement (0 - Step Force, 1 - Impulse).
%%-------------------------------------------------------------------%%
    % Raw Data
    v = gradient(s,t);
    a = gradient(v,t);

    % Butterworth Filter
    if exp == 0         % Step Force Filter Parameters
        Wp = 10/fps/2;      % Passband (Cutoff) Freq.
        Ws = 15/fps/2;      % Stopband Corner Freq.
        Rp = 0.1;           % Passband Ripple [dB]
        Rs = 1;             % Stopband attenuation [dB]
    else                % Impulse Filter Parameters
        Wp = 100/fps/2;     % Passband (Cutoff) Freq.
        Ws = 120/fps/2;     % Stopband Corner Freq.
        Rp = 0.01;          % Passband Ripple [dB]
```

```
        Rs = 0.05;          % Stopband attenuation [dB]
    end
    [N,Wn] = buttord(Wp,Ws,Rp,Rs);  % Returns lowest order (N)
    [b,a]=butter(N,Wn,'low');       % Creates a lowpass Butterworth filter
        s_iir = filtfilt(b,a,S);
            % Zero-phase digital filtering by processing the input data,
            % in both the forward and reverse directions.
    v_iir = gradient(s_iir,t);
    a_iir = gradient(v_iir,t);

    %Output
    kin_raw = [t,s,v,a];
    kin_filt = [t,s_iir,v_iir,a_iir];

    kin_raw = kin_raw(idx:end,:);
    kin_filt = kin_filt(idx:end,:);
end
```

```
function [kin_raw,kin_filt] = acc_kin(t,a,exp)
%% Kinematic Calculations for Accelerometer Data ----------------------%%
% Author: Craig Martin
% Description: Calculates displacement and velocity from acceleration data
% using the trapazoidal method. Calculations are performed for raw data and
% data filtered using a polynomial fit.
% Input: t - time series, a - acceleration series, exp - Type of
% Experiement (0 - Step Force, 1 - Impulse).
%%-------------------------------------------------------------------------%%
    %% Curve Fitting
    % Fit Parameters
    if exp == 0 %FRC
        pwr = 1-10^-4;
    else
        pwr = 1-10^-9;
    end
    % Smoothing Spline
    [curve,~,~] = fit(t, a,'smoothingspline','SmoothingParam', pwr);
    a_spl = curve(t);

    %% Integration
    for n = 1 : length(t)
        v(n,1) =  trapz(t(1:n), a(1:n), 1);
        v_spl(n,1) =  trapz(t(1:n), a_spl(1:n), 1);
```

```
    end
    for n = 1 : length(t)
        s(n,1) =  trapz(t(1:n), v(1:n), 1);
        s_spl(n,1) =  trapz(t(1:n), v_spl(1:n), 1);
    end
    kin_raw = [t,s,v,a];
    kin_filt = [t,s_spl,v_spl,a_spl];
end
```

```
function [A] = interp_nan(A,B)
%% Interpolate NaN ------------------------------------------------------%%
% Author: Craig Martin
% Description: Finds cells that do not contain a number (nan) in A and
% performs linear interpolation with respect to B.
%%-------------------------------------------------------------------------%%
    A_nan = isnan(A);
    if sum(A_nan) > 0
        A(A_nan) = interp1(B(~A_nan),A(~A_nan),B(A_nan));
    end
end
```

Appendix C

Kinematic Plots for Step Force Experiment

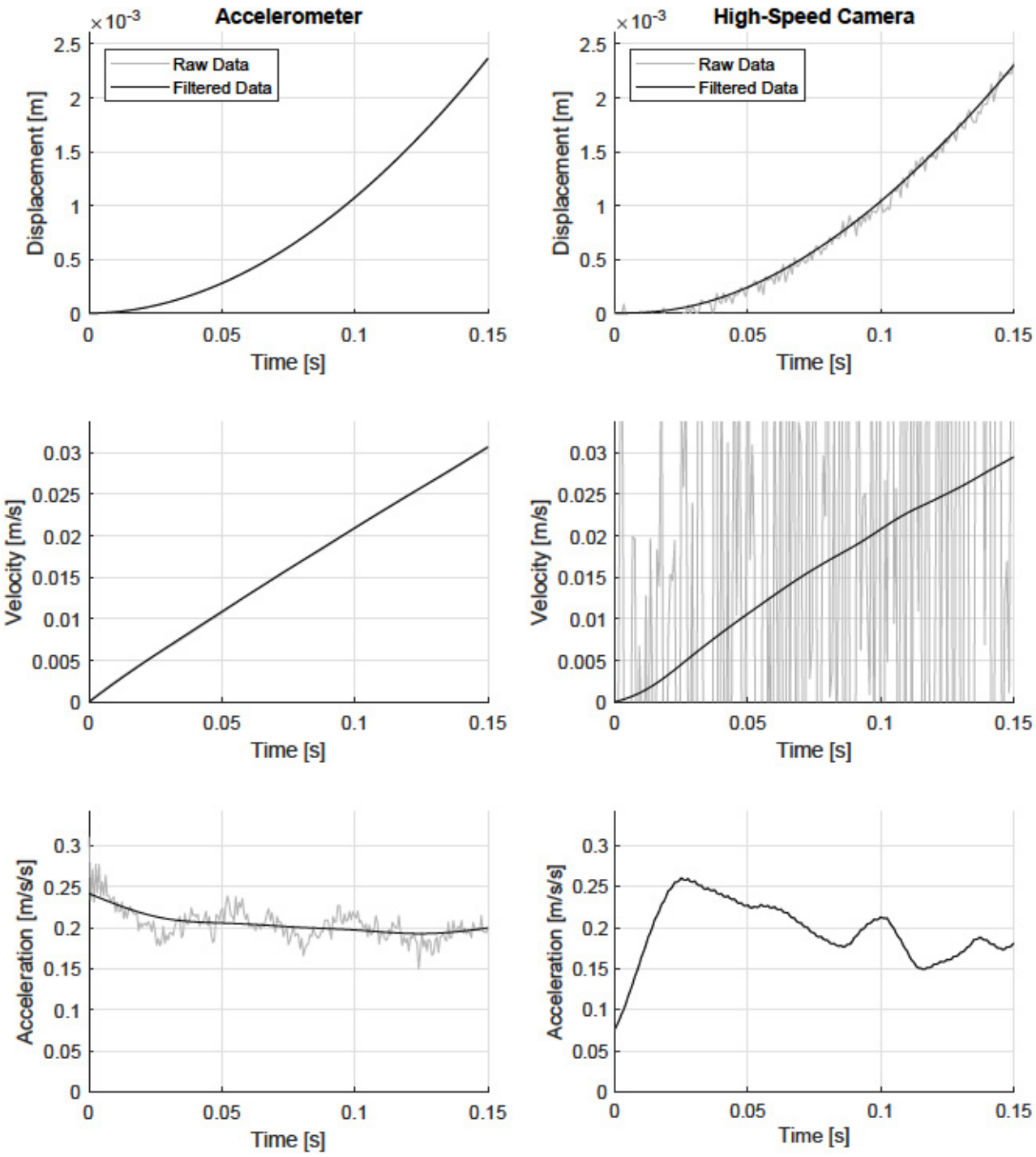

Figure C.1: Step-Force Kinematics of a Disk: 3% of Ice Mass (Run 1)

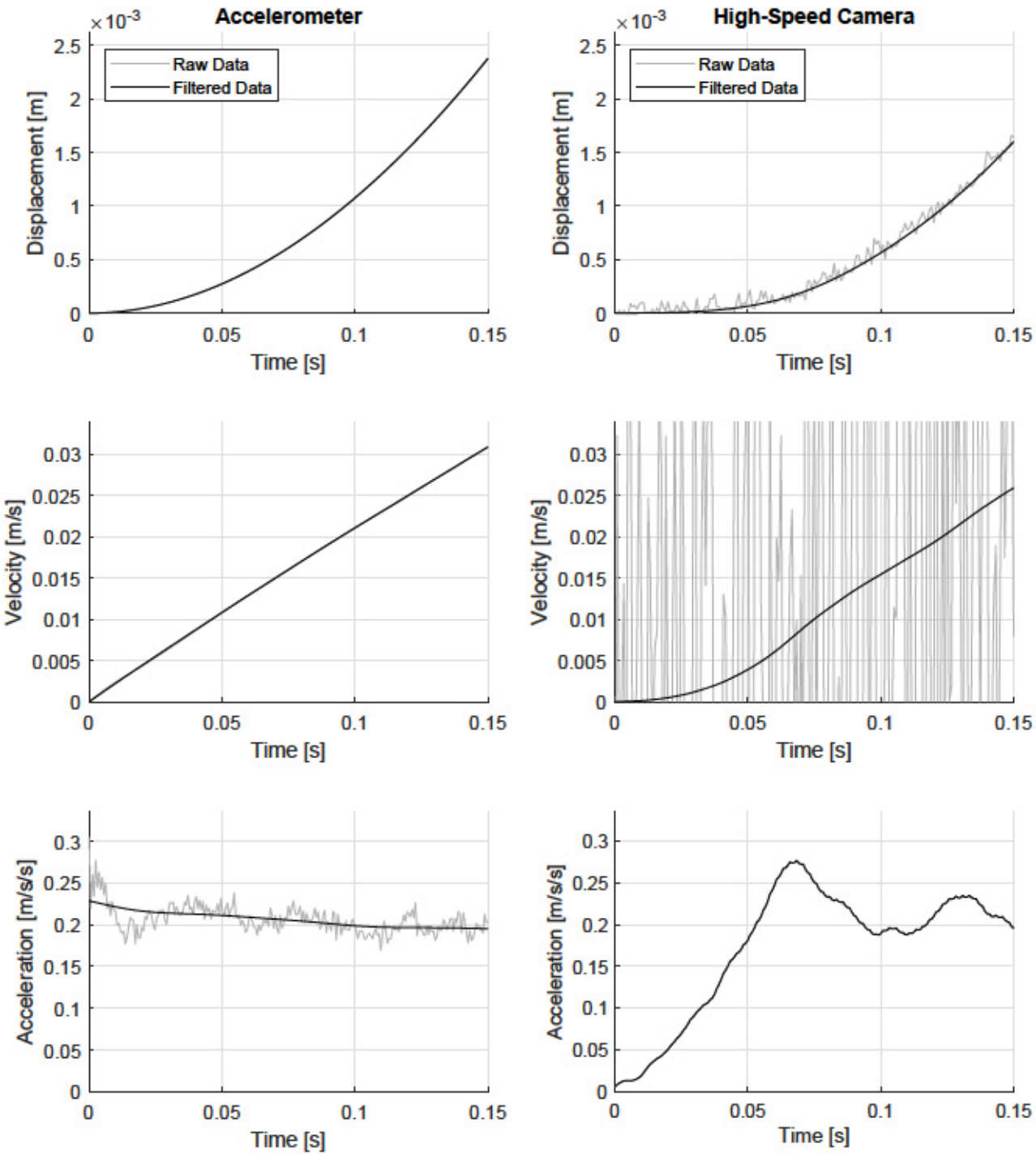

Figure C.2: Step-Force Kinematics of a Disk: 3% of Ice Mass (Run 2)

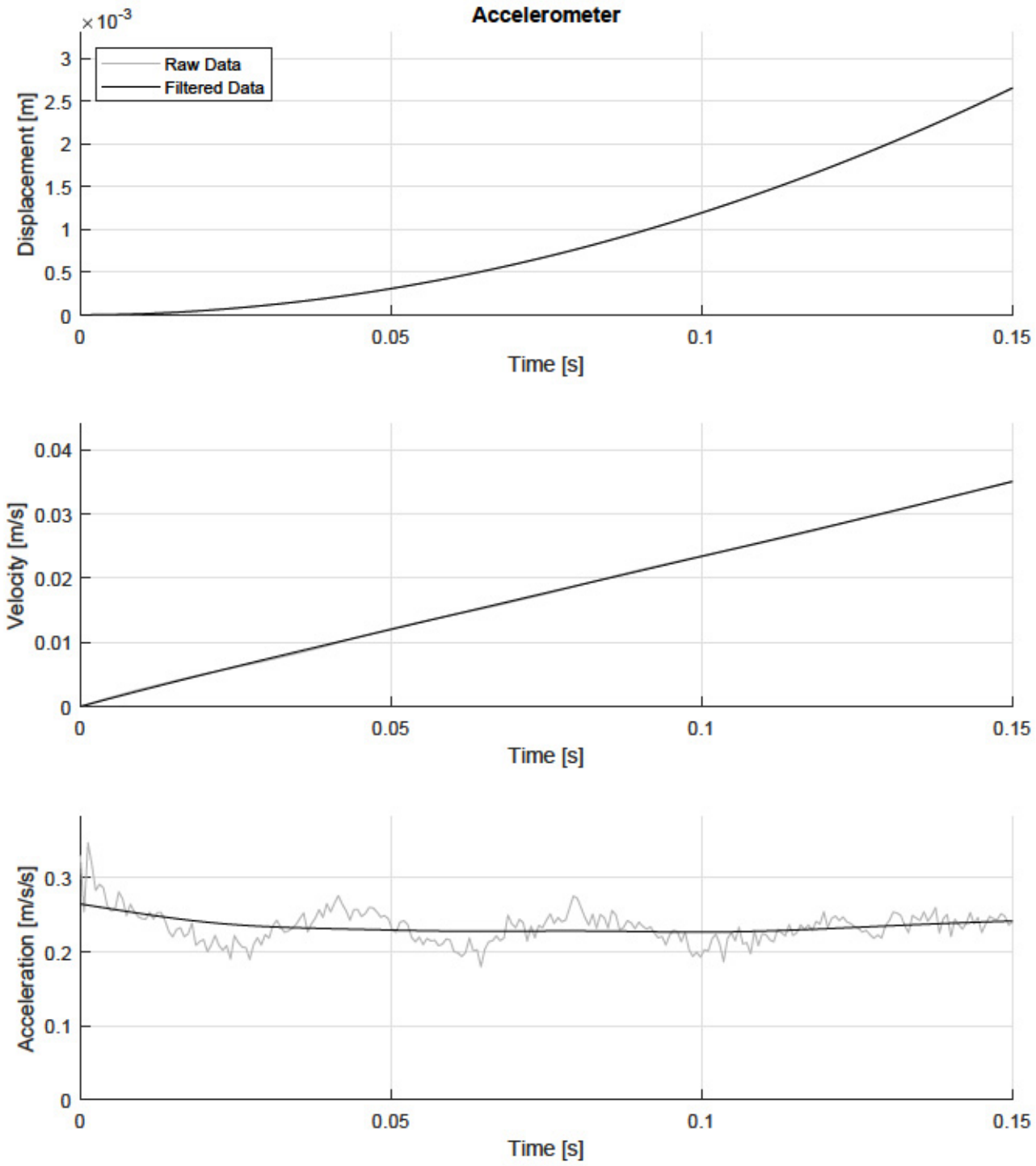

Figure C.3: Step-Force Kinematics of a Disk: 3% of Ice Mass (Run 3)

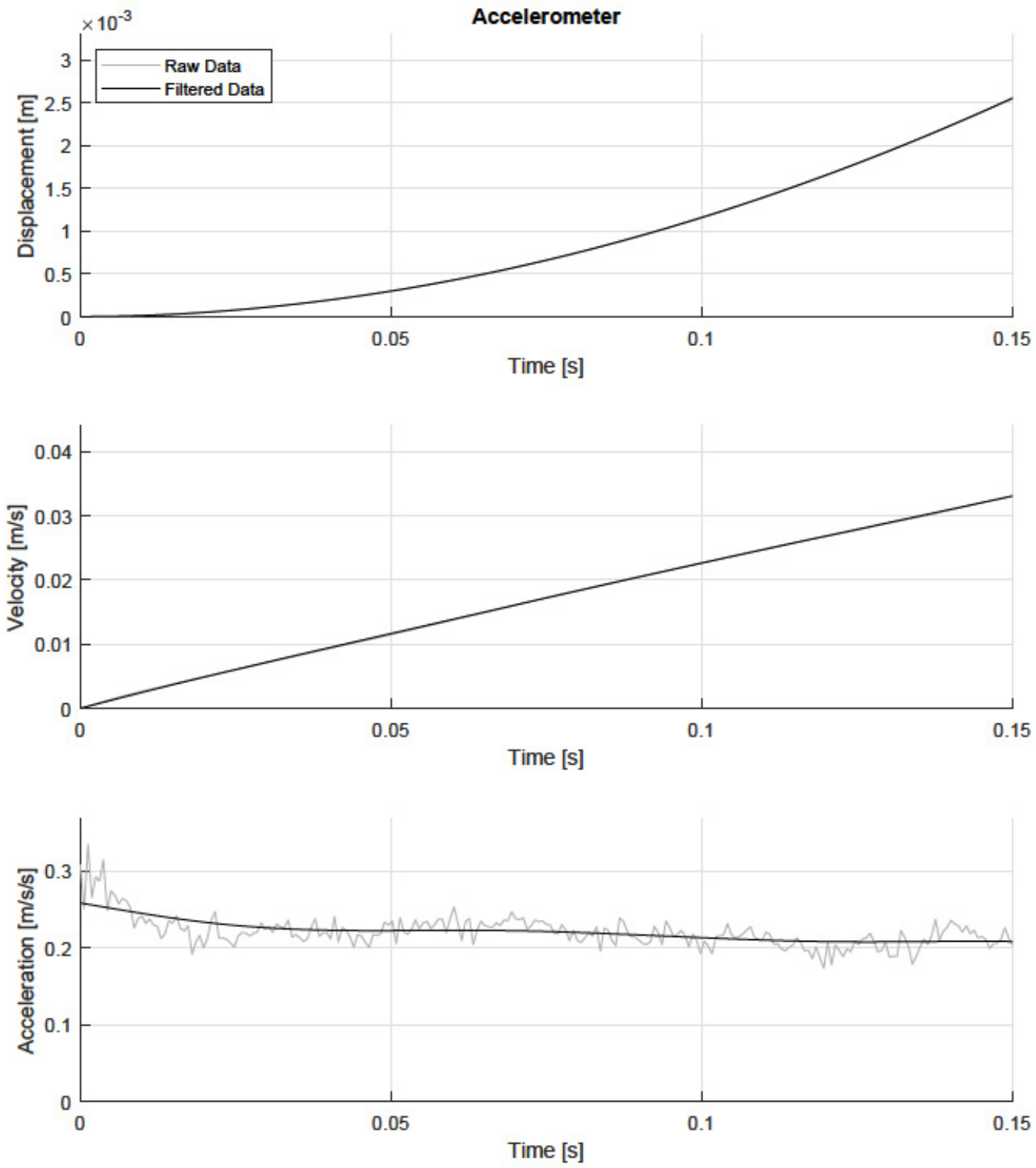

Figure C.4: Step-Force Kinematics of a Disk: 3% of Ice Mass (Run 4)

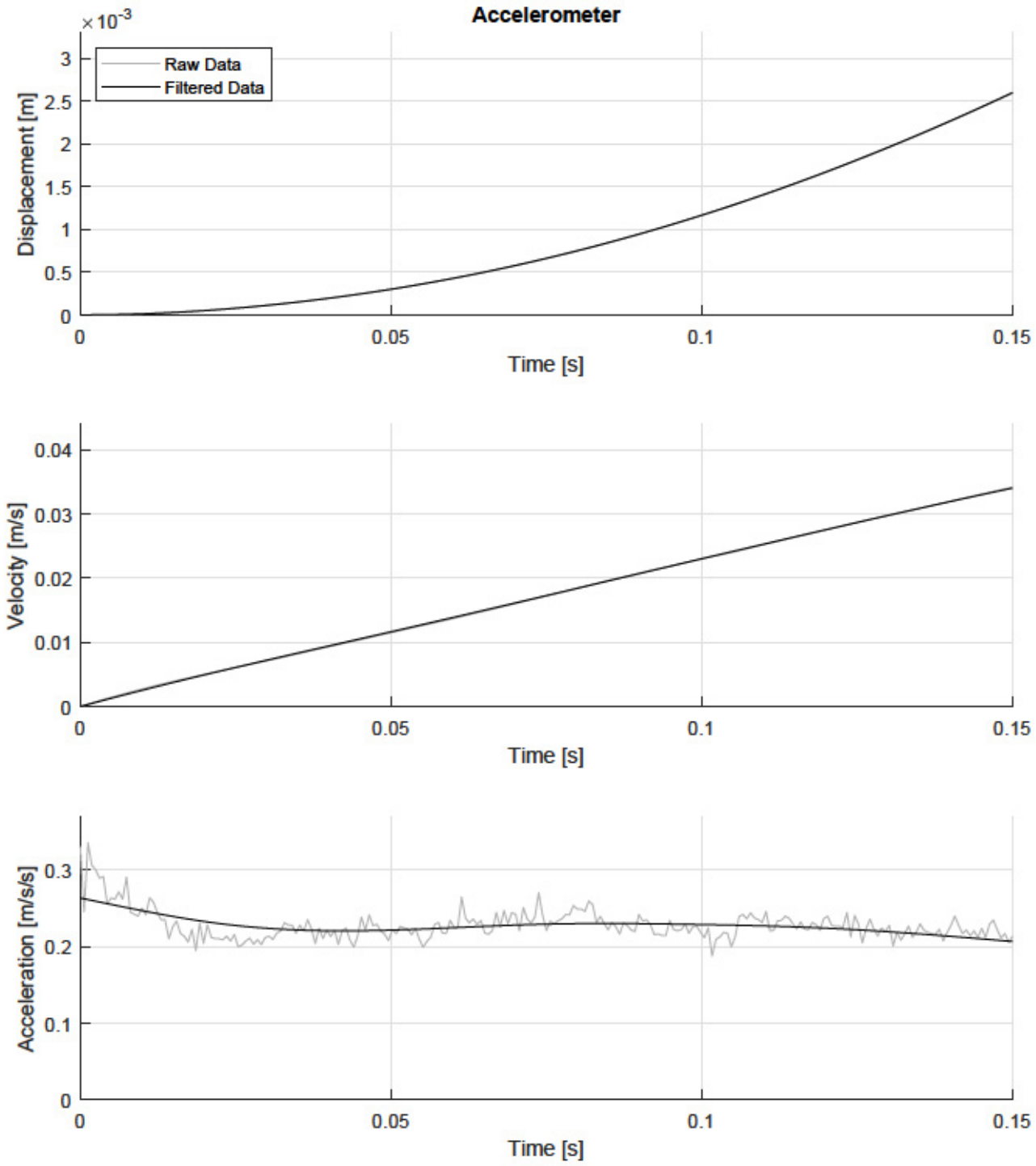

Figure C.5: Step-Force Kinematics of a Disk: 3% of Ice Mass (Run 5)

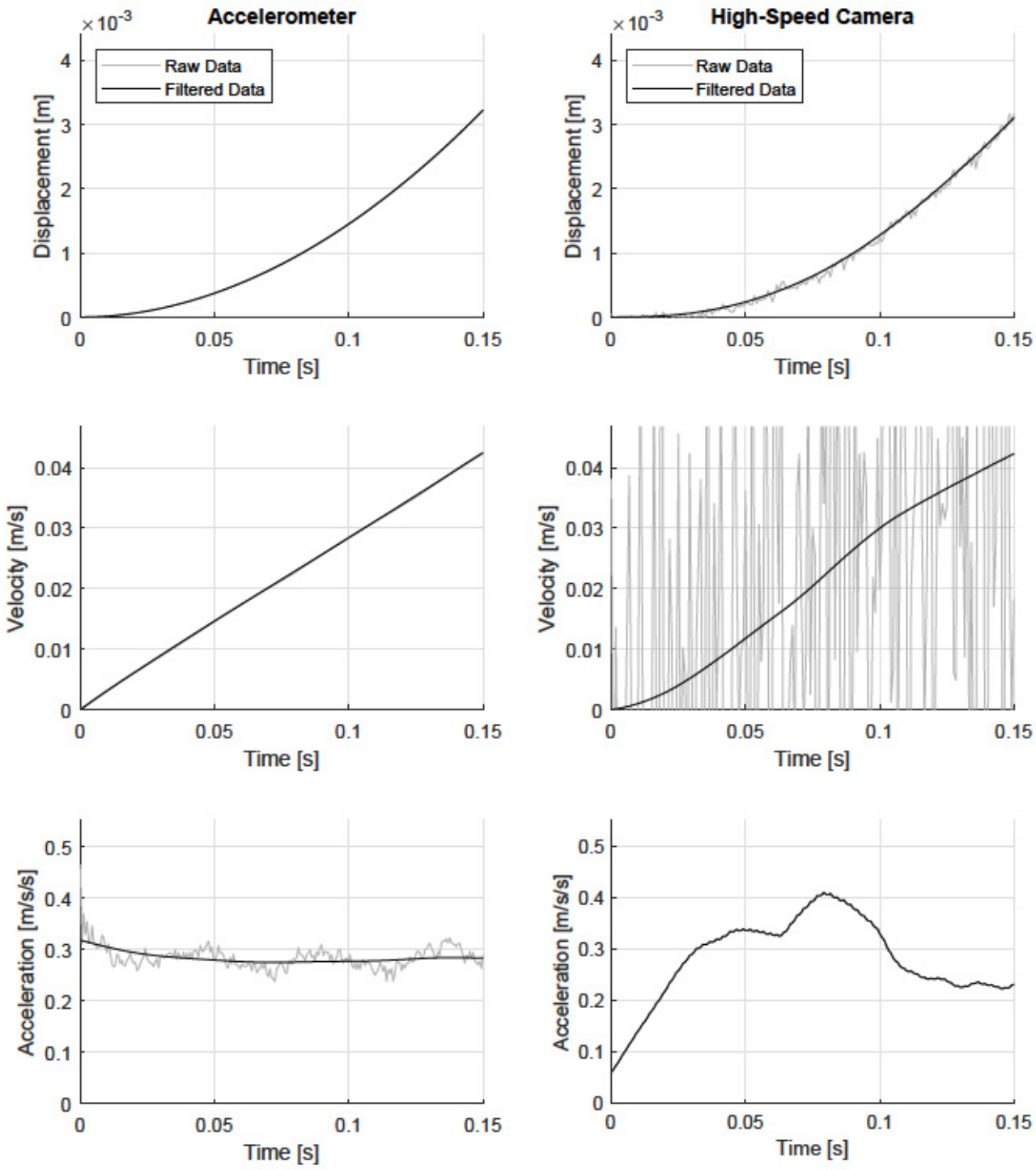

Figure C.6: Step-Force Kinematics of a Disk: 4% of Ice Mass (Run 1)

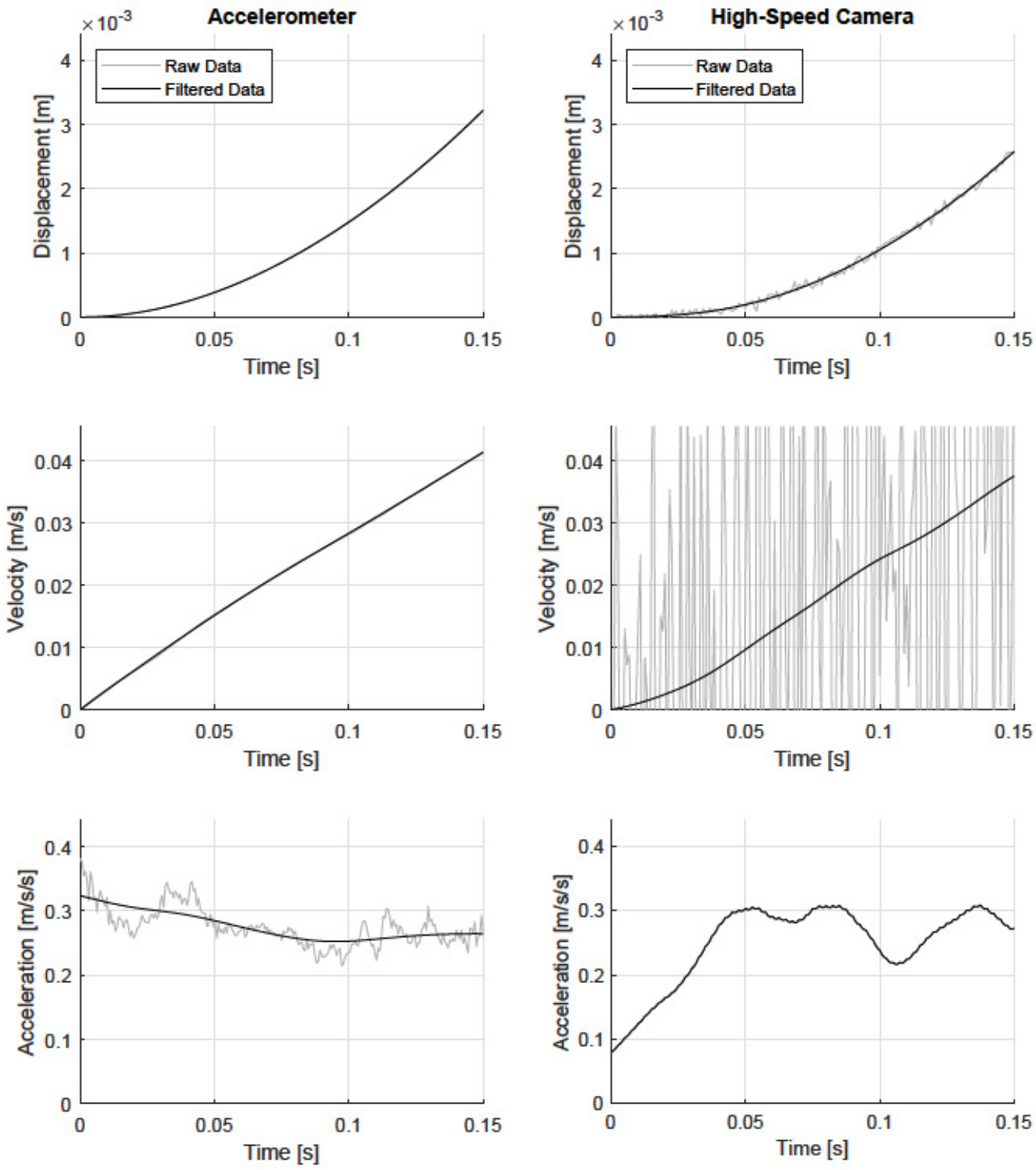

Figure C.7: Step-Force Kinematics of a Disk: 4% of Ice Mass (Run 2)

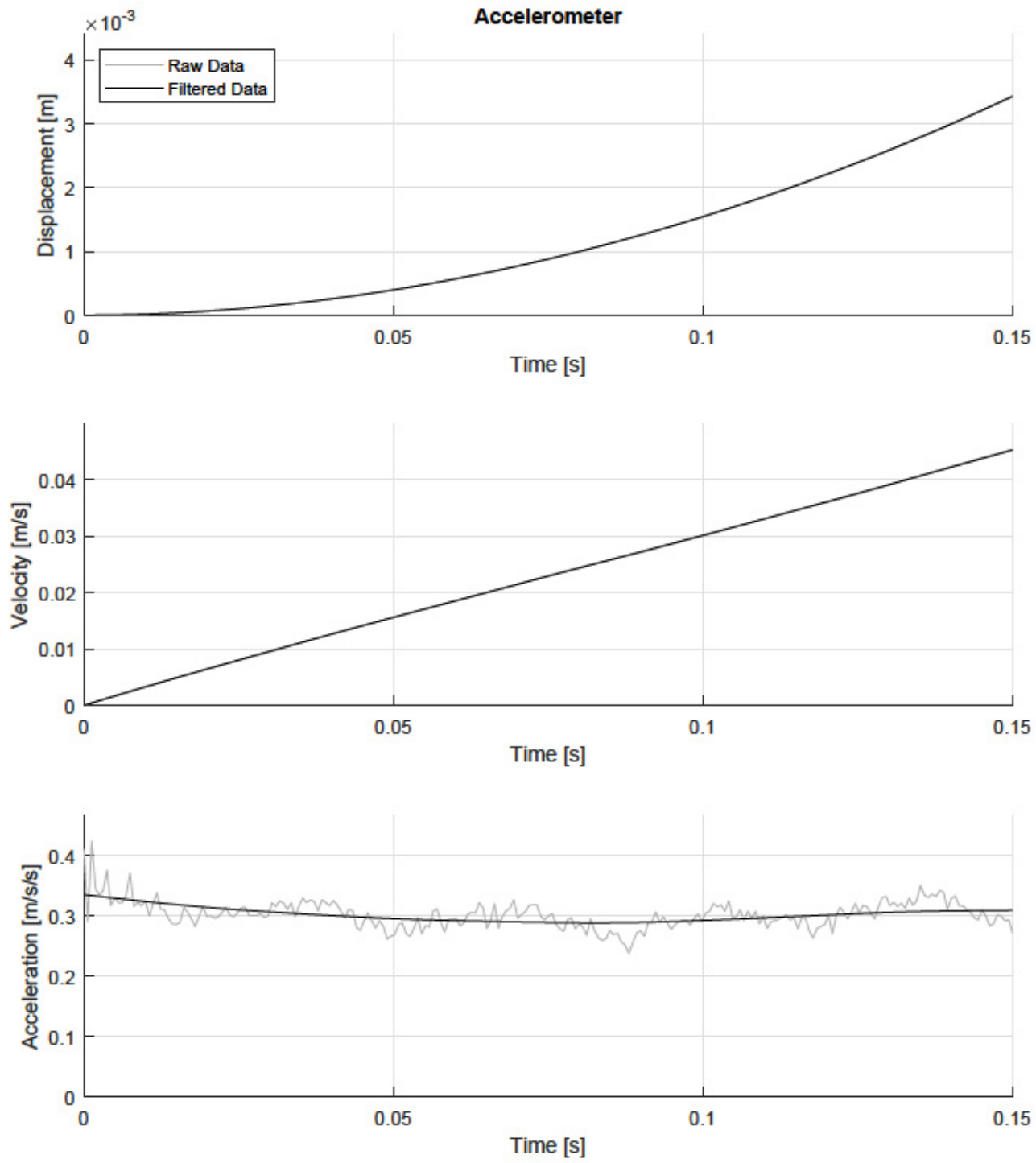

Figure C.8: Step-Force Kinematics of a Disk: 4% of Ice Mass (Run 3)

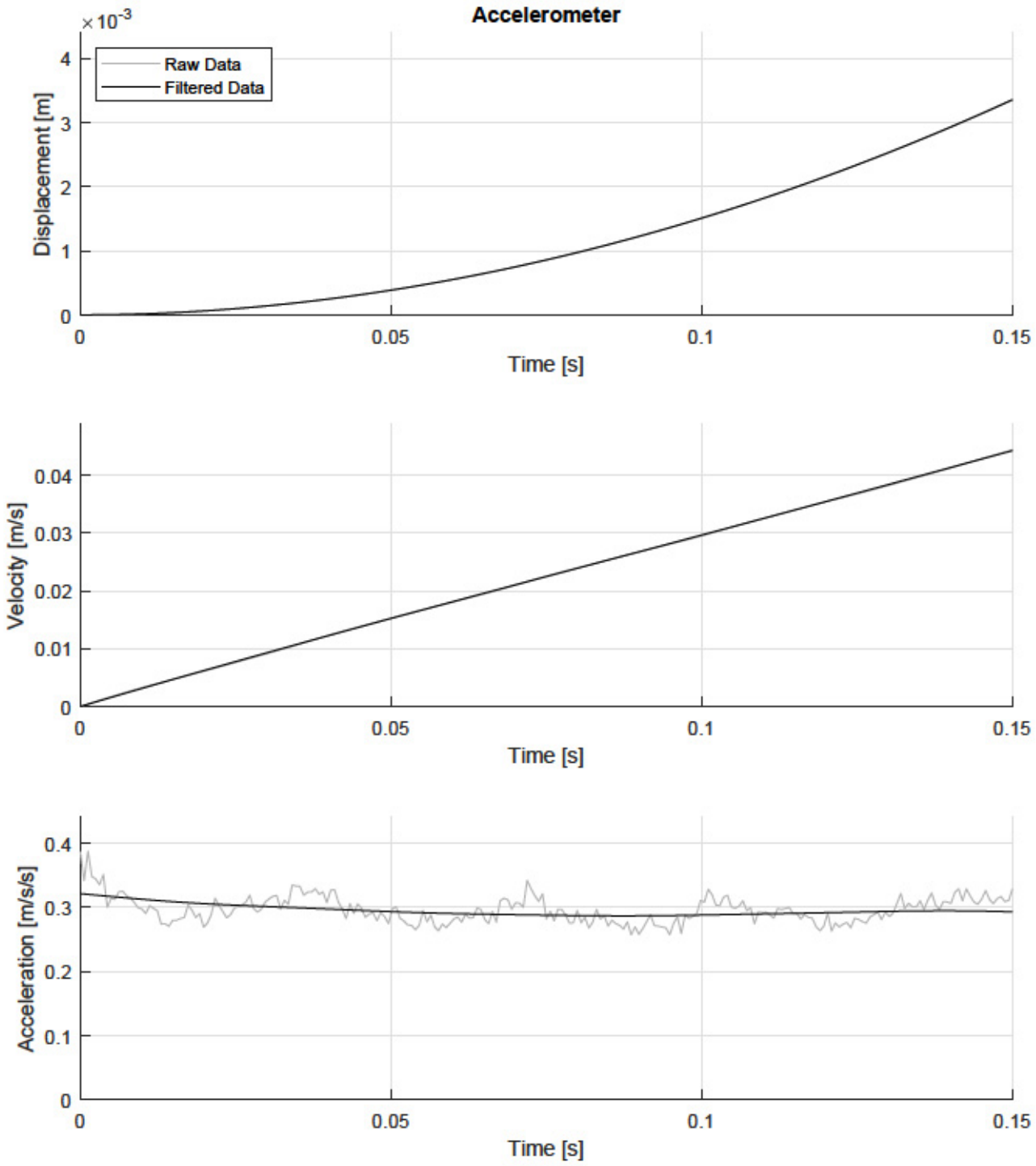

Figure C.9: Step-Force Kinematics of a Disk: 4% of Ice Mass (Run 4)

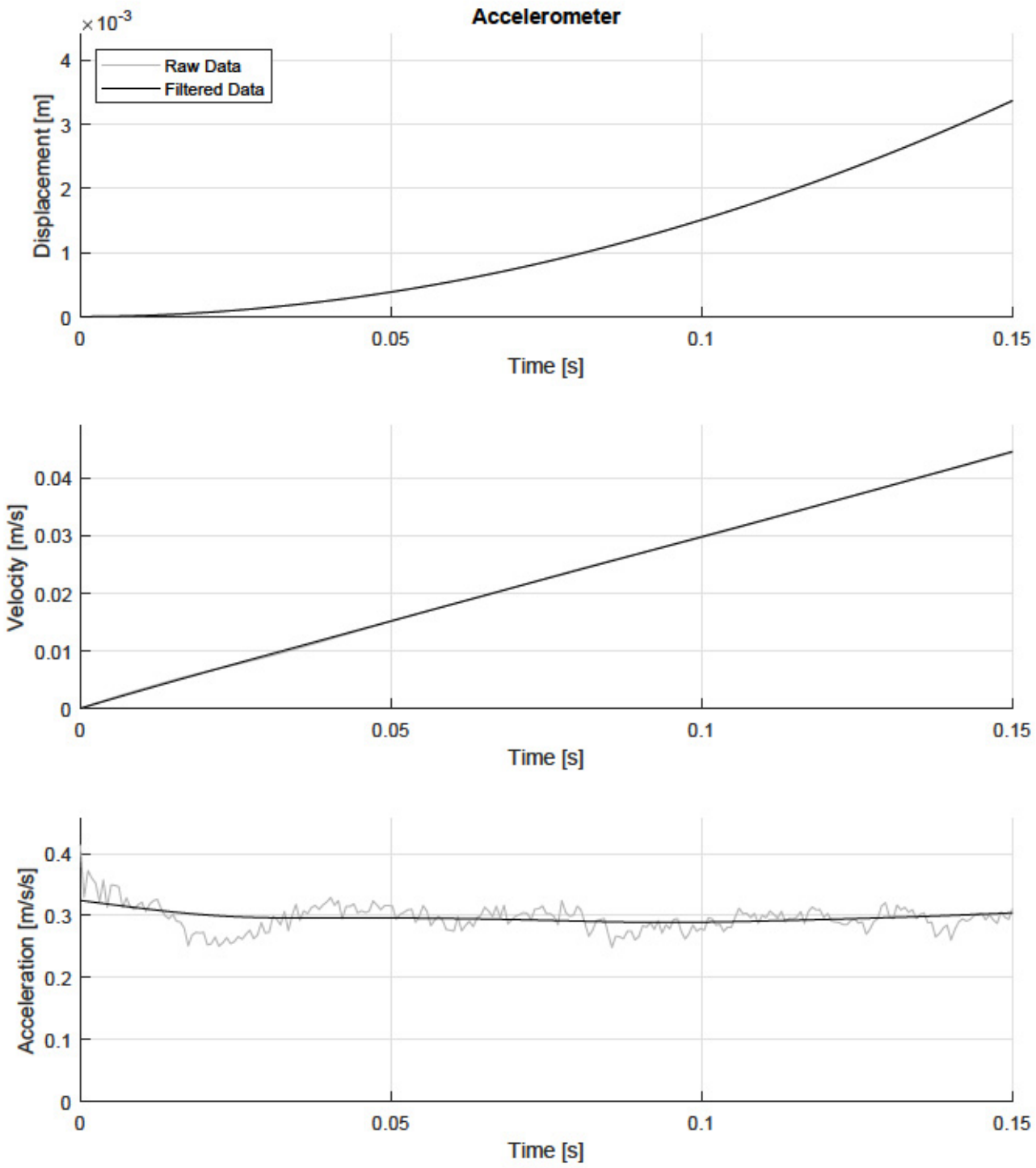

Figure C.10: Step-Force Kinematics of a Disk: 4% of Ice Mass (Run 5)

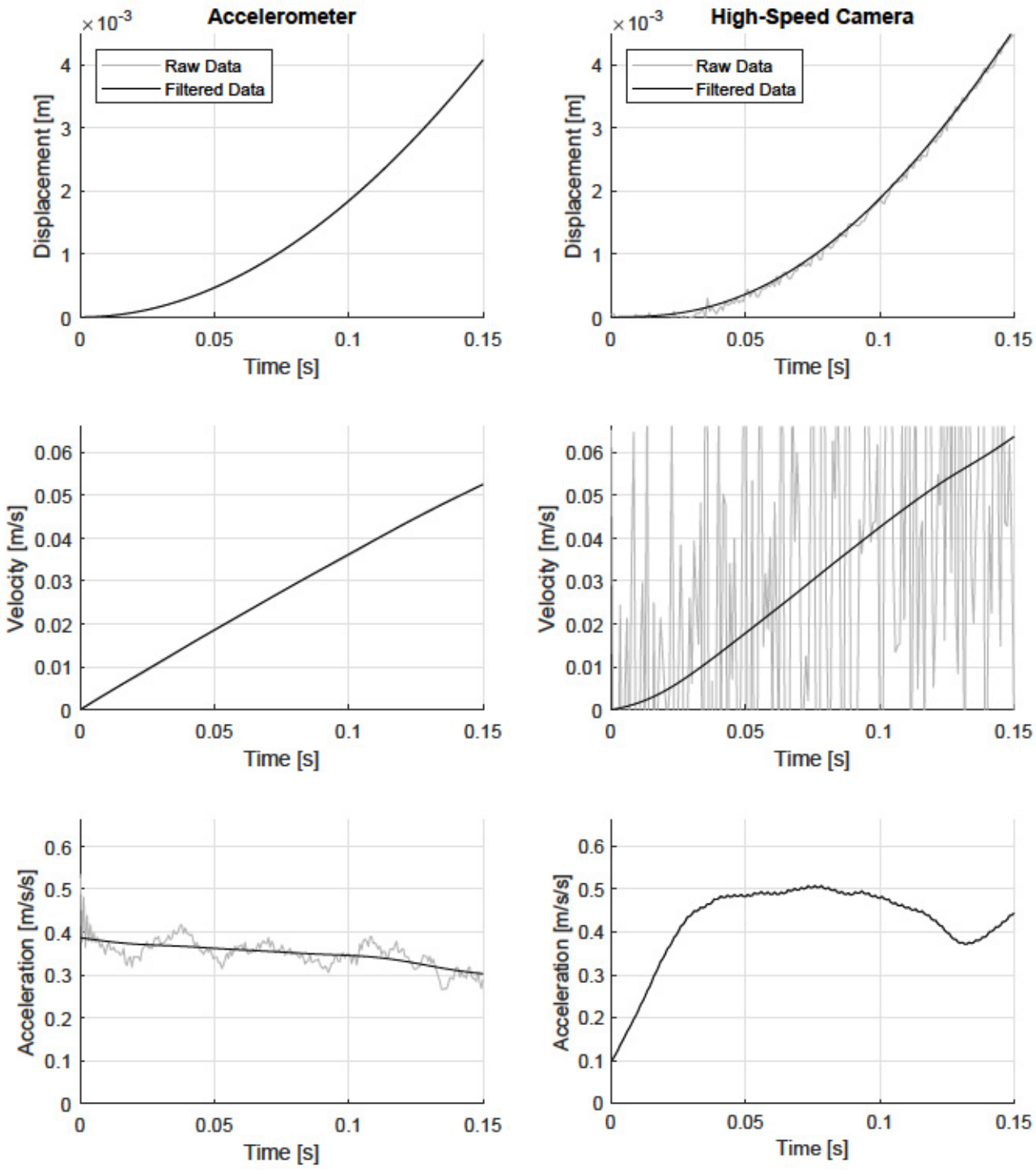

Figure C.11: Step-Force Kinematics of a Disk: 5% of Ice Mass (Run 1)

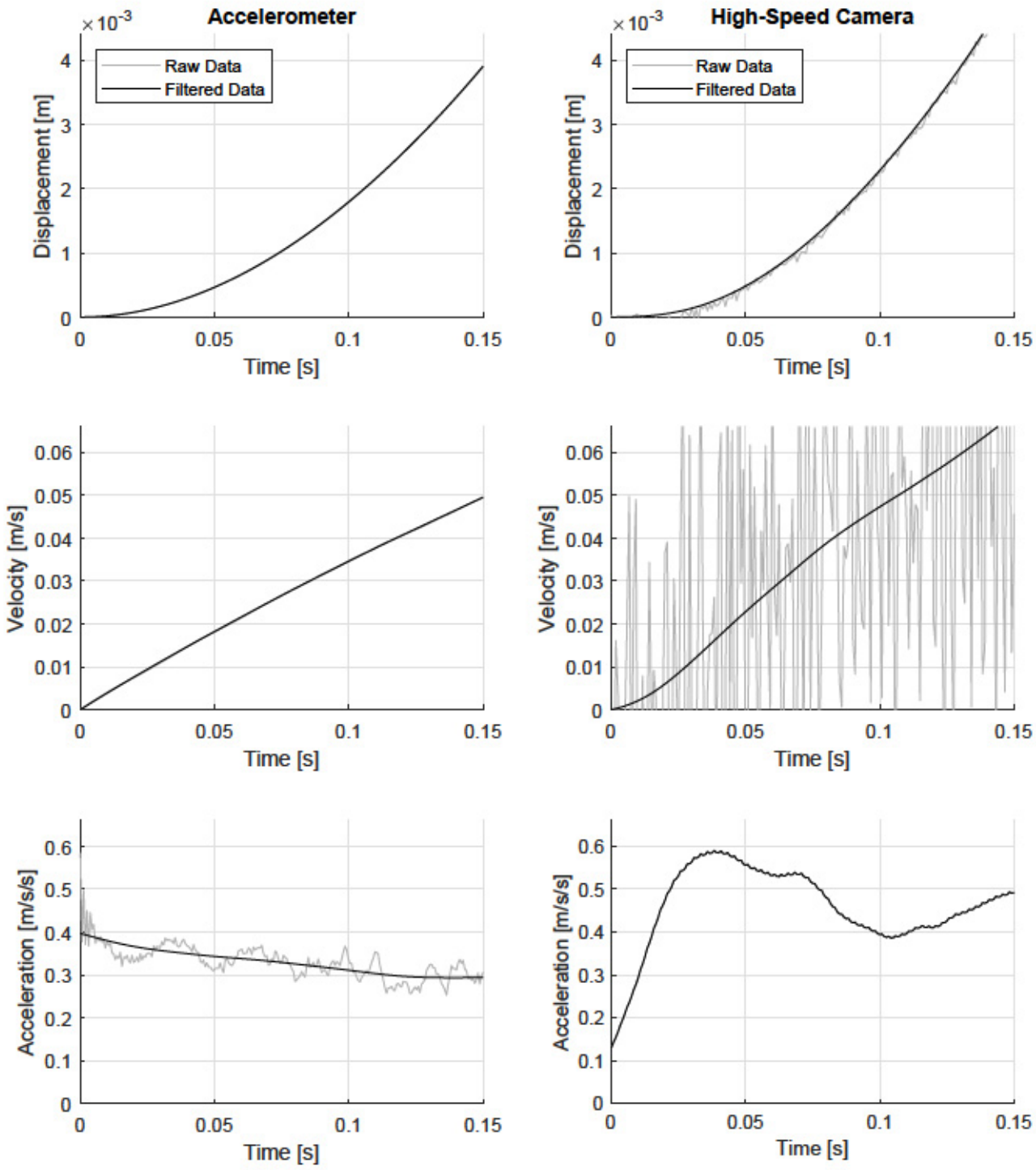

Figure C.12: Step-Force Kinematics of a Disk: 5% of Ice Mass (Run 2)

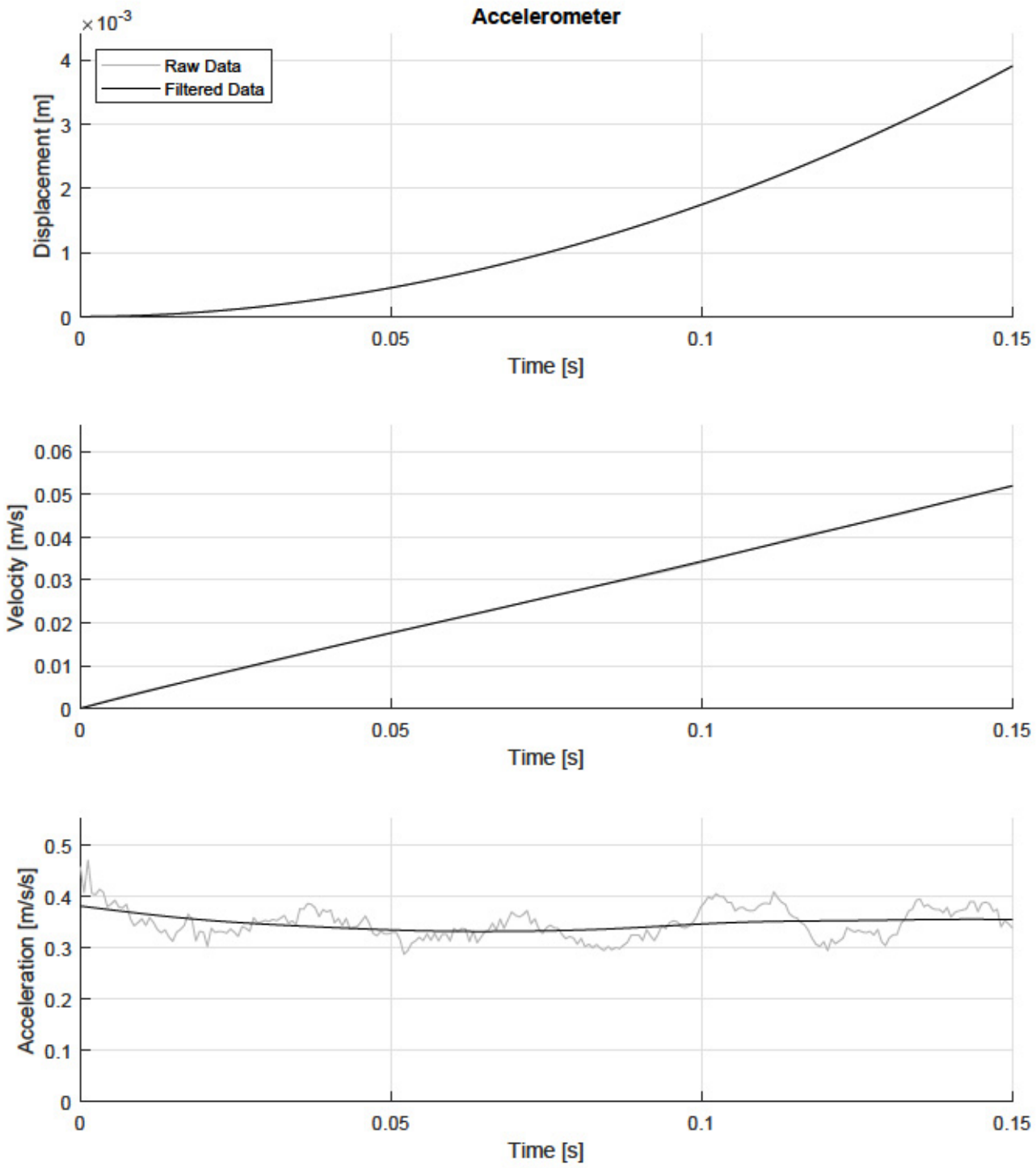

Figure C.13: Step-Force Kinematics of a Disk: 5% of Ice Mass (Run 3)

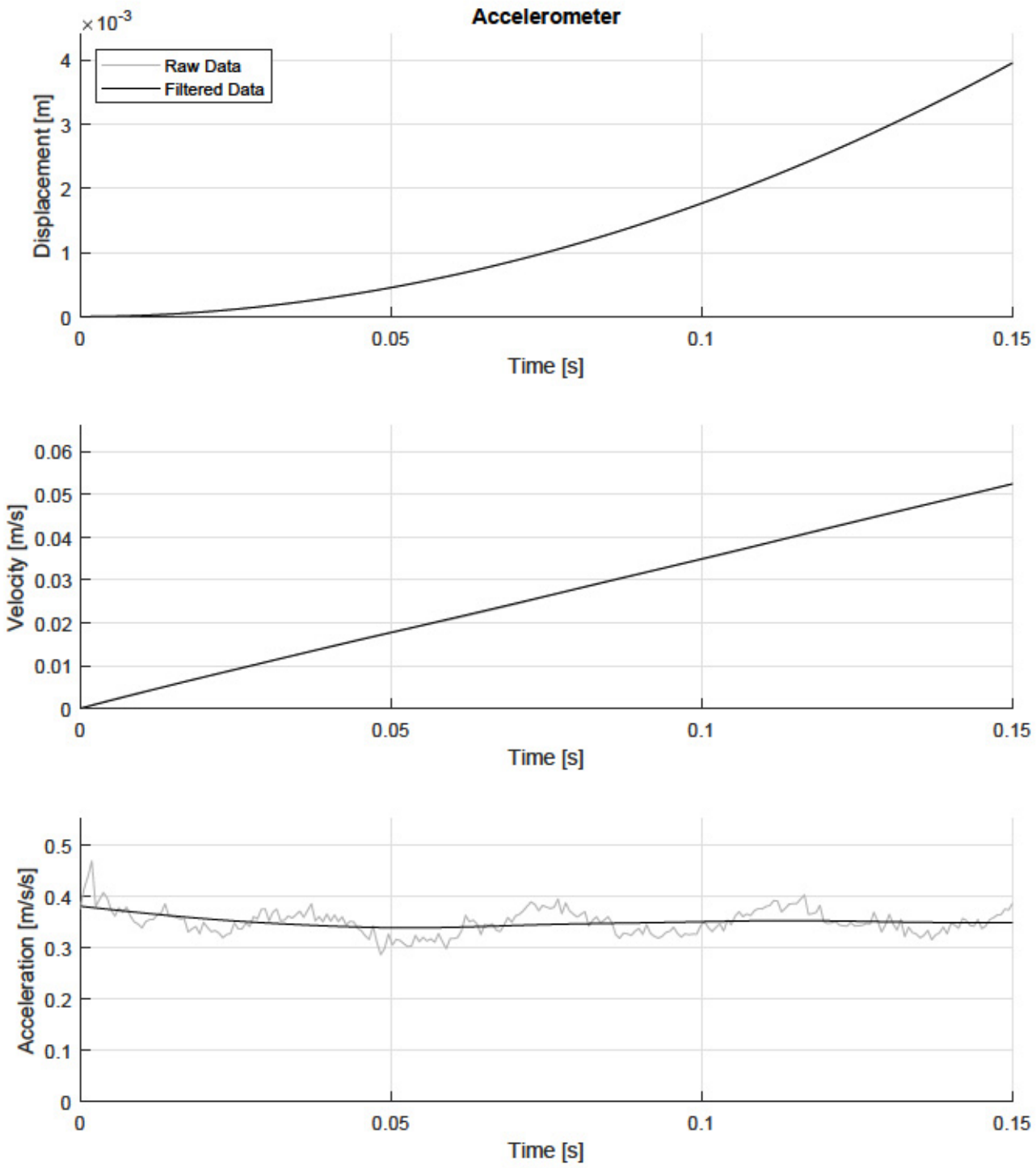

Figure C.14: Step-Force Kinematics of a Disk: 5% of Ice Mass (Run 4)

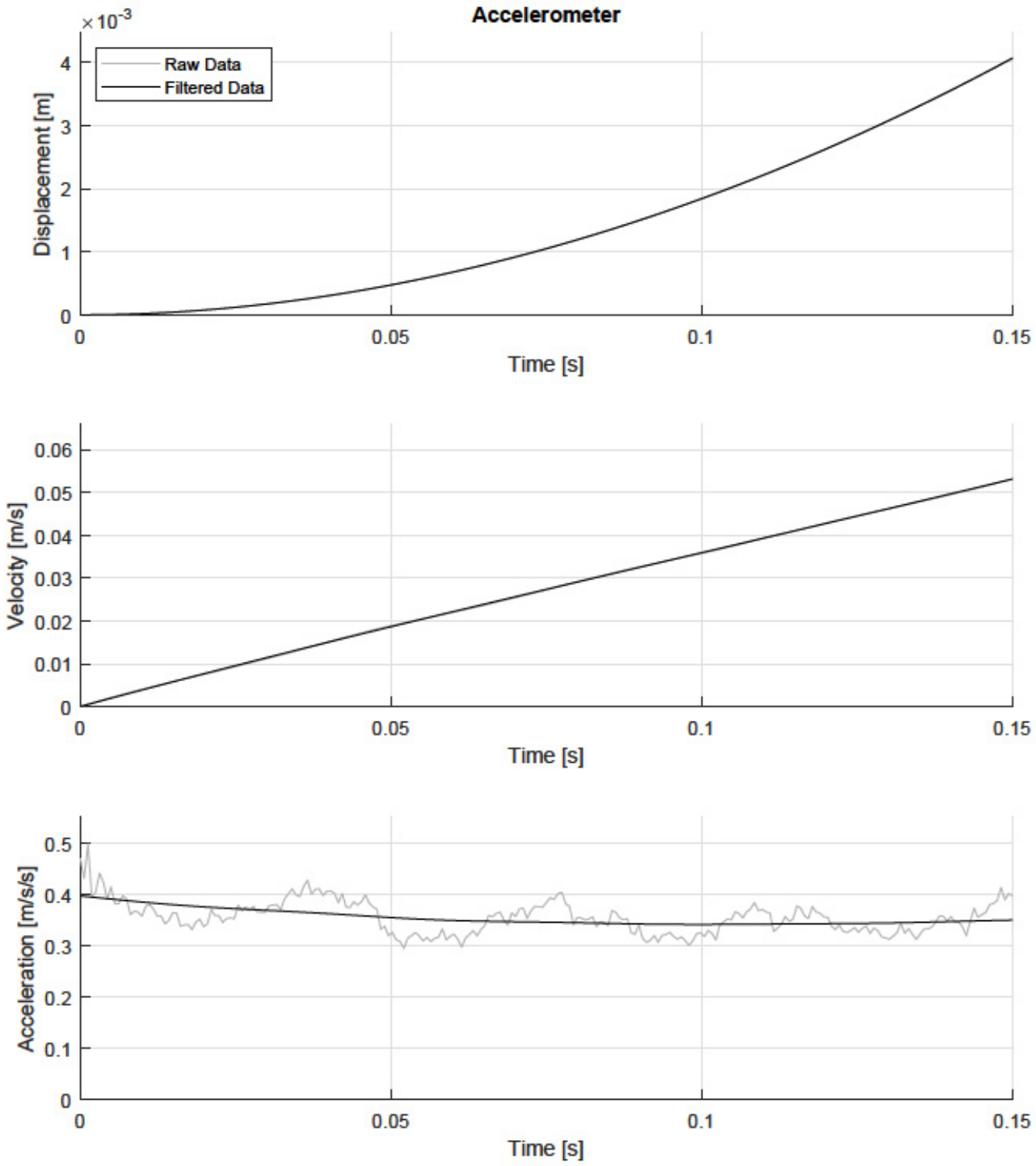

Figure C.15: Step-Force Kinematics of a Disk: 5% of Ice Mass (Run 5)

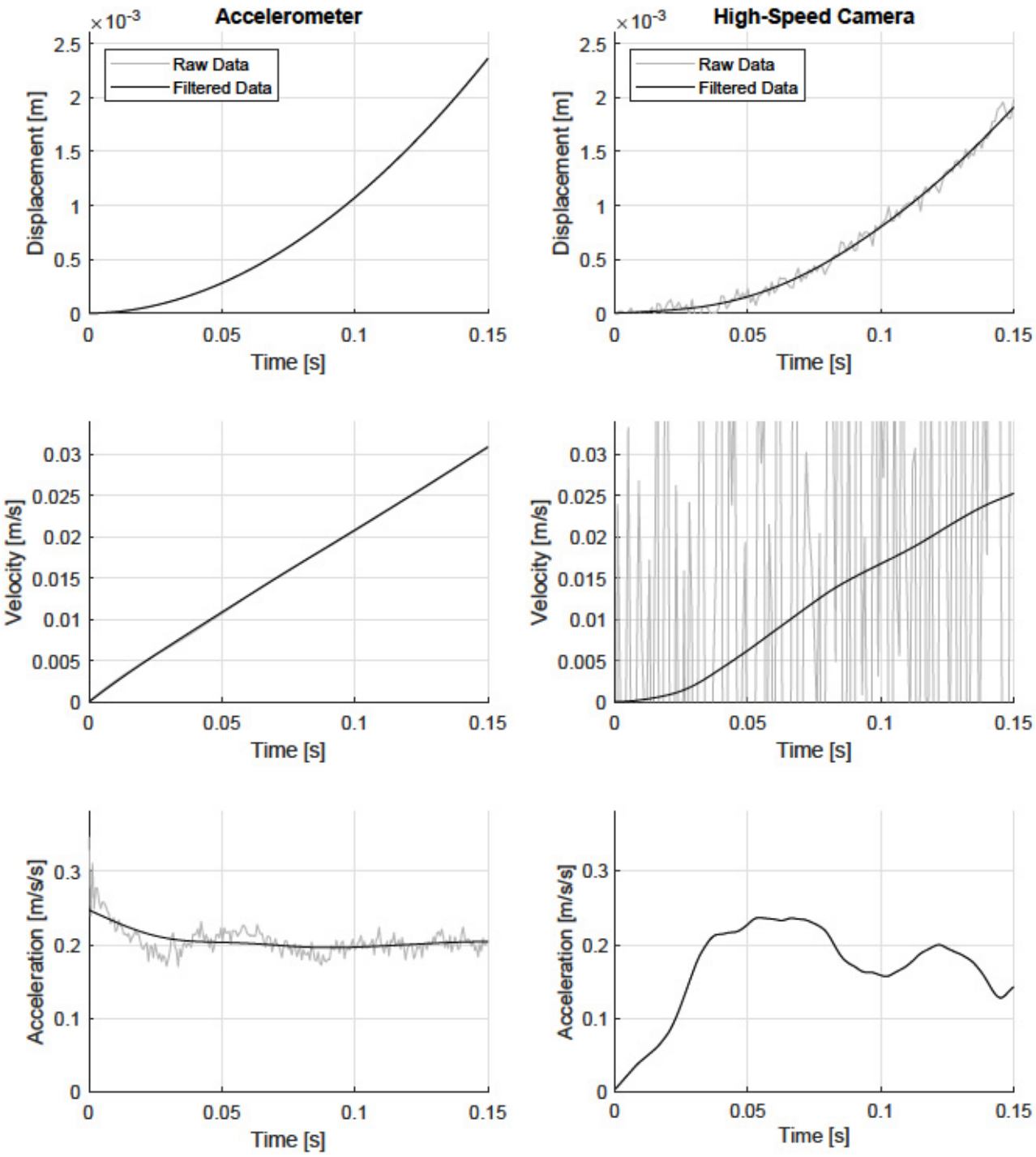

Figure C.16: Step-Force Kinematics of a 5-Sided Polygon: 3% of Ice Mass (Run 1)

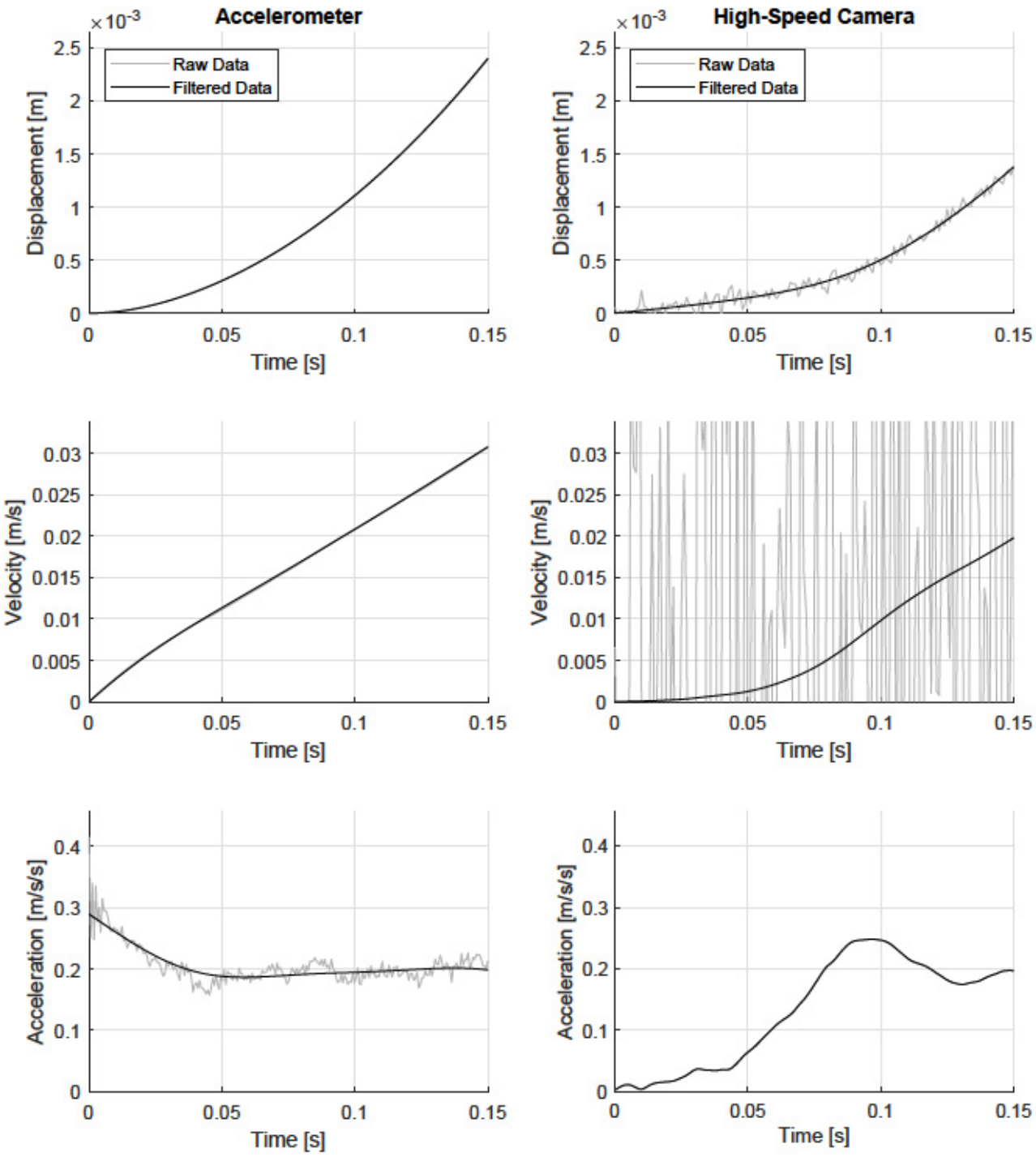

Figure C.17: Step-Force Kinematics of a 5-Sided Polygon: 3% of Ice Mass (Run 2)

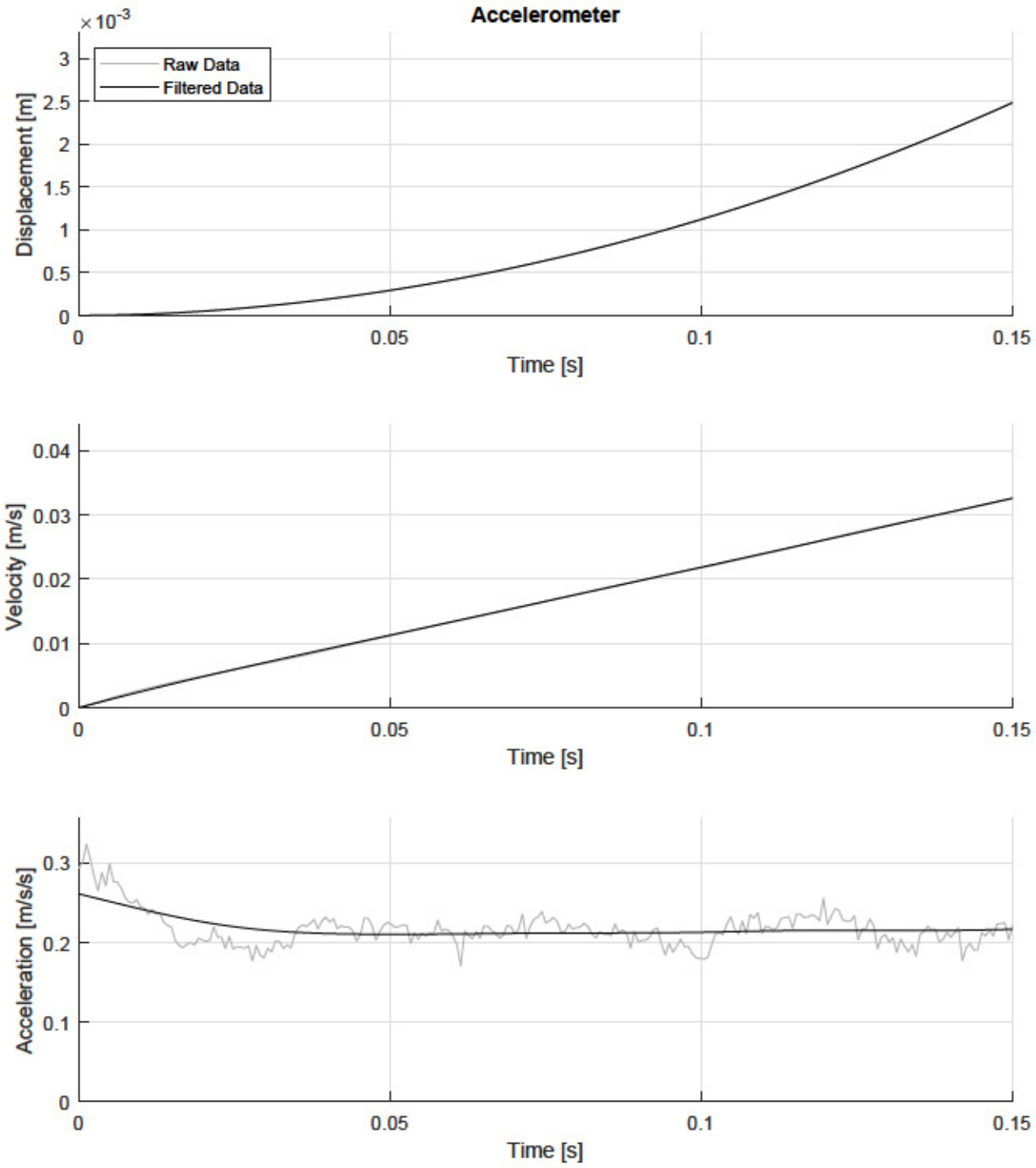

Figure C.18: Step-Force Kinematics of a 5-Sided Polygon: 3% of Ice Mass (Run 3)

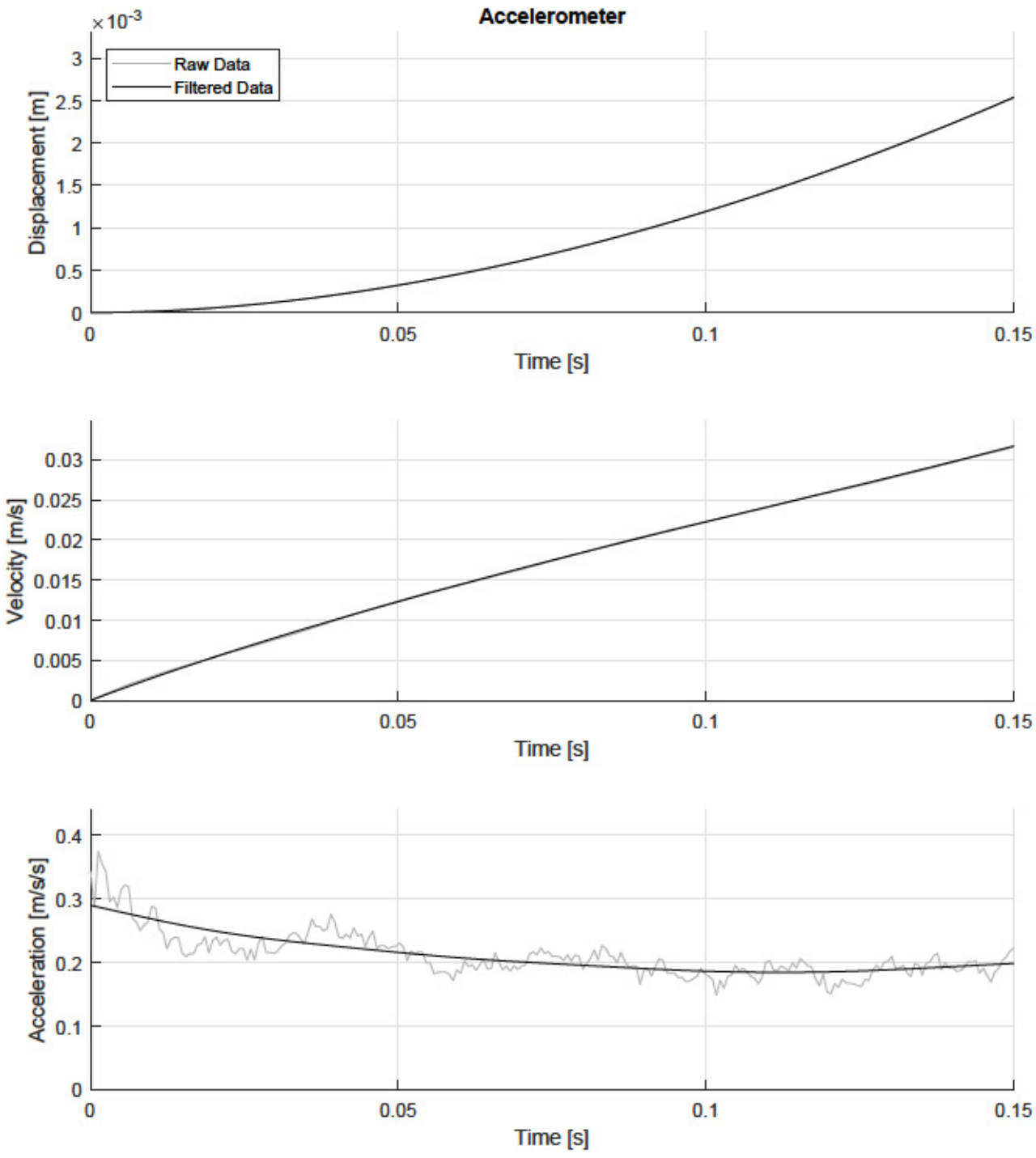

Figure C.19: Step-Force Kinematics of a 5-Sided Polygon: 3% of Ice Mass (Run 4)

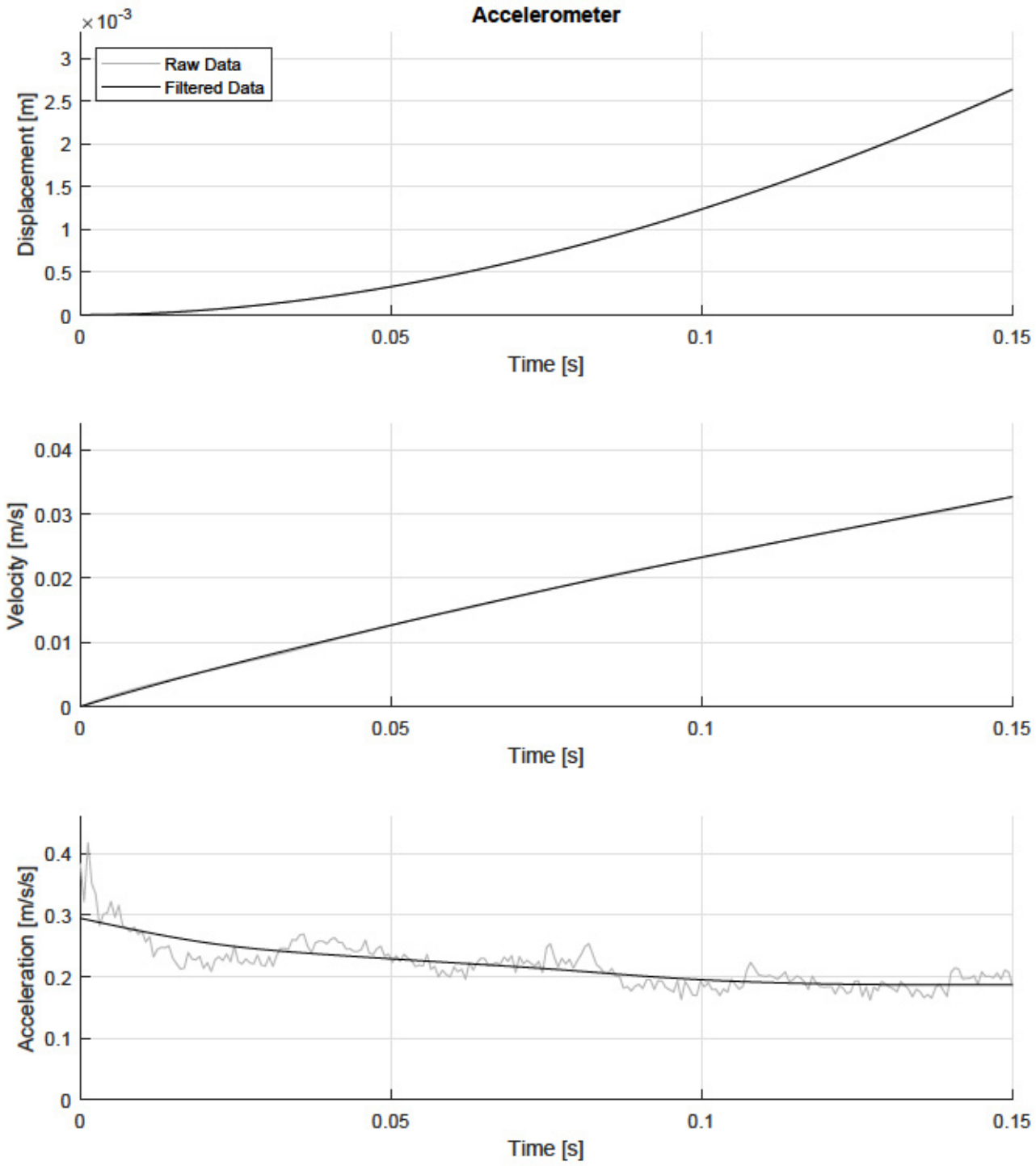

Figure C.20: Step-Force Kinematics of a 5-Sided Polygon: 3% of Ice Mass (Run 5)

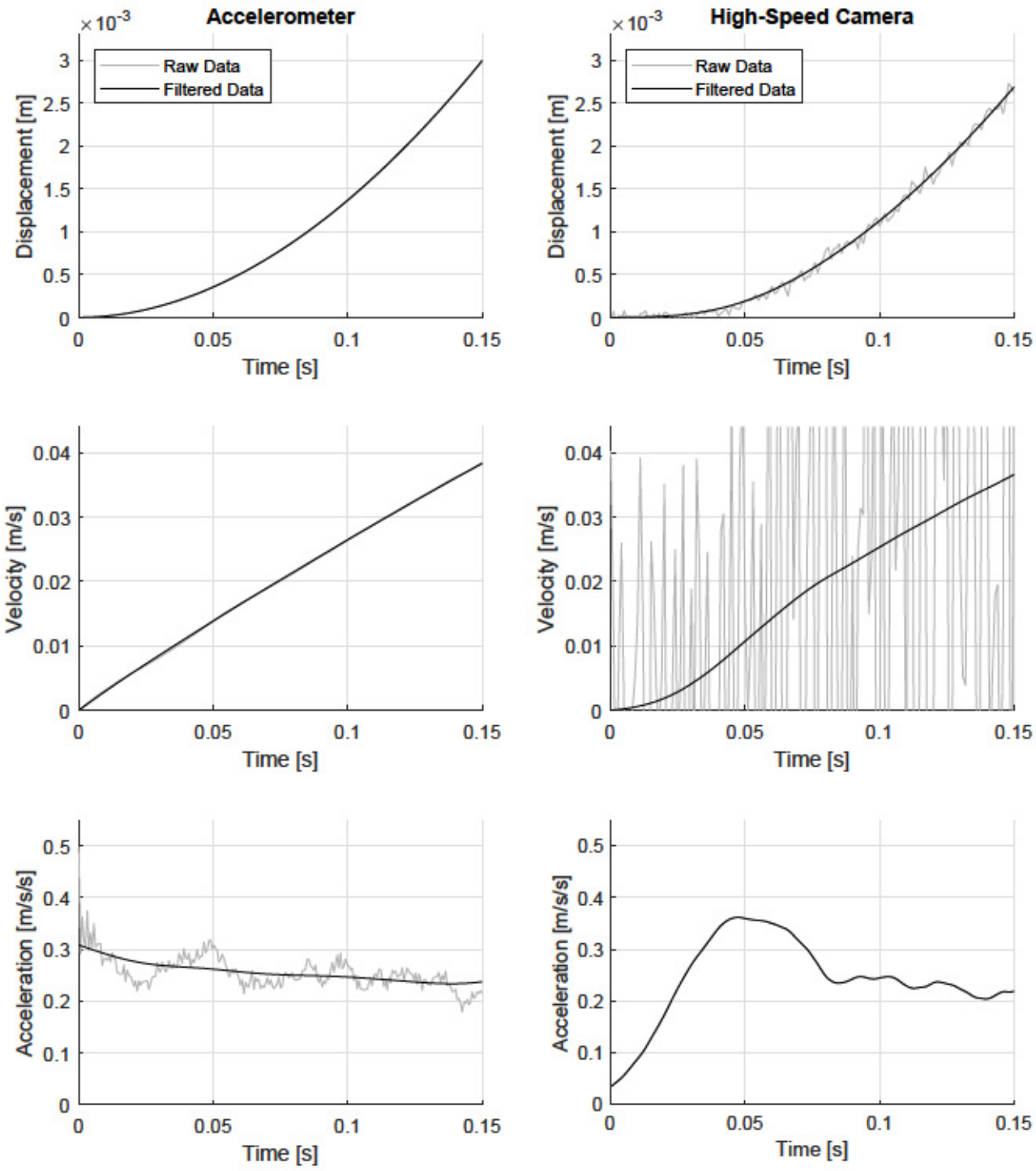

Figure C.21: Step-Force Kinematics of a 5-Sided Polygon: 4% of Ice Mass (Run 1)

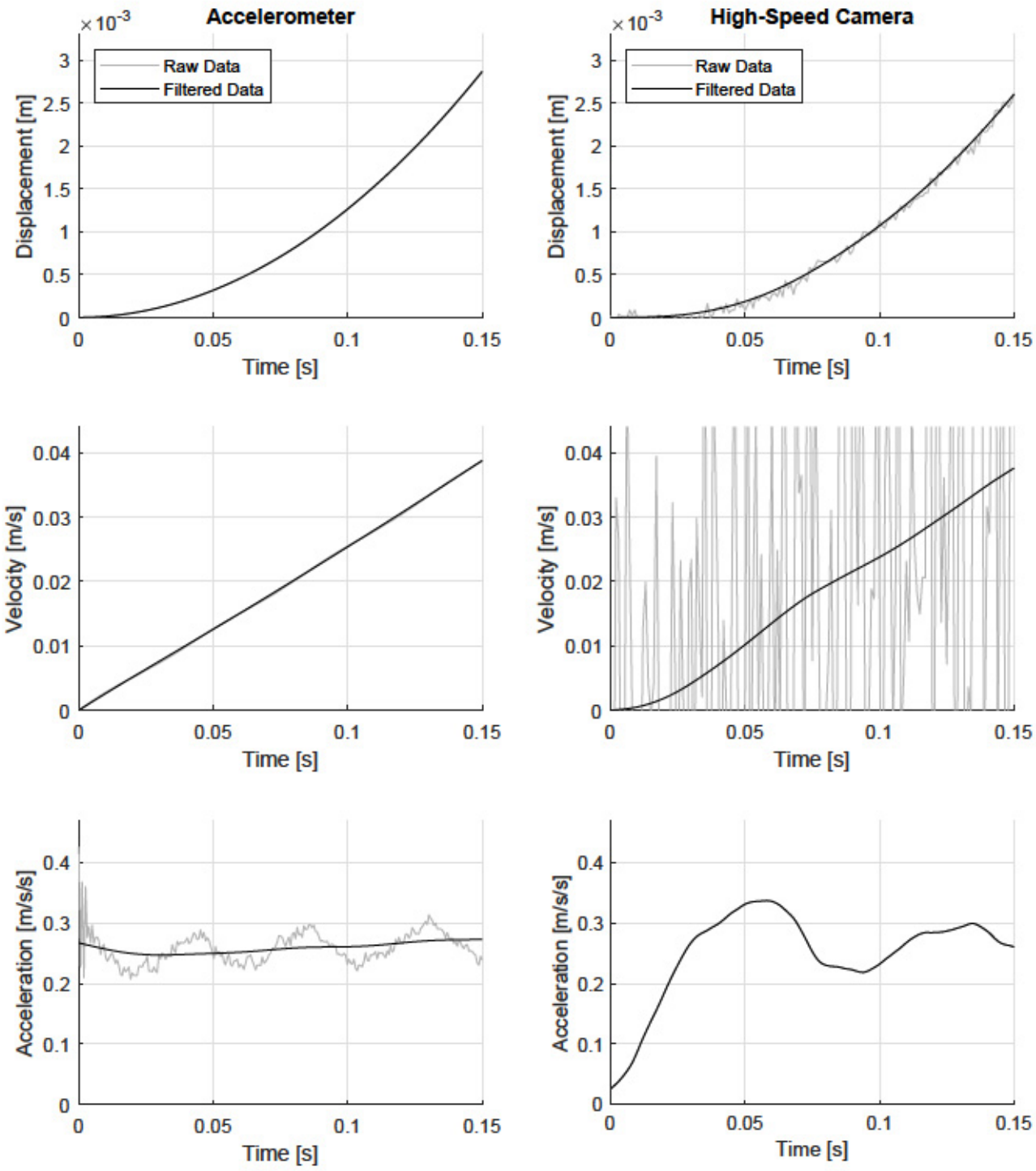

Figure C.22: Step-Force Kinematics of a 5-Sided Polygon: 4% of Ice Mass (Run 2)

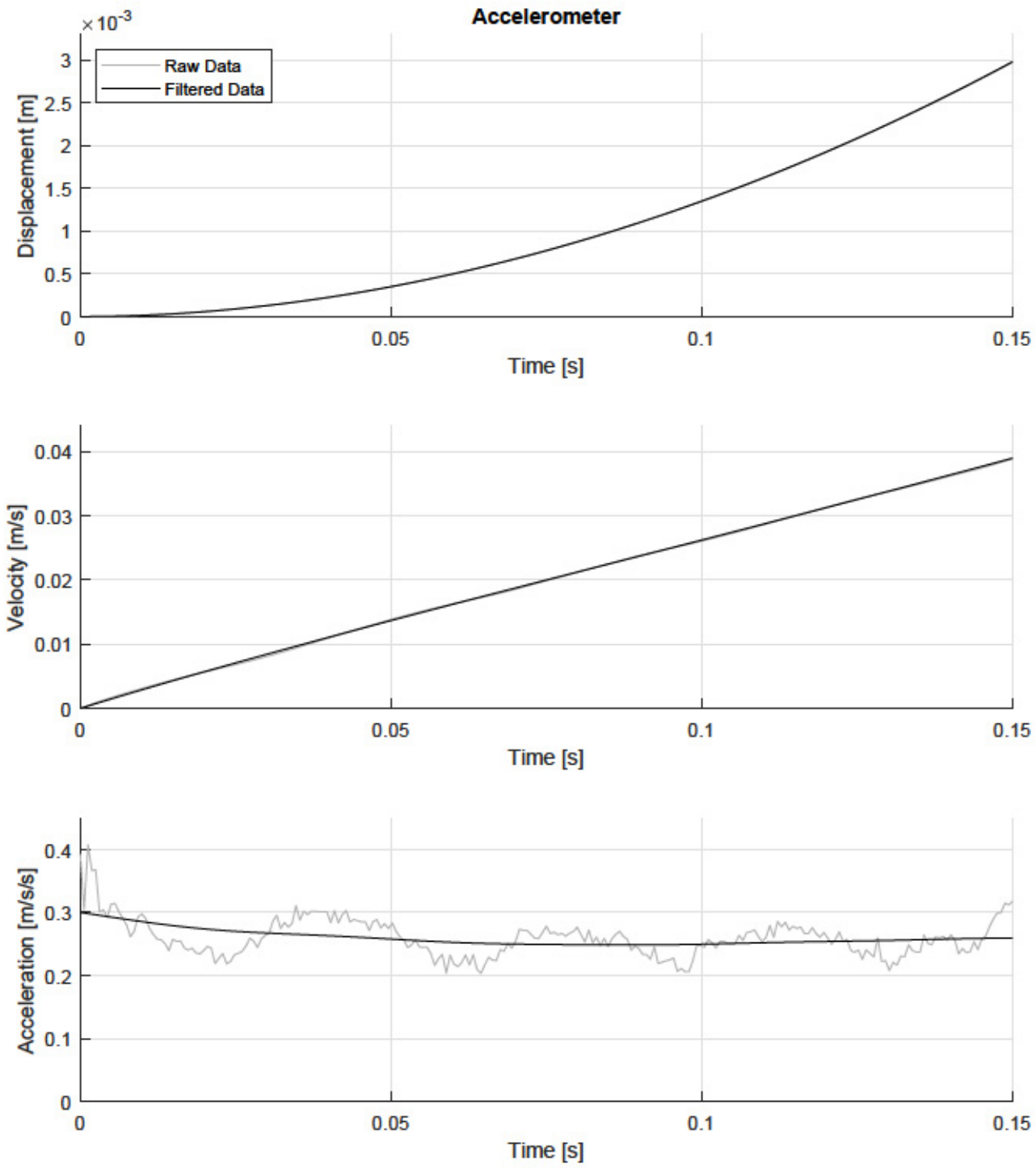

Figure C.23: Step-Force Kinematics of a 5-Sided Polygon: 4% of Ice Mass (Run 3)

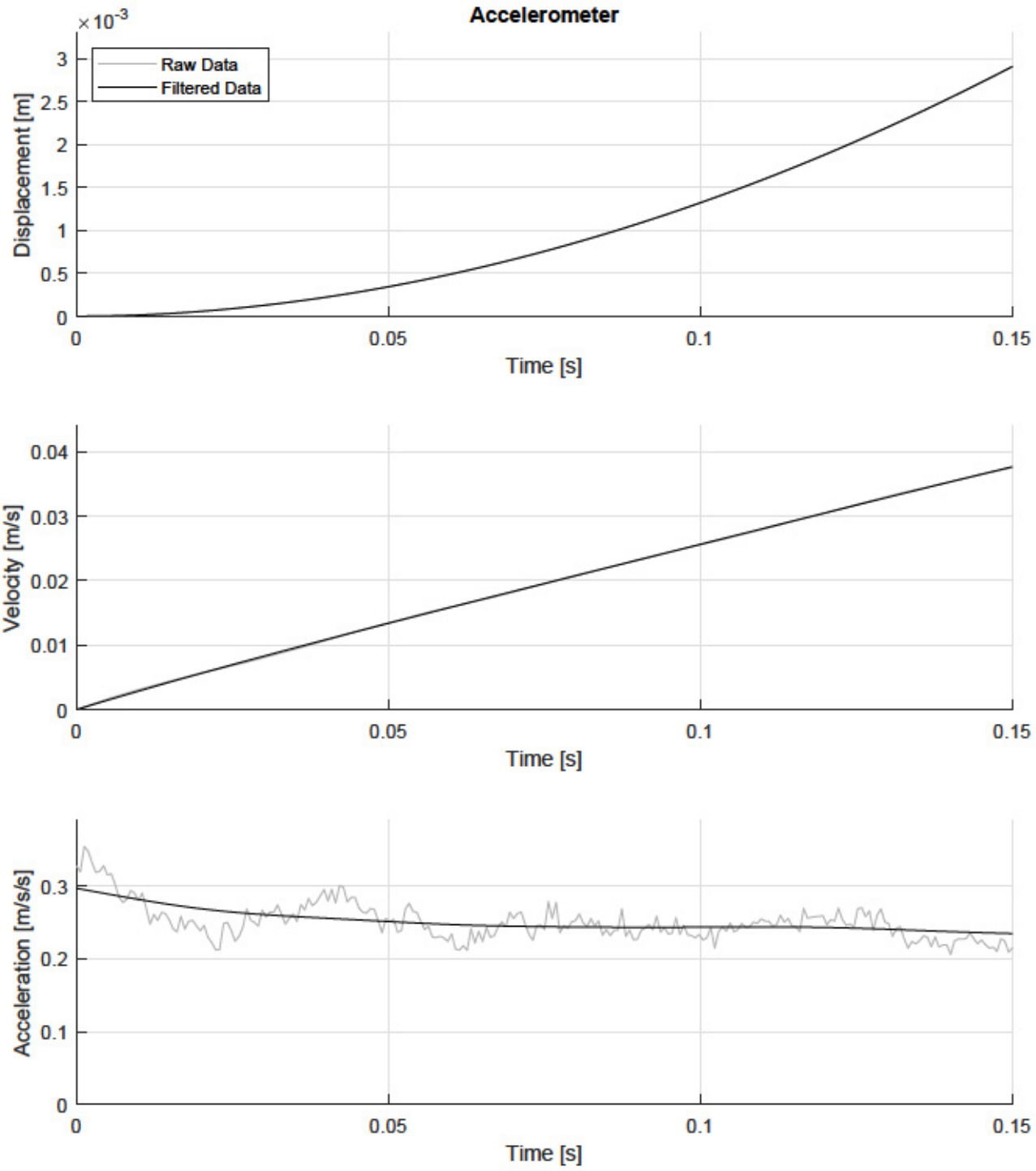

Figure C.24: Step-Force Kinematics of a 5-Sided Polygon: 4% of Ice Mass (Run 4)

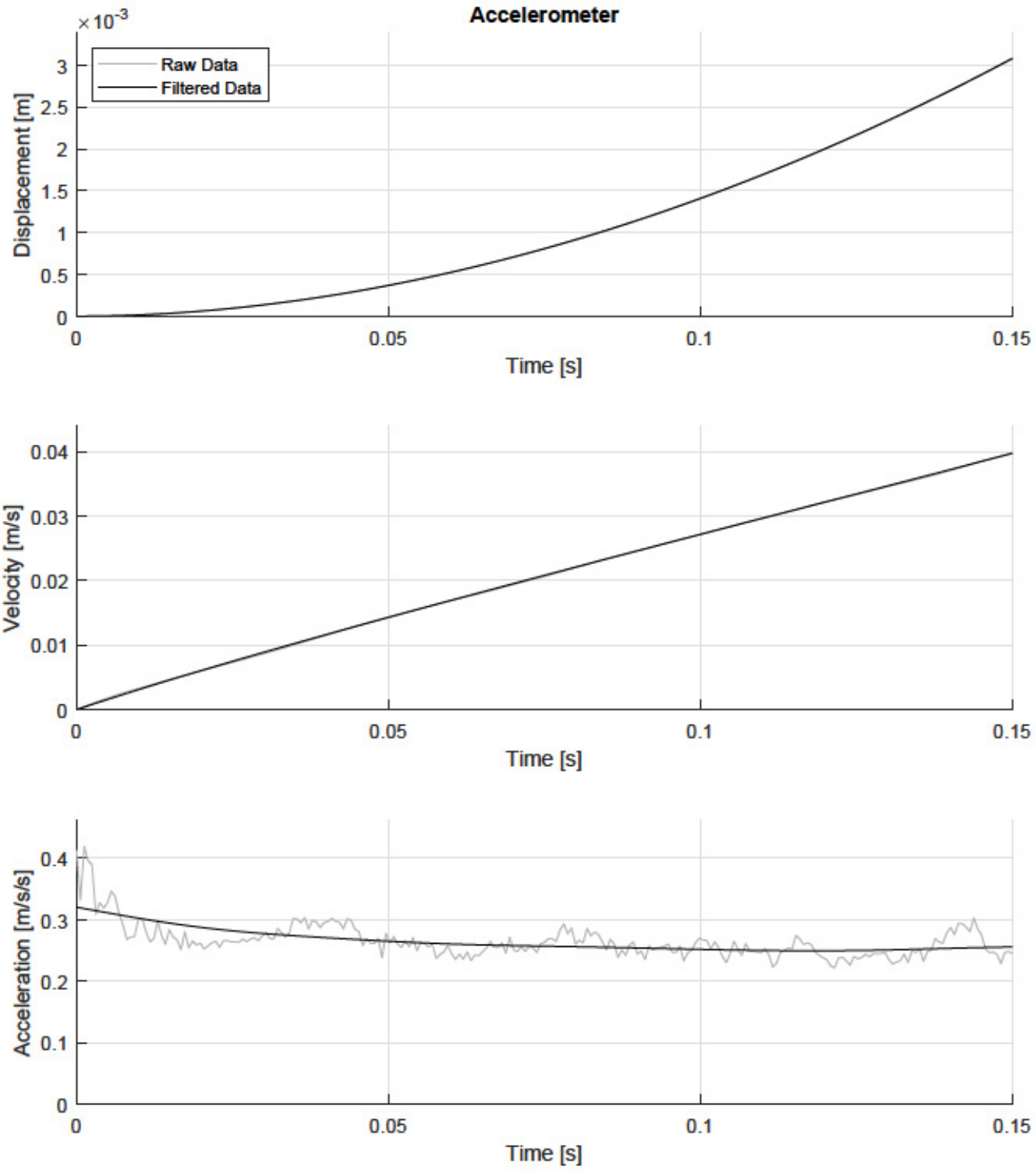

Figure C.25: Step-Force Kinematics of a 5-Sided Polygon: 4% of Ice Mass (Run 5)

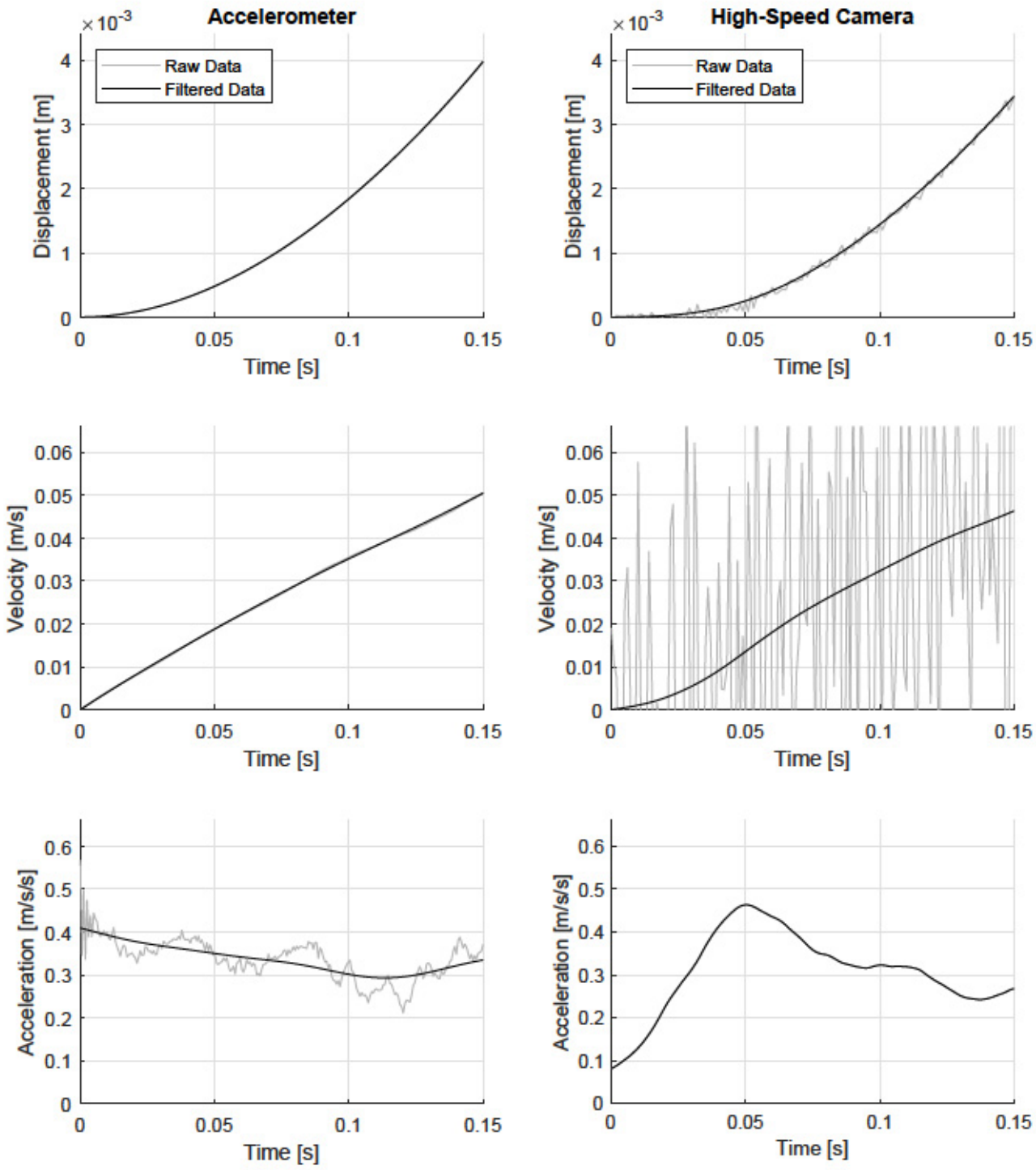

Figure C.26: Step-Force Kinematics of a 5-Sided Polygon: 5% of Ice Mass (Run 1)

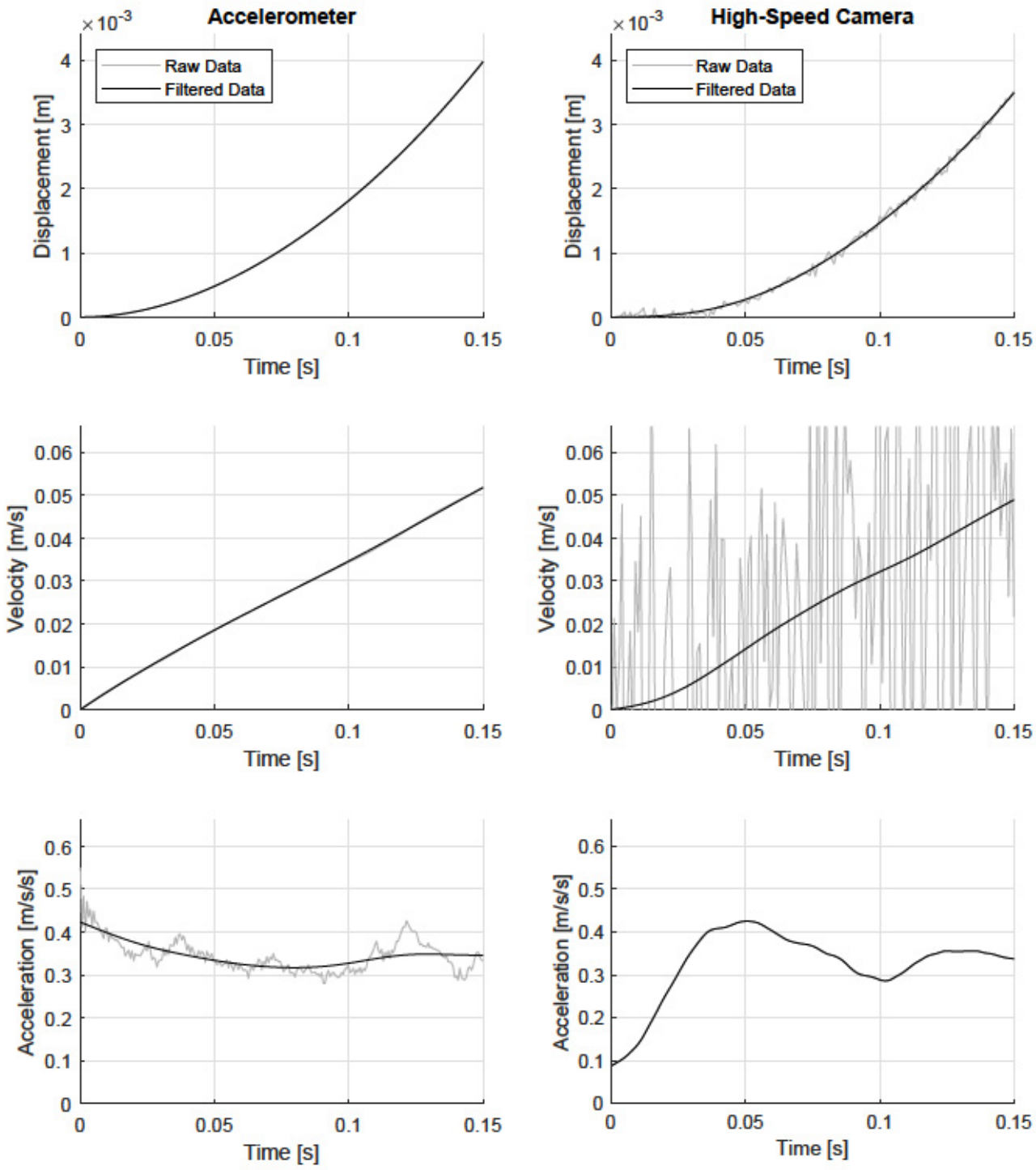

Figure C.27: Step-Force Kinematics of a 5-Sided Polygon: 5% of Ice Mass (Run 2)

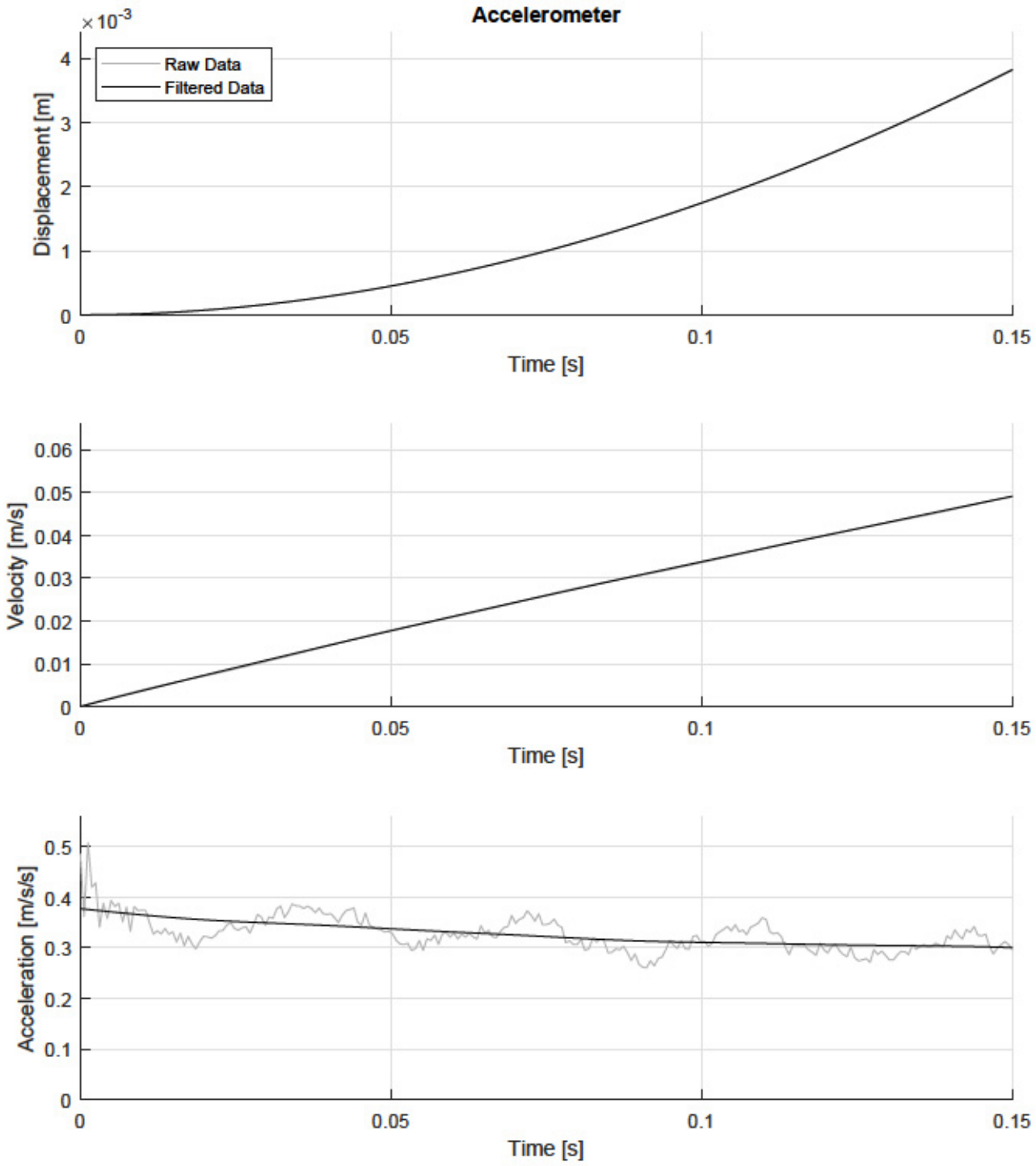

Figure C.28: Step-Force Kinematics of a 5-Sided Polygon: 5% of Ice Mass (Run 3)

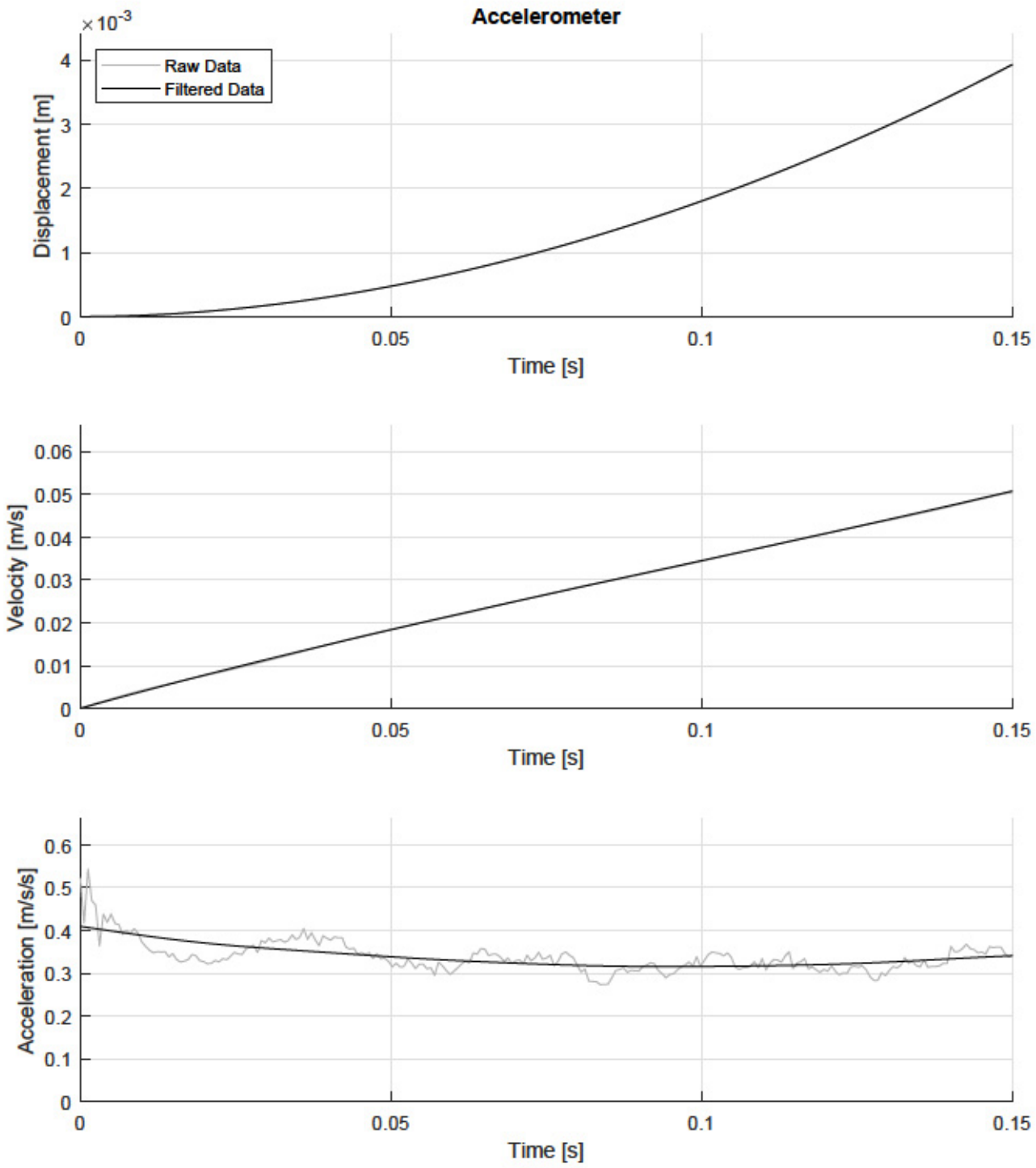

Figure C.29: Step-Force Kinematics of a 5-Sided Polygon: 5% of Ice Mass (Run 4)

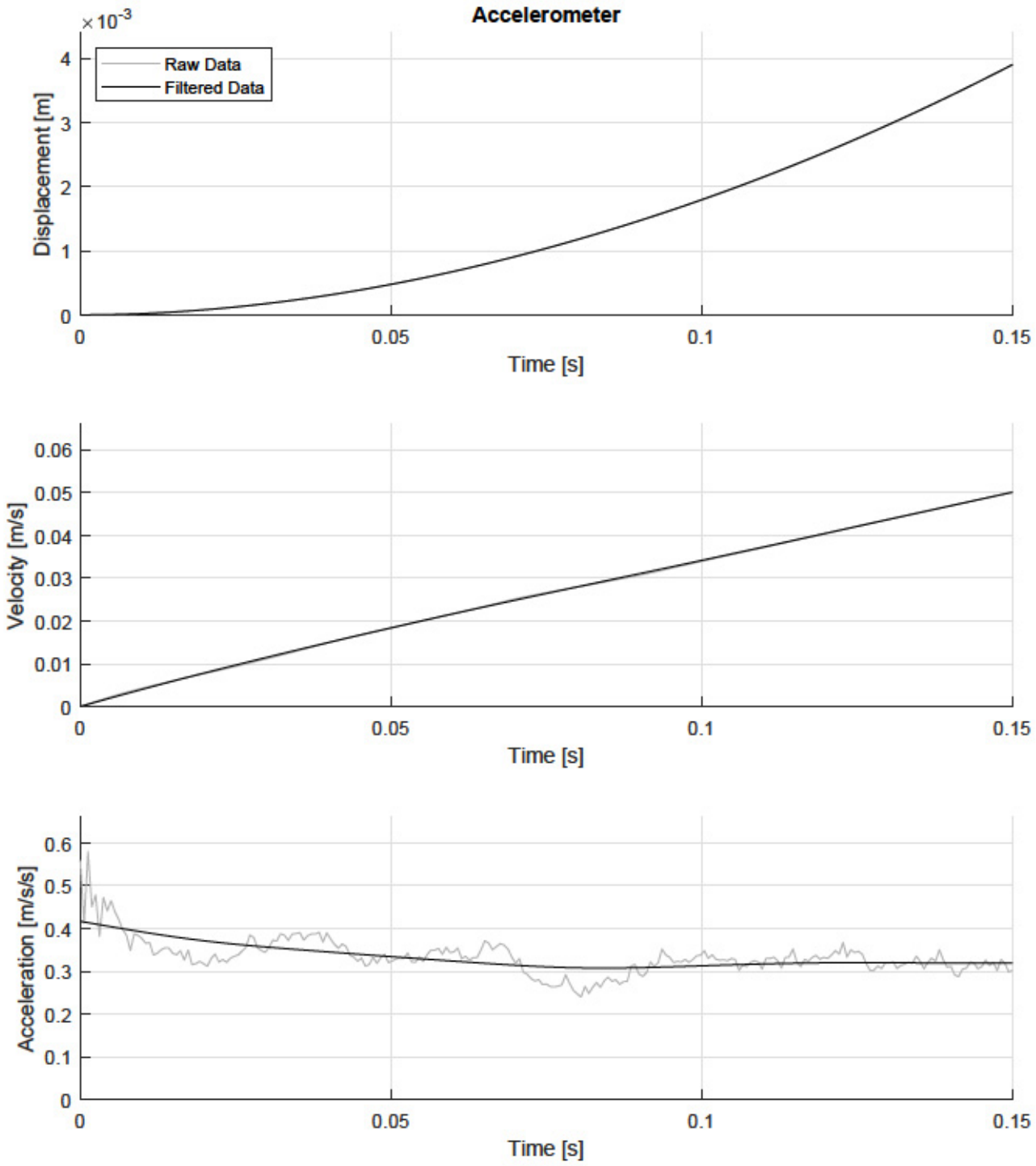

Figure C.30: Step-Force Kinematics of a 5-Sided Polygon: 5% of Ice Mass (Run 5)

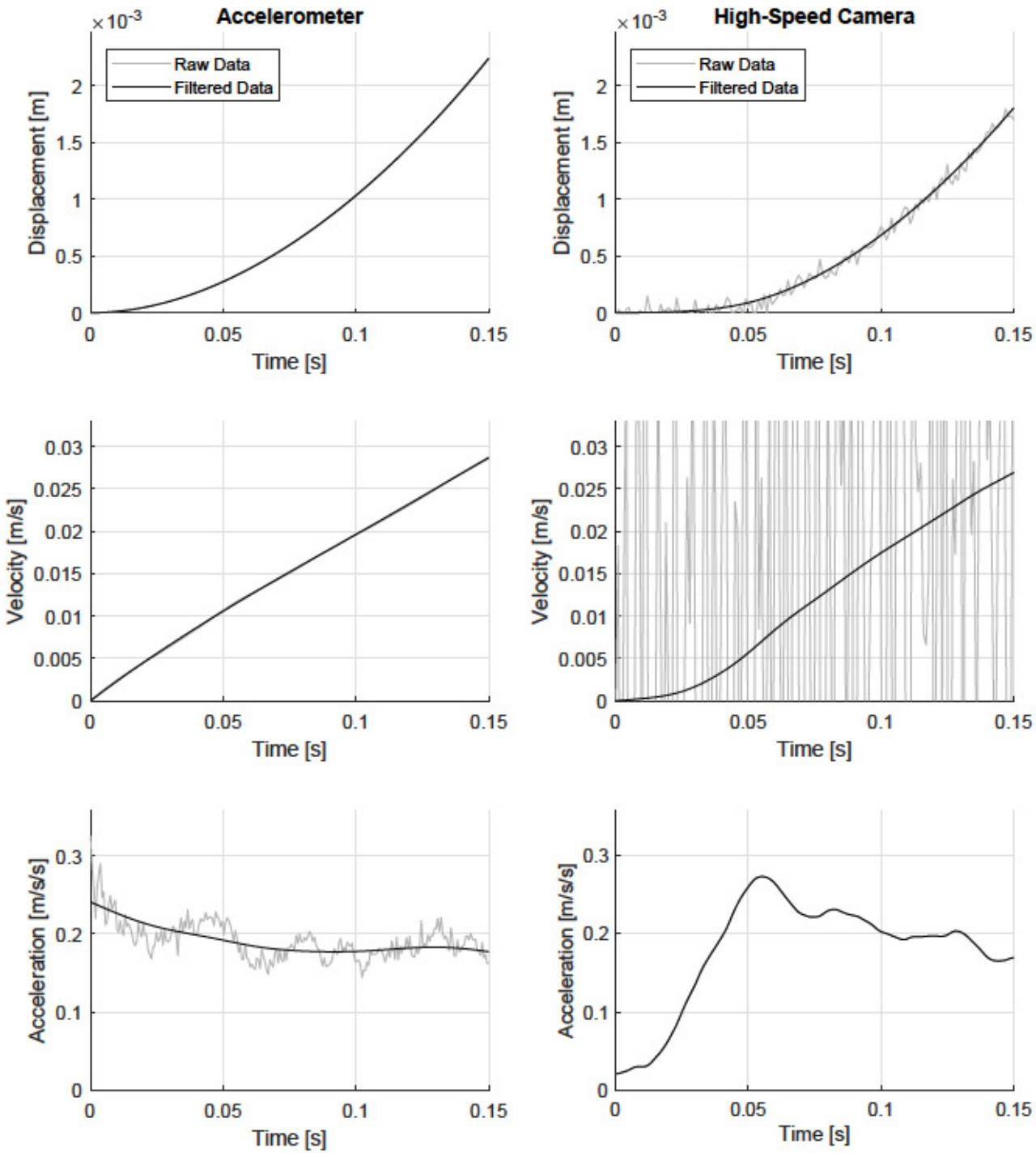

Figure C.31: Step-Force Kinematics of a 4-Sided Polygon: 3% of Ice Mass (Run 1)

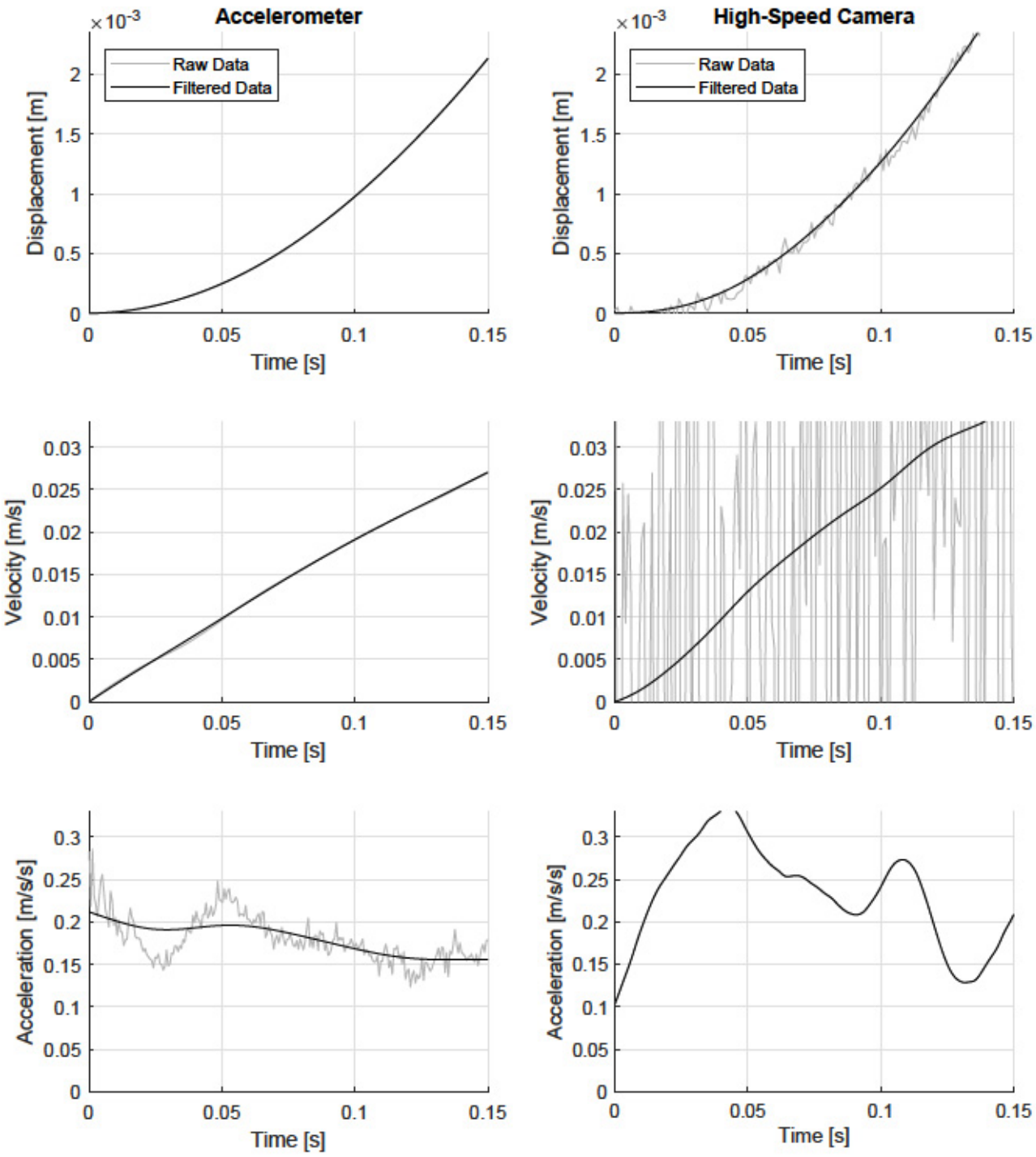

Figure C.32: Step-Force Kinematics of a 4-Sided Polygon: 3% of Ice Mass (Run 2)

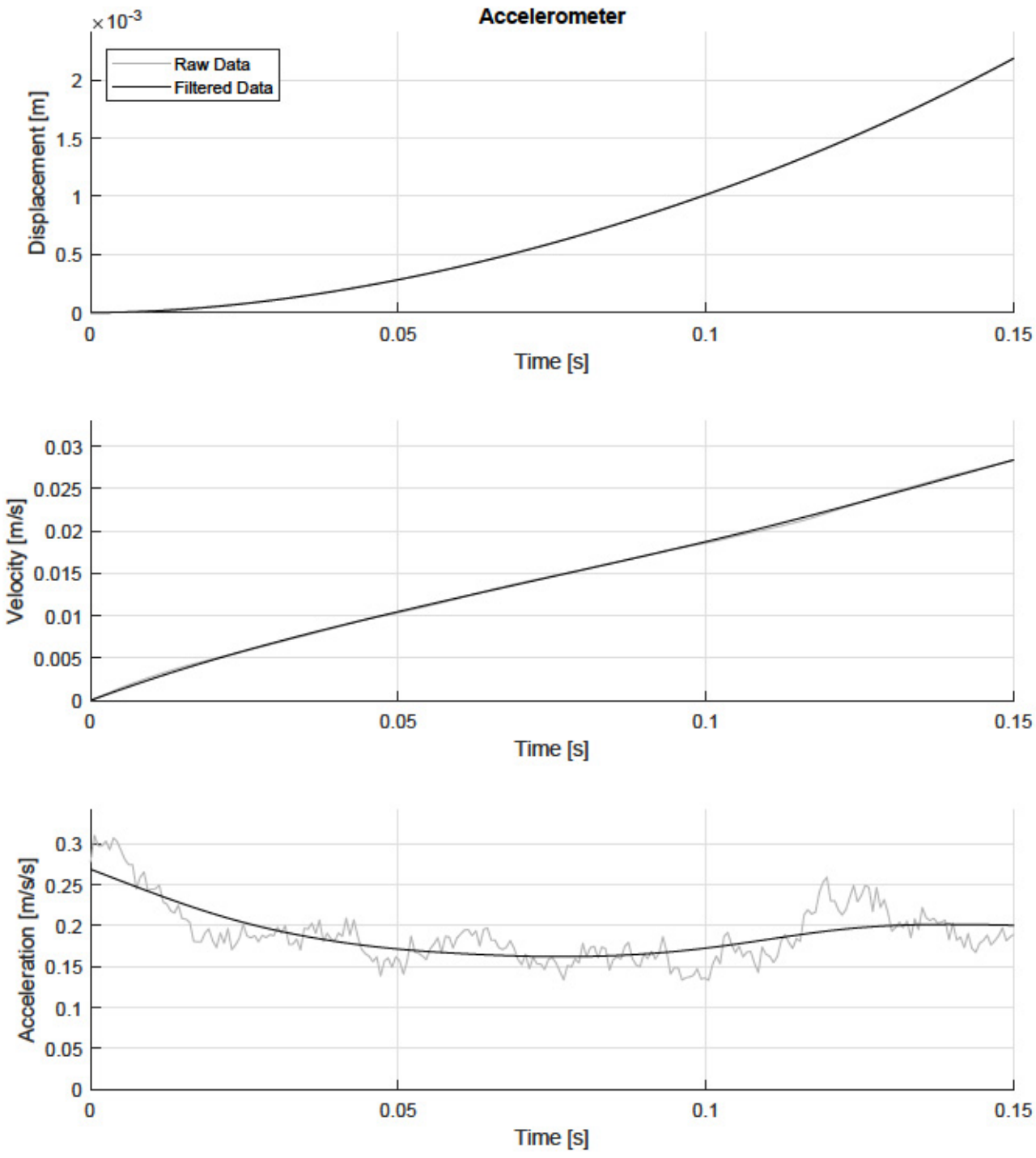

Figure C.33: Step-Force Kinematics of a 4-Sided Polygon: 3% of Ice Mass (Run 3)

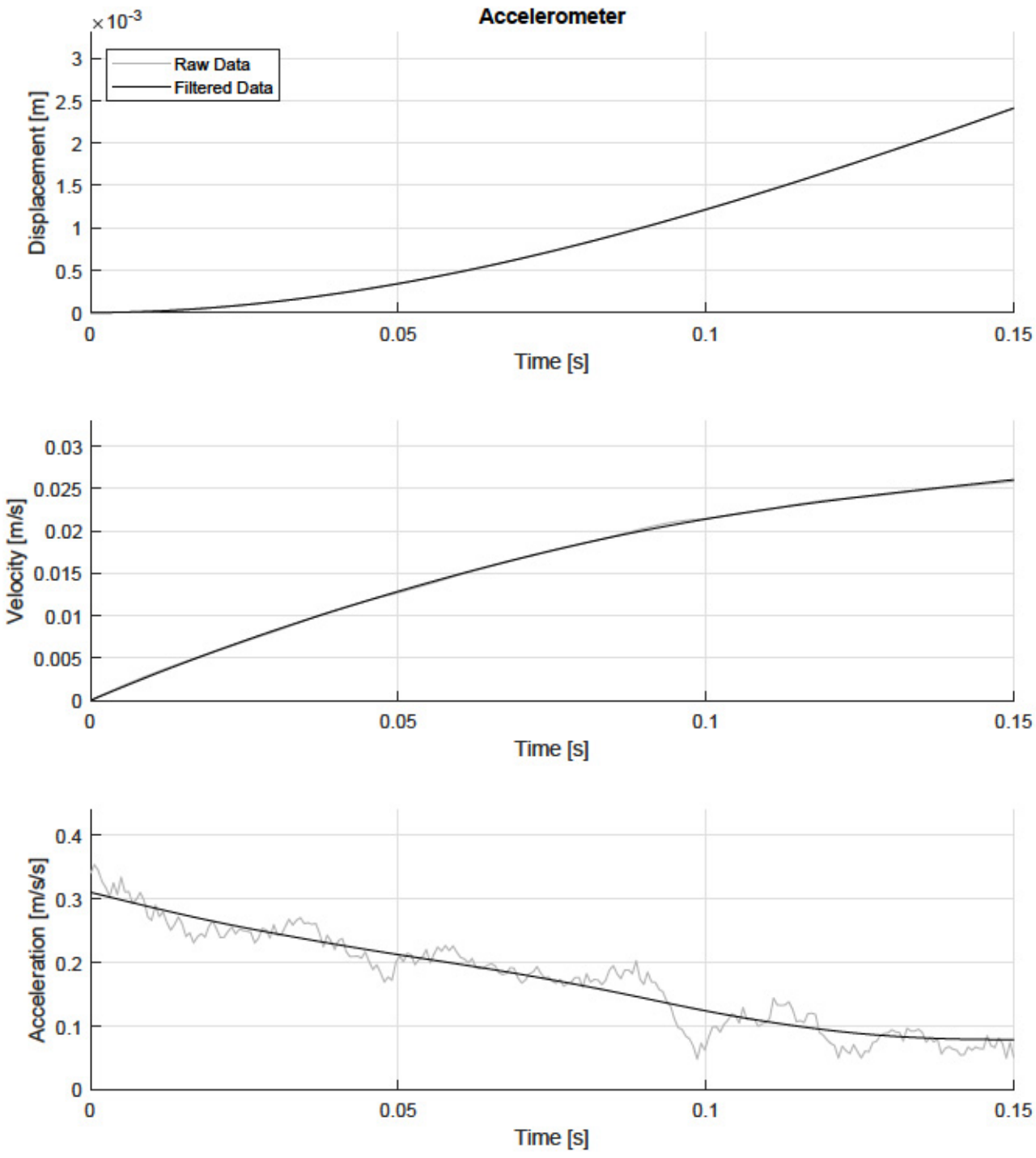

Figure C.34: Step-Force Kinematics of a 4-Sided Polygon: 3% of Ice Mass (Run 4)

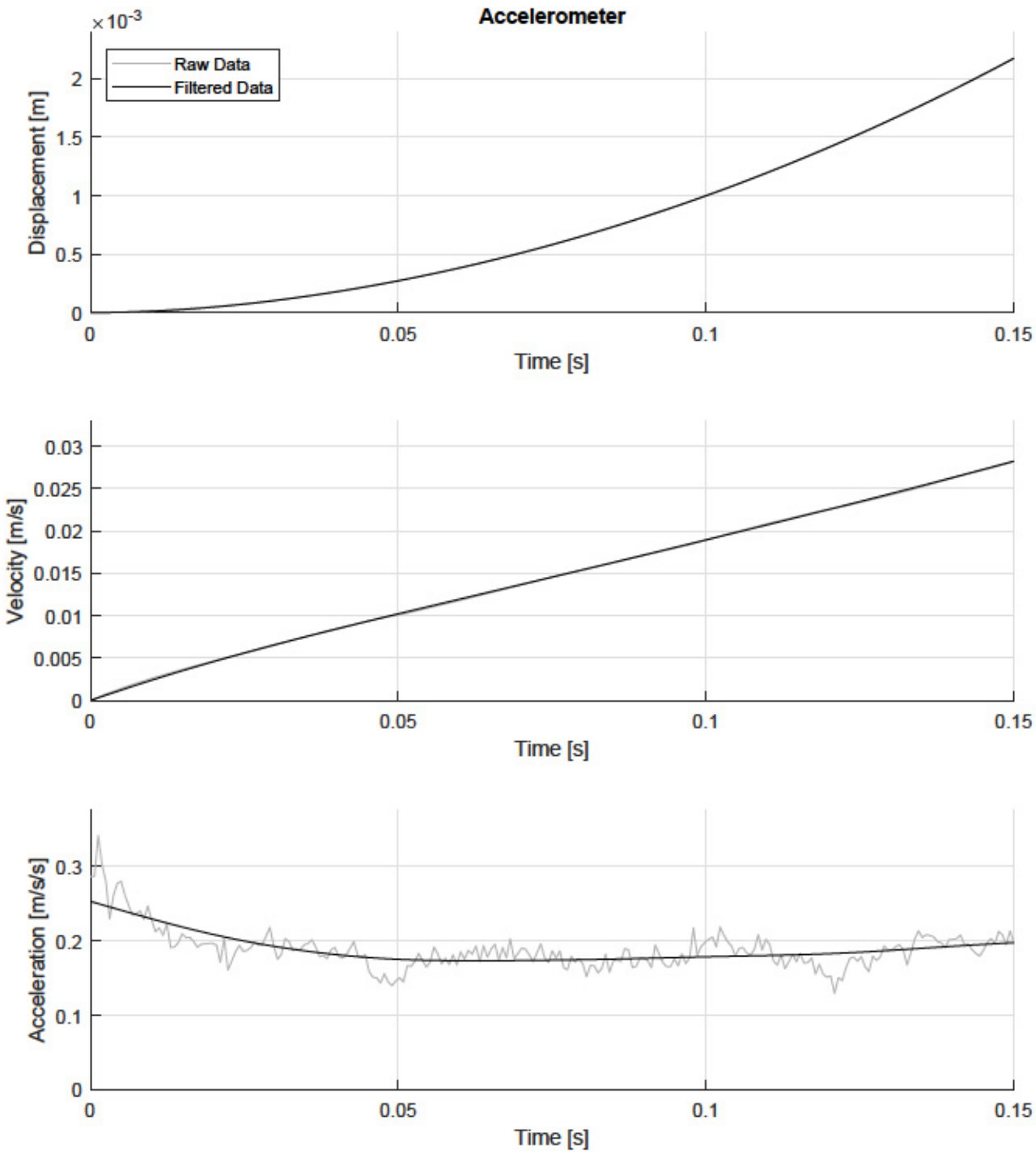

Figure C.35: Step-Force Kinematics of a 4-Sided Polygon: 3% of Ice Mass (Run 5)

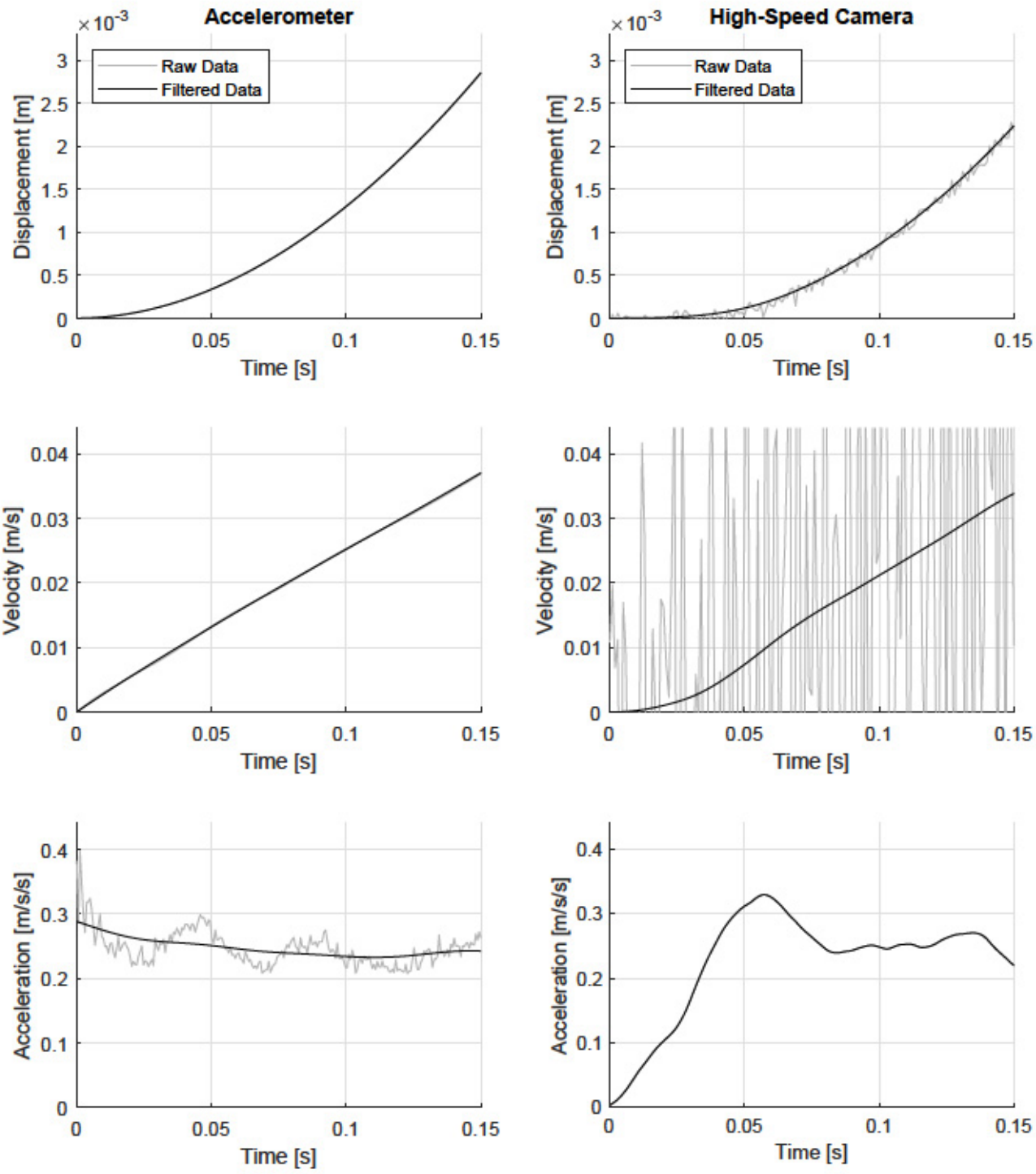

Figure C.36: Step-Force Kinematics of a 4-Sided Polygon: 4% of Ice Mass (Run 1)

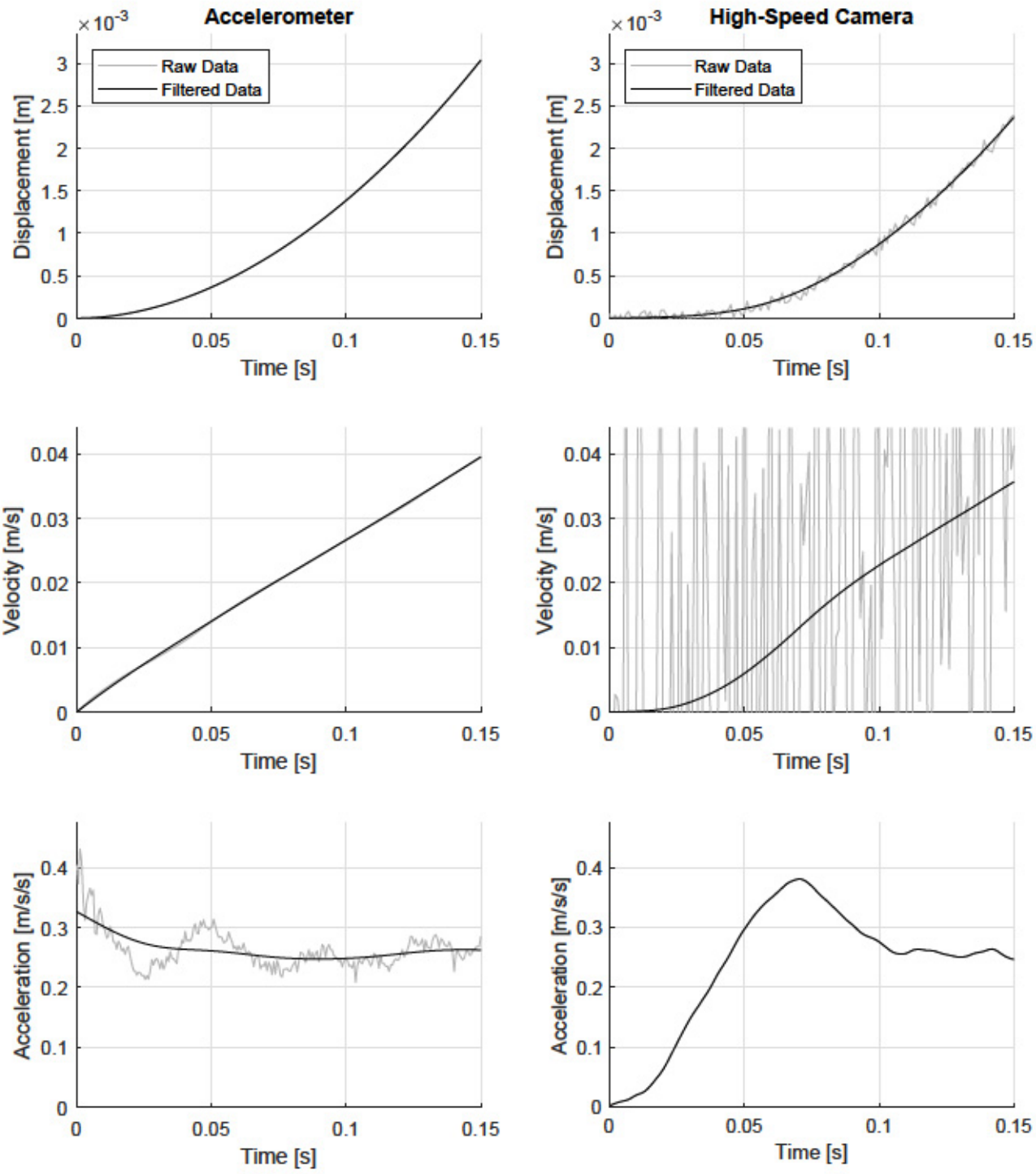

Figure C.37: Step-Force Kinematics of a 4-Sided Polygon: 4% of Ice Mass (Run 2)

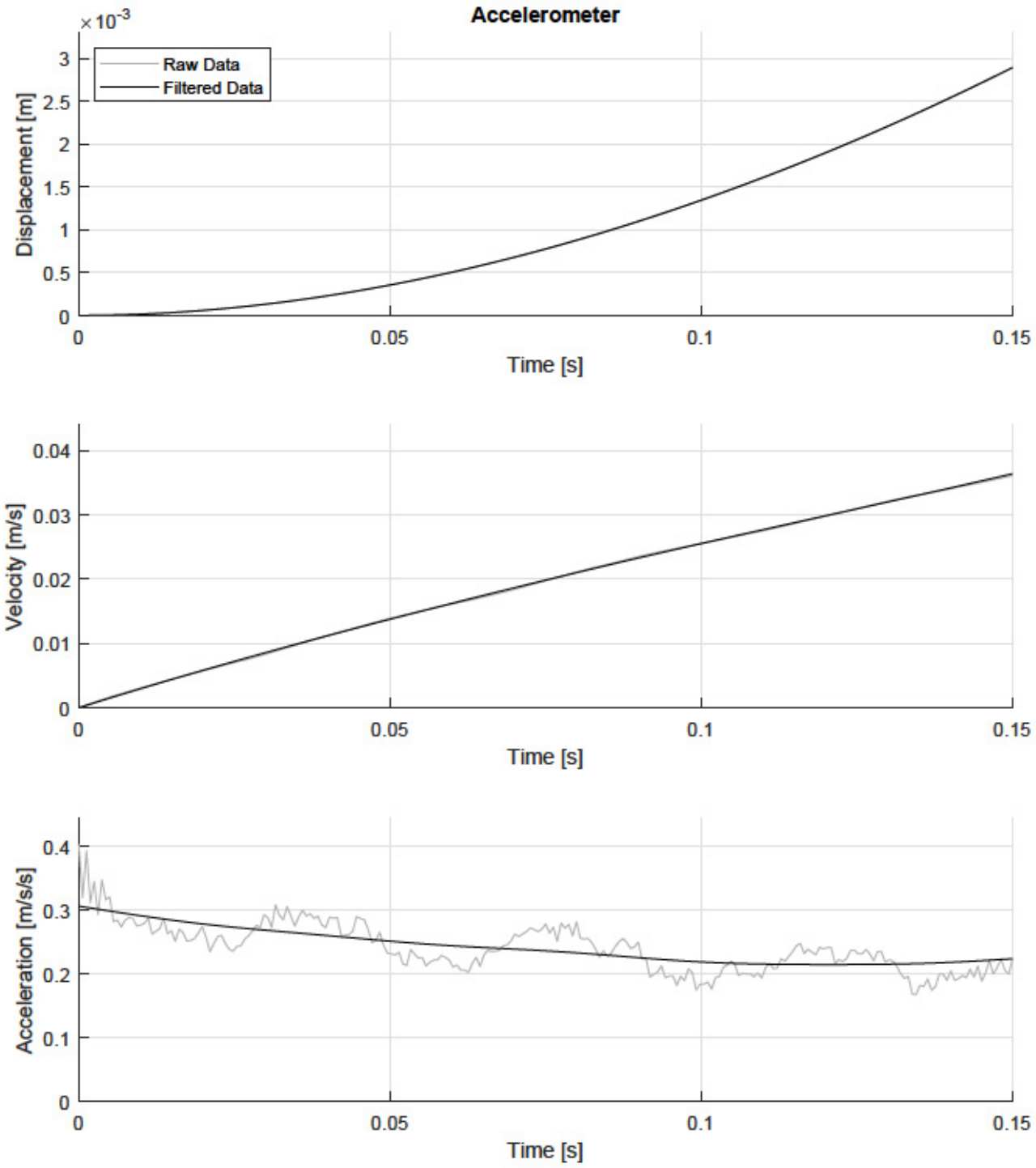

Figure C.38: Step-Force Kinematics of a 4-Sided Polygon: 4% of Ice Mass (Run 3)

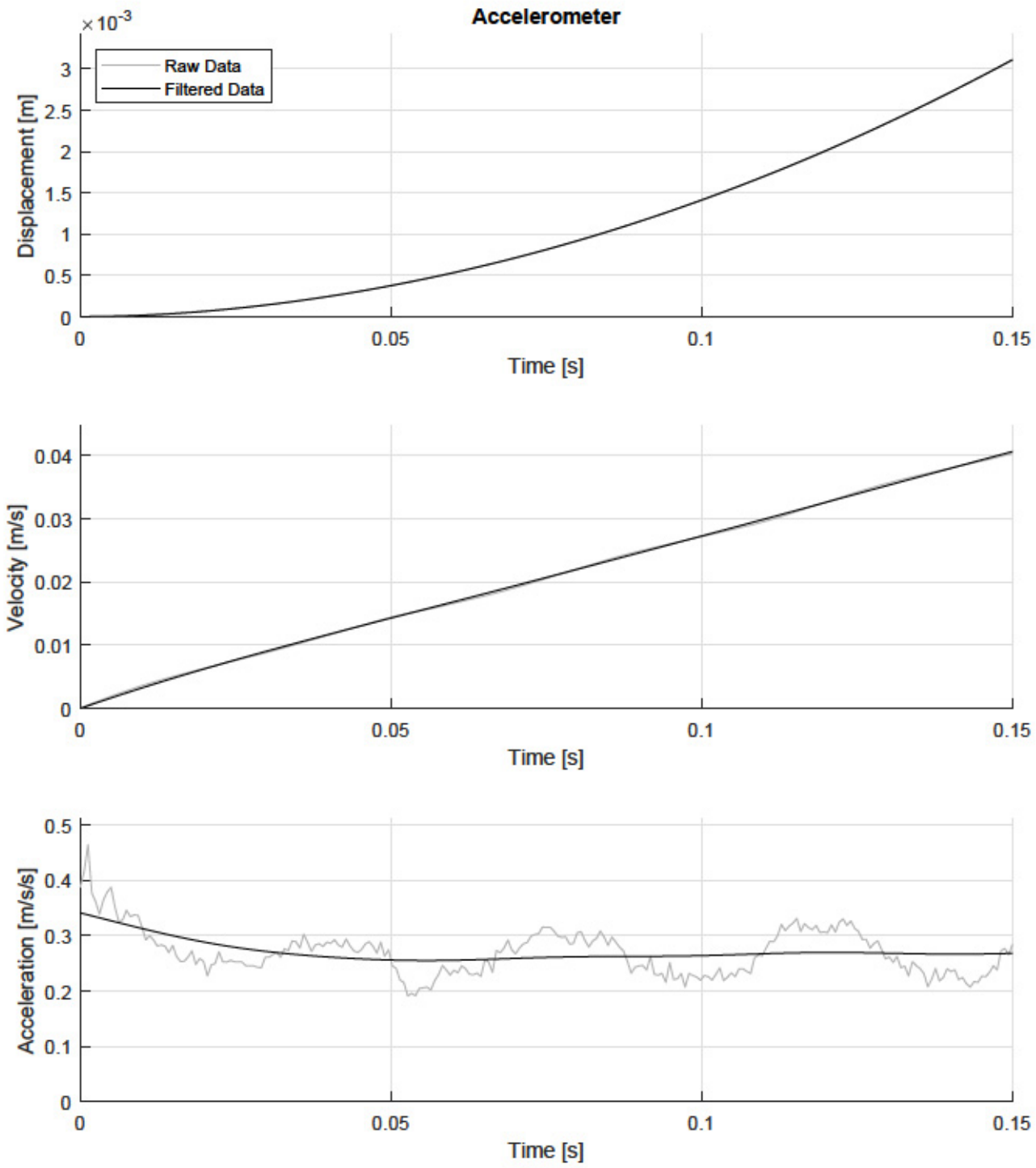

Figure C.39: Step-Force Kinematics of a 4-Sided Polygon: 4% of Ice Mass (Run 4)

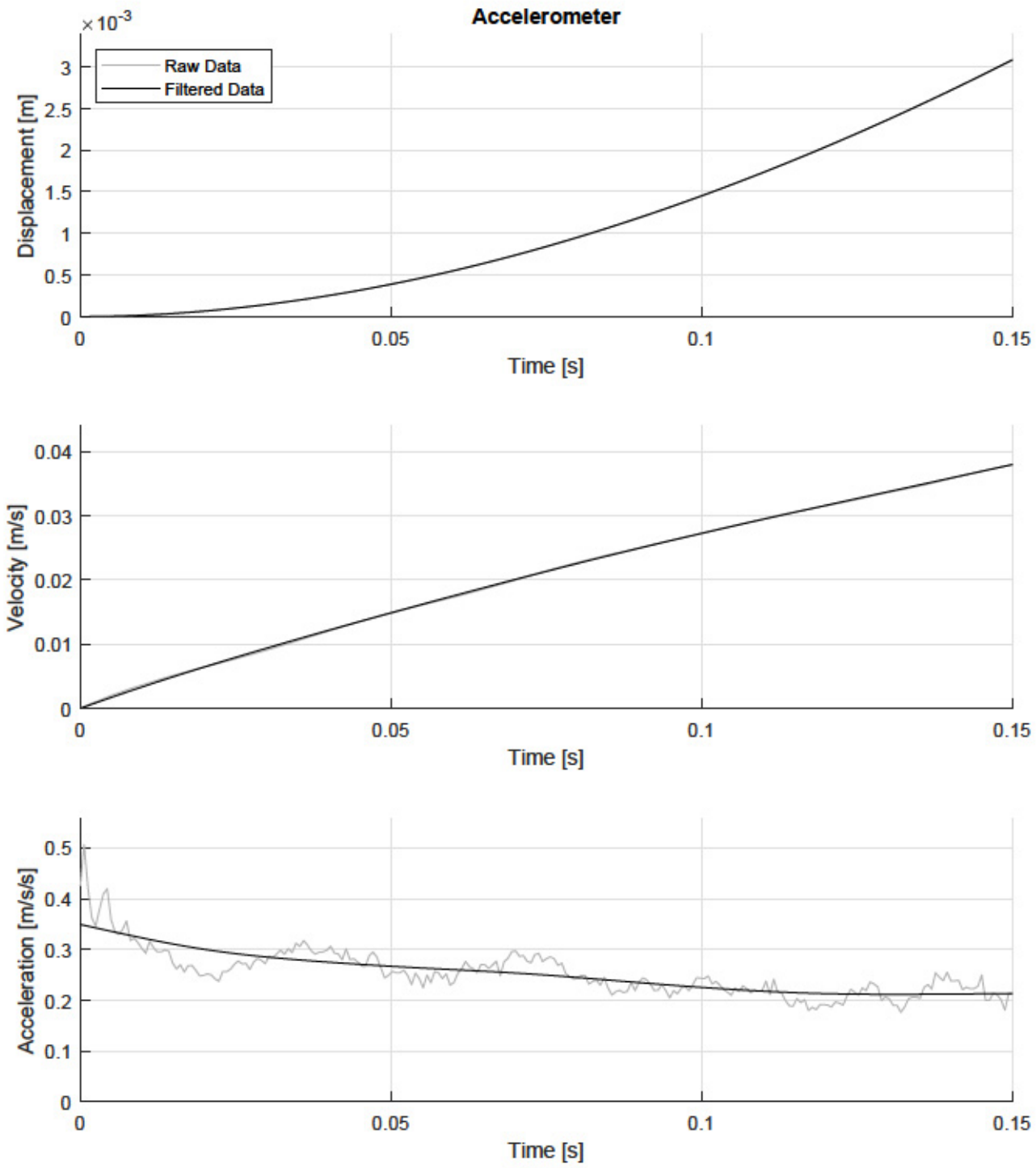

Figure C.40: Step-Force Kinematics of a 4-Sided Polygon: 4% of Ice Mass (Run 5)

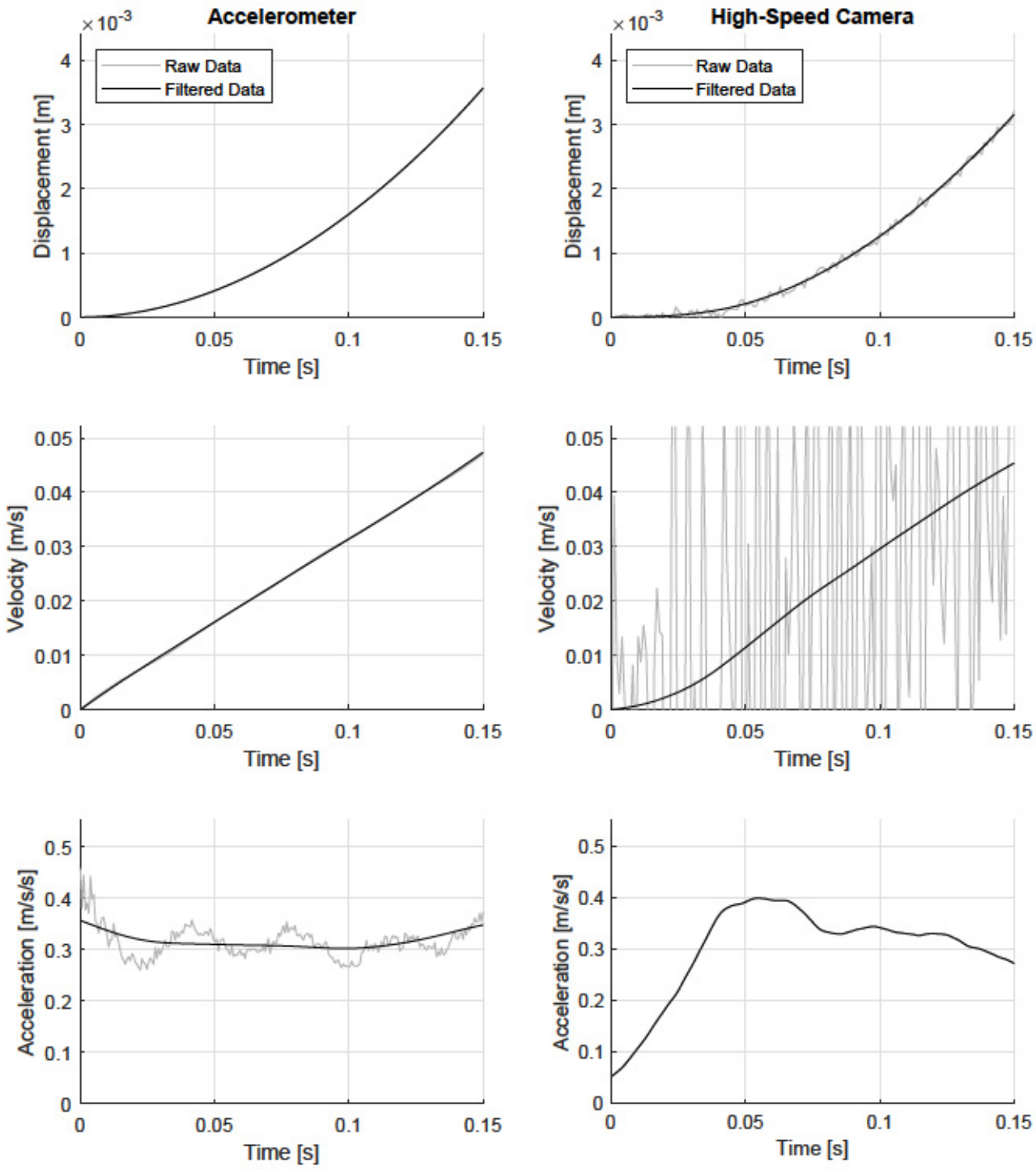

Figure C.41: Step-Force Kinematics of a 4-Sided Polygon: 5% of Ice Mass (Run 1)

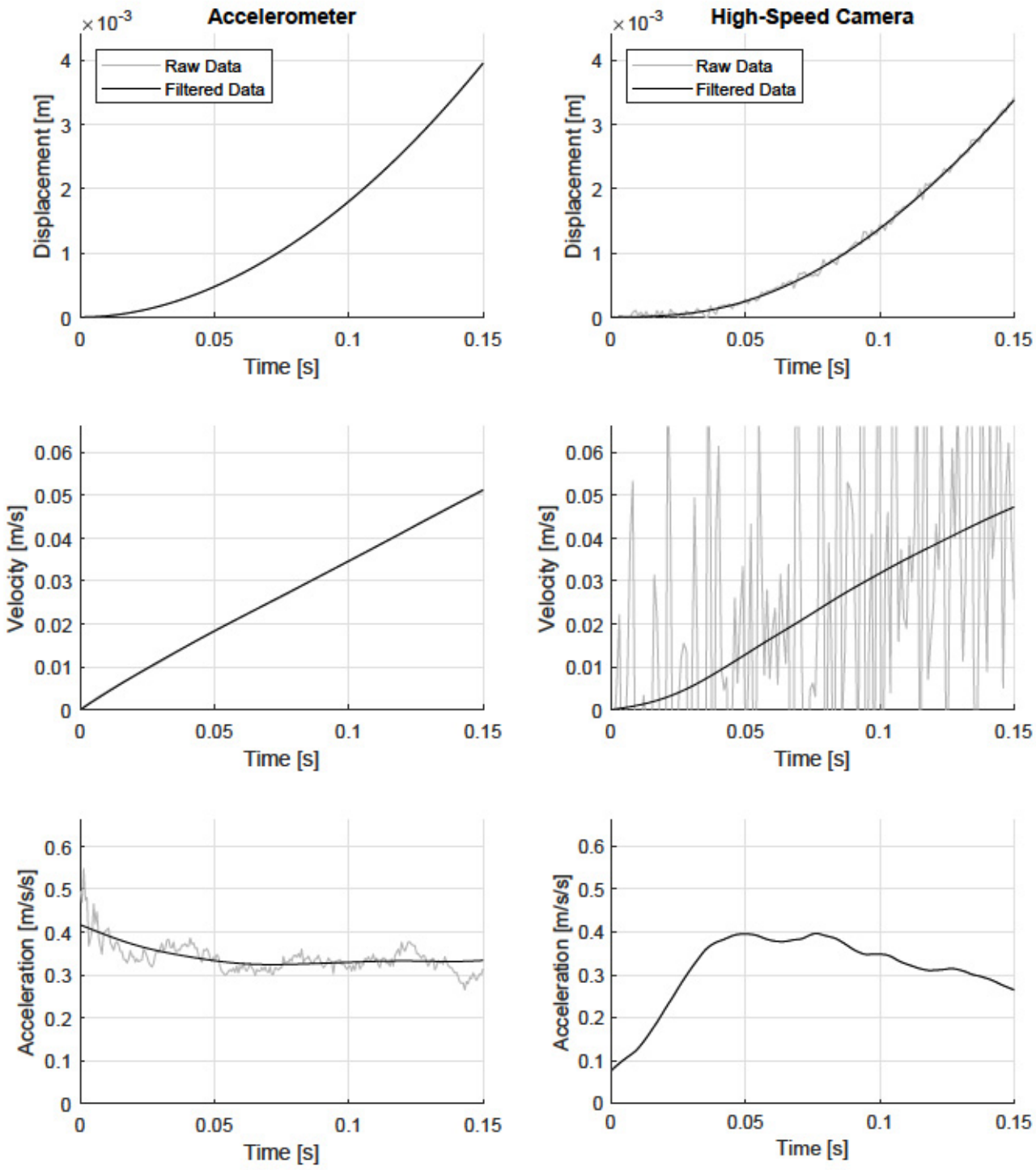

Figure C.42: Step-Force Kinematics of a 4-Sided Polygon: 5% of Ice Mass (Run 2)

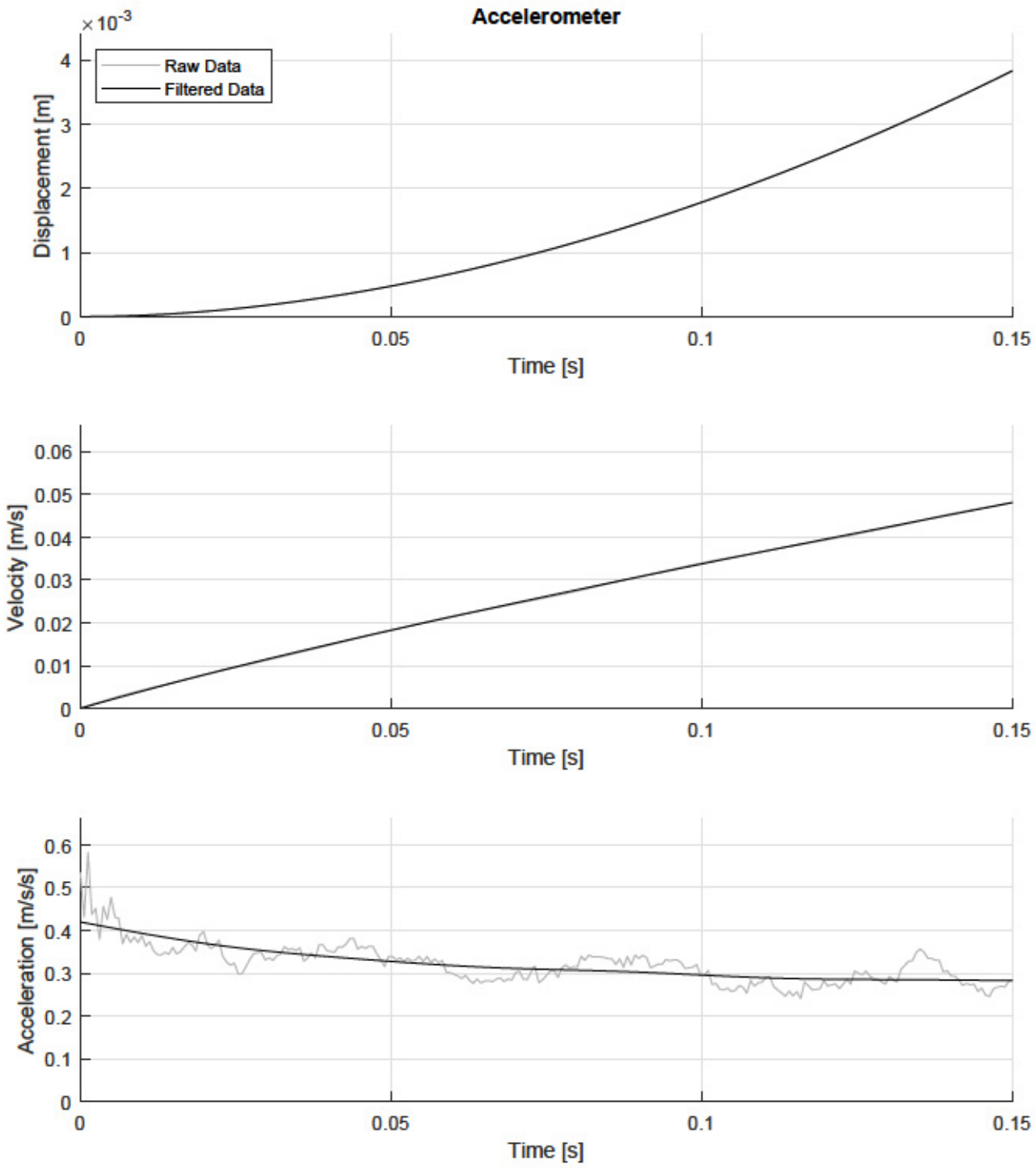

Figure C.43: Step-Force Kinematics of a 4-Sided Polygon: 5% of Ice Mass (Run 3)

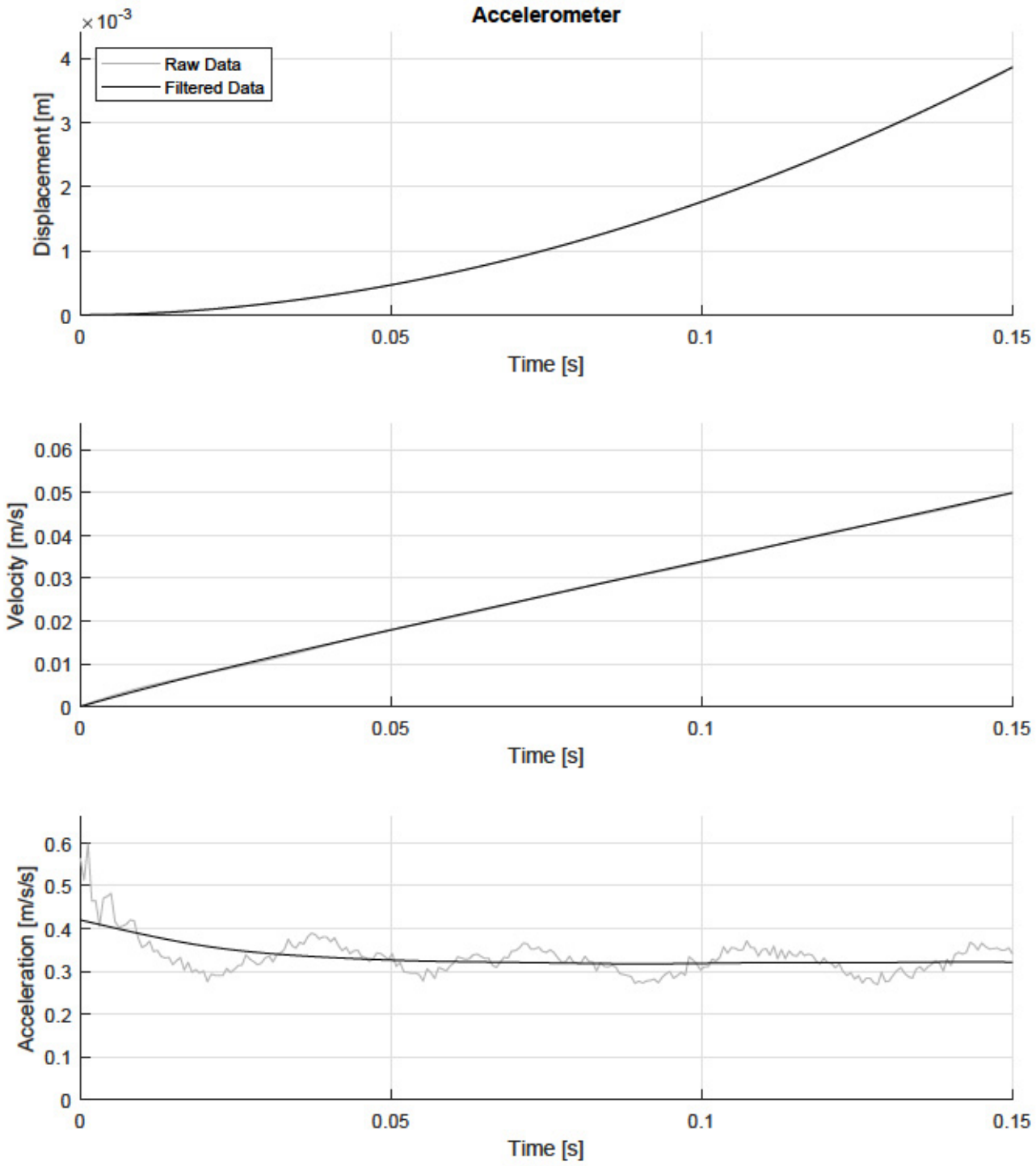

Figure C.44: Step-Force Kinematics of a 4-Sided Polygon: 5% of Ice Mass (Run 4)

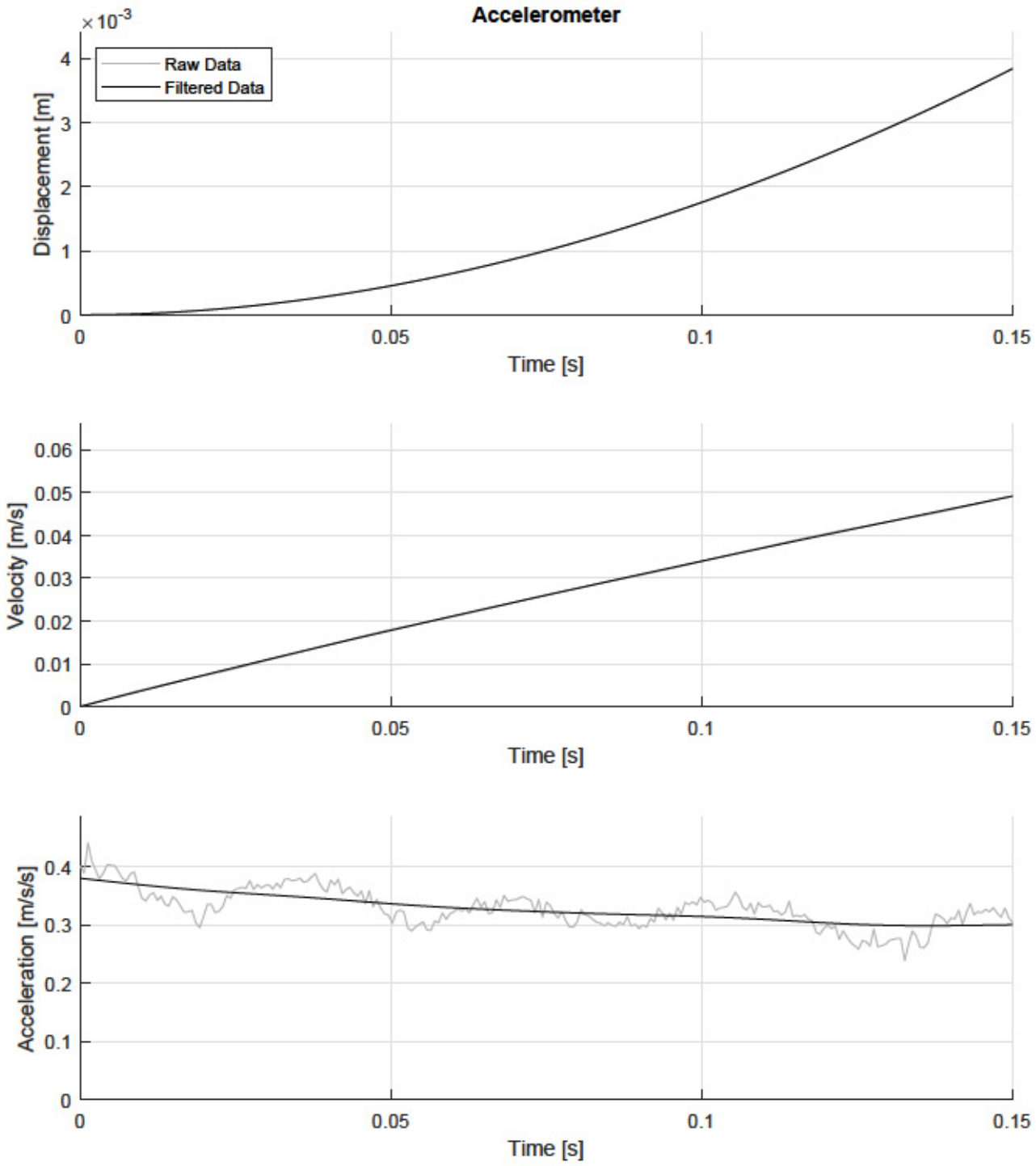

Figure C.45: Step-Force Kinematics of a 4-Sided Polygon: 5% of Ice Mass (Run 5)

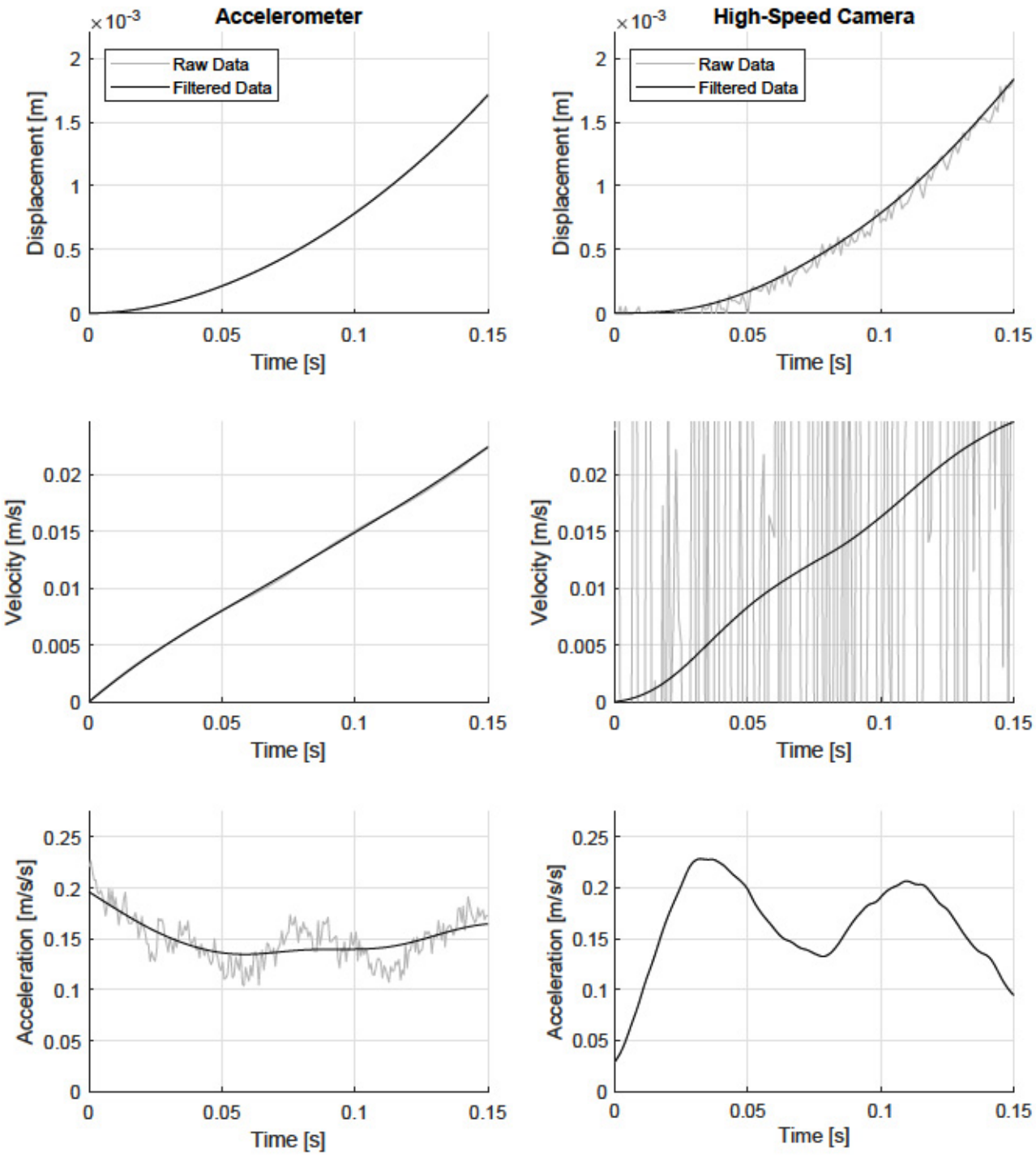

Figure C.46: Step-Force Kinematics of a 3-Sided Polygon: 3% of Ice Mass (Run 1)

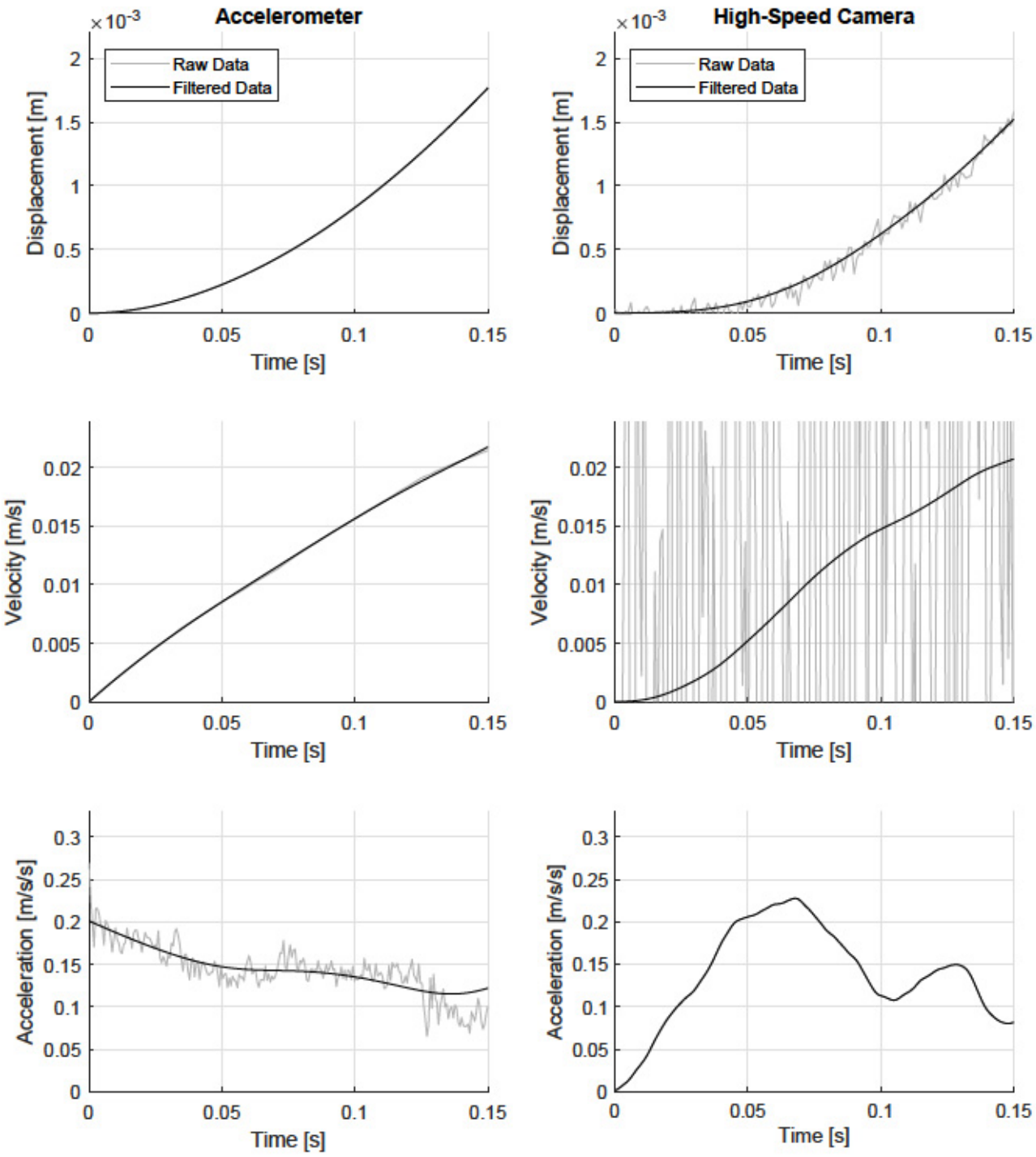

Figure C.47: Step-Force Kinematics of a 3-Sided Polygon: 3% of Ice Mass (Run 2)

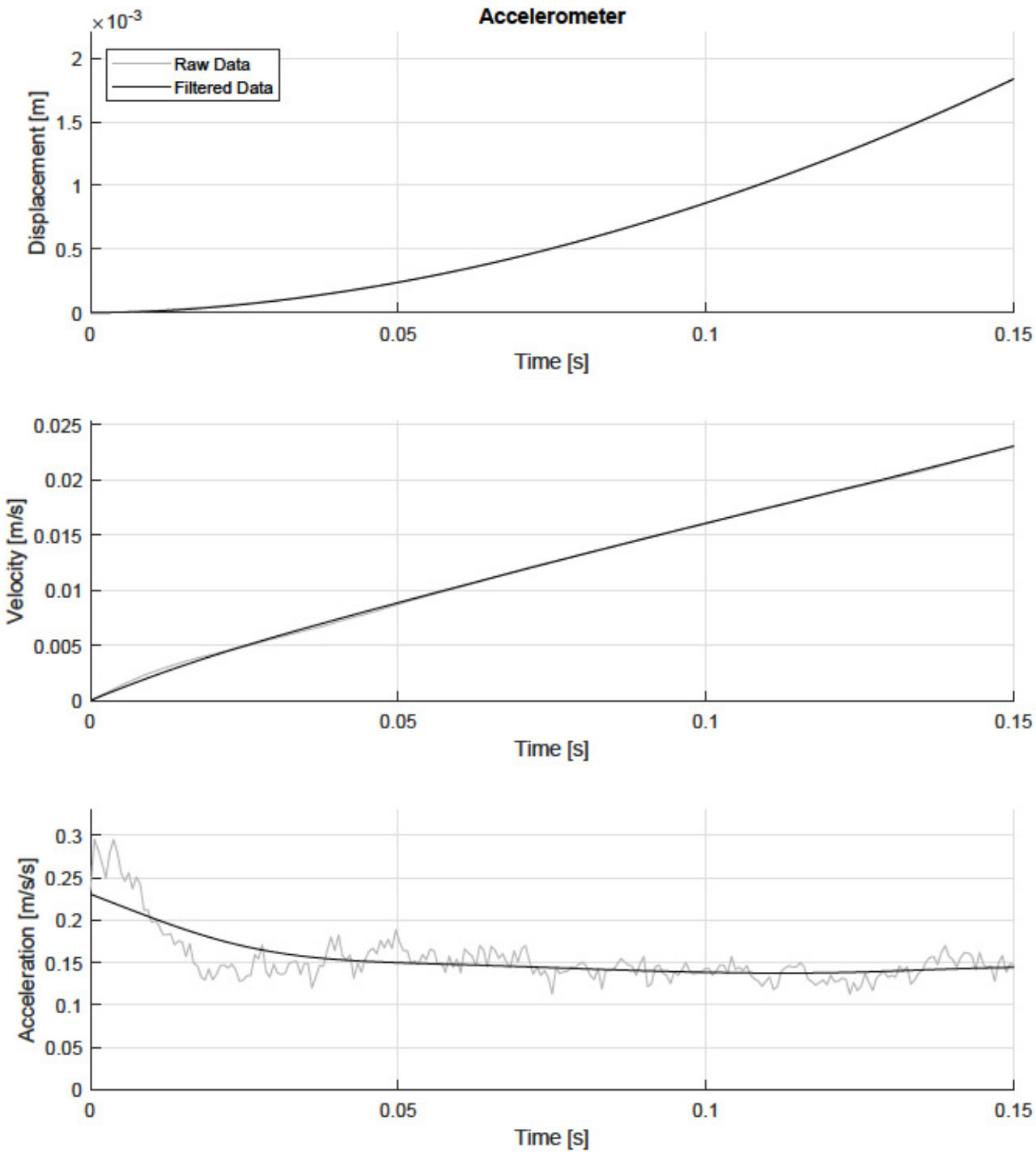

Figure C.48: Step-Force Kinematics of a 3-Sided Polygon: 3% of Ice Mass (Run 3)

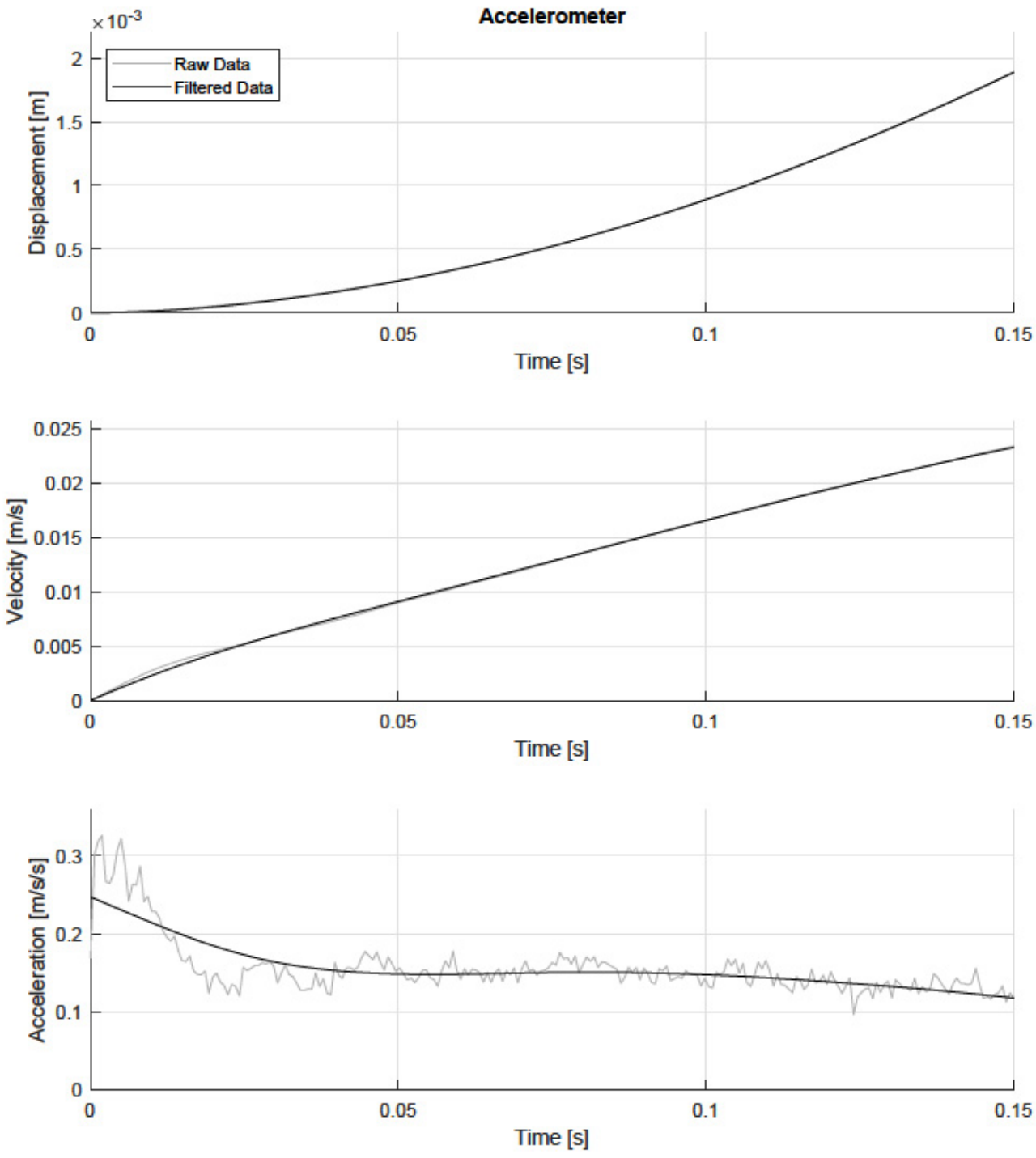

Figure C.49: Step-Force Kinematics of a 3-Sided Polygon: 3% of Ice Mass (Run 4)

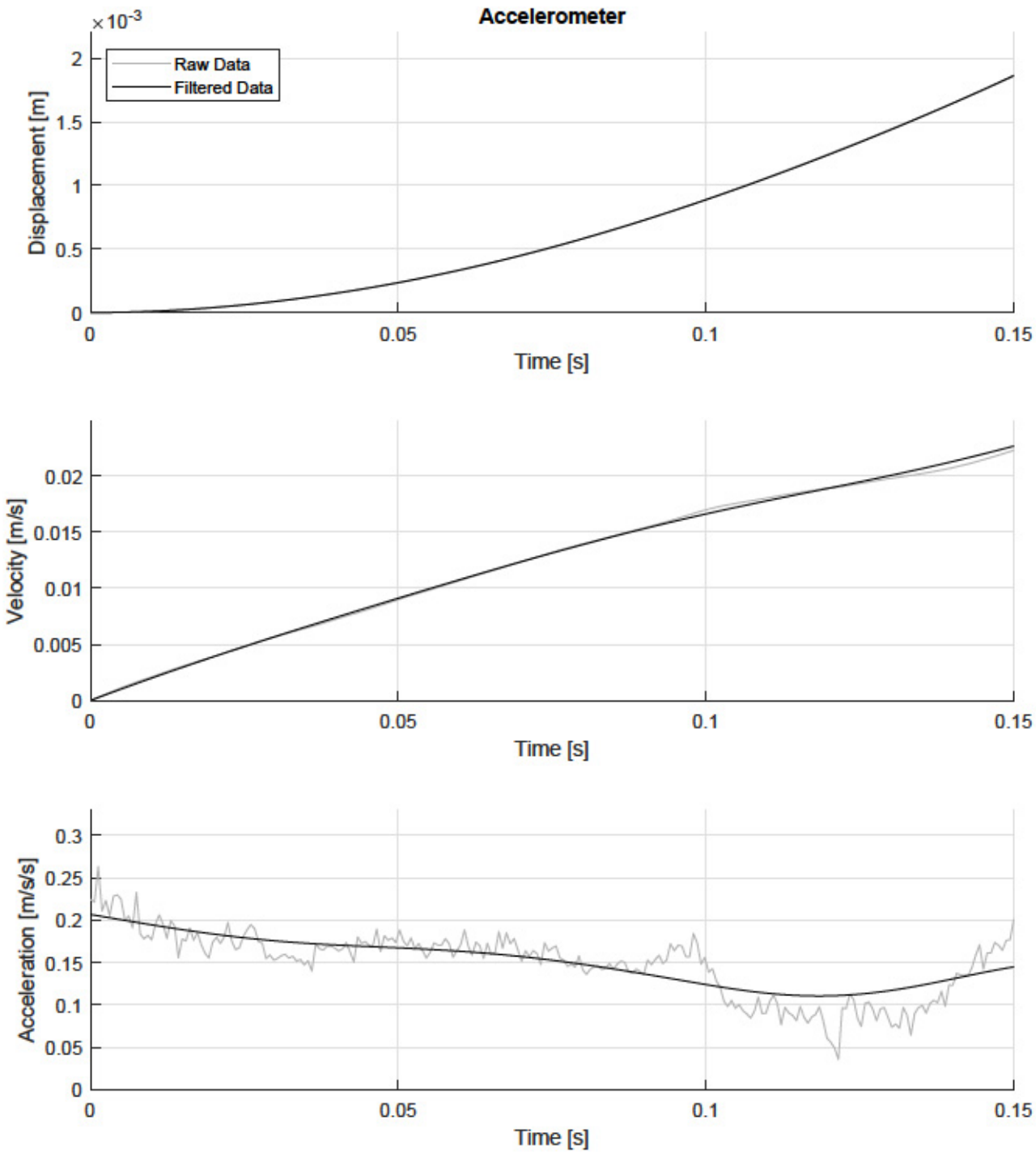

Figure C.50: Step-Force Kinematics of a 3-Sided Polygon: 3% of Ice Mass (Run 5)

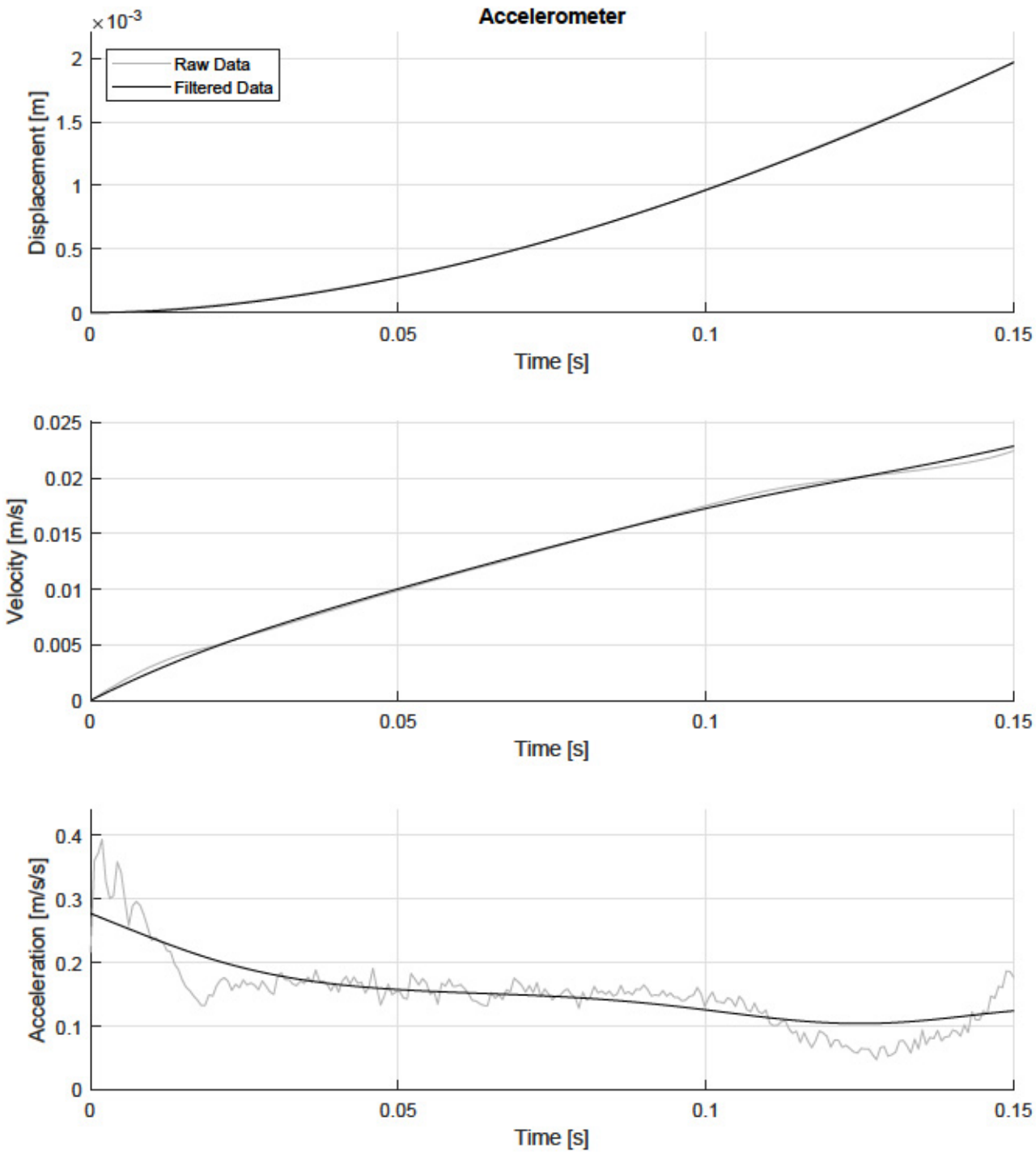

Figure C.51: Step-Force Kinematics of a 3-Sided Polygon: 3% of Ice Mass (Run 6)

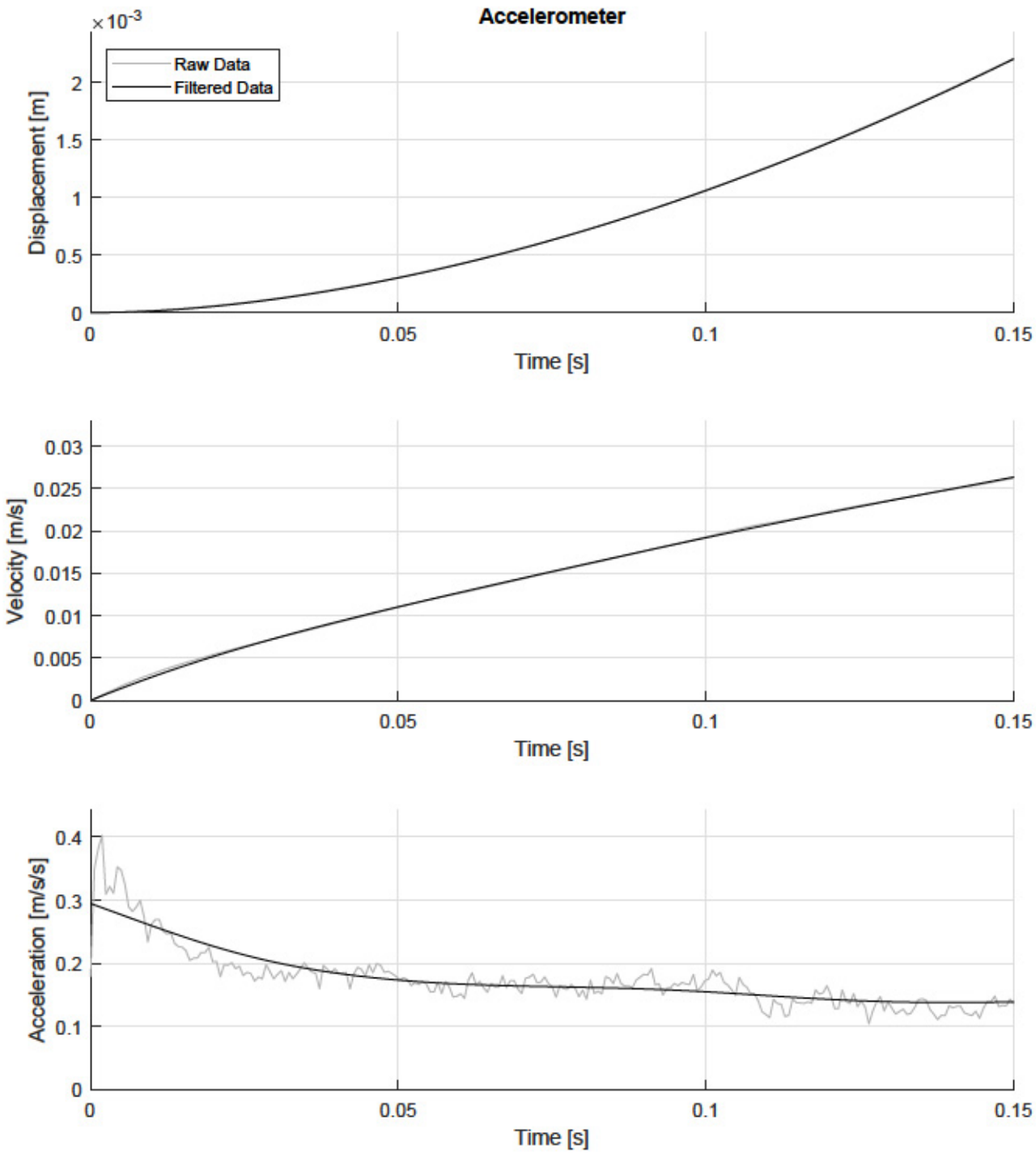

Figure C.52: Step-Force Kinematics of a 3-Sided Polygon: 3% of Ice Mass (Run 7)

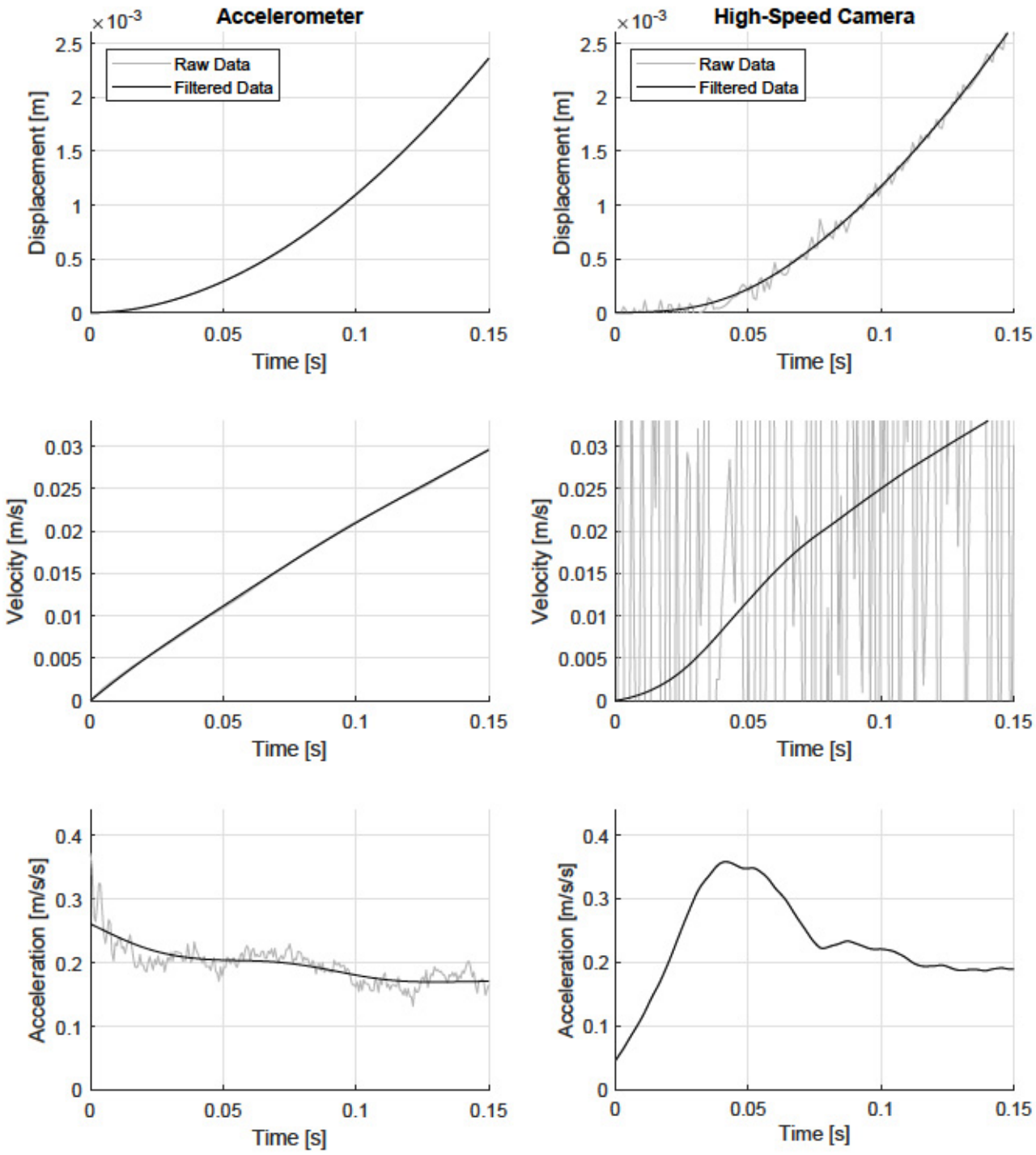

Figure C.53: Step-Force Kinematics of a 3-Sided Polygon: 4% of Ice Mass (Run 1)

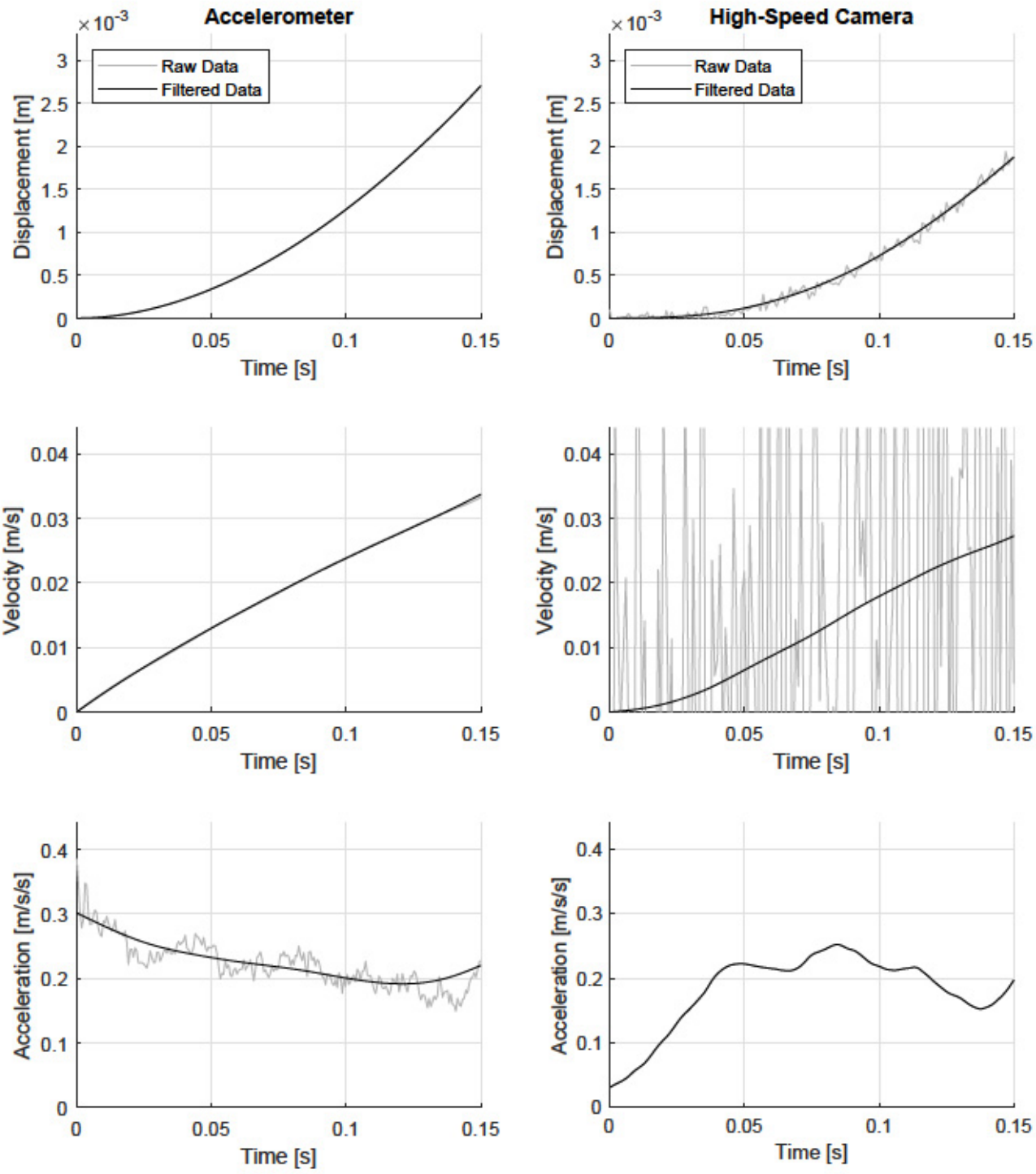

Figure C.54: Step-Force Kinematics of a 3-Sided Polygon: 4% of Ice Mass (Run 2)

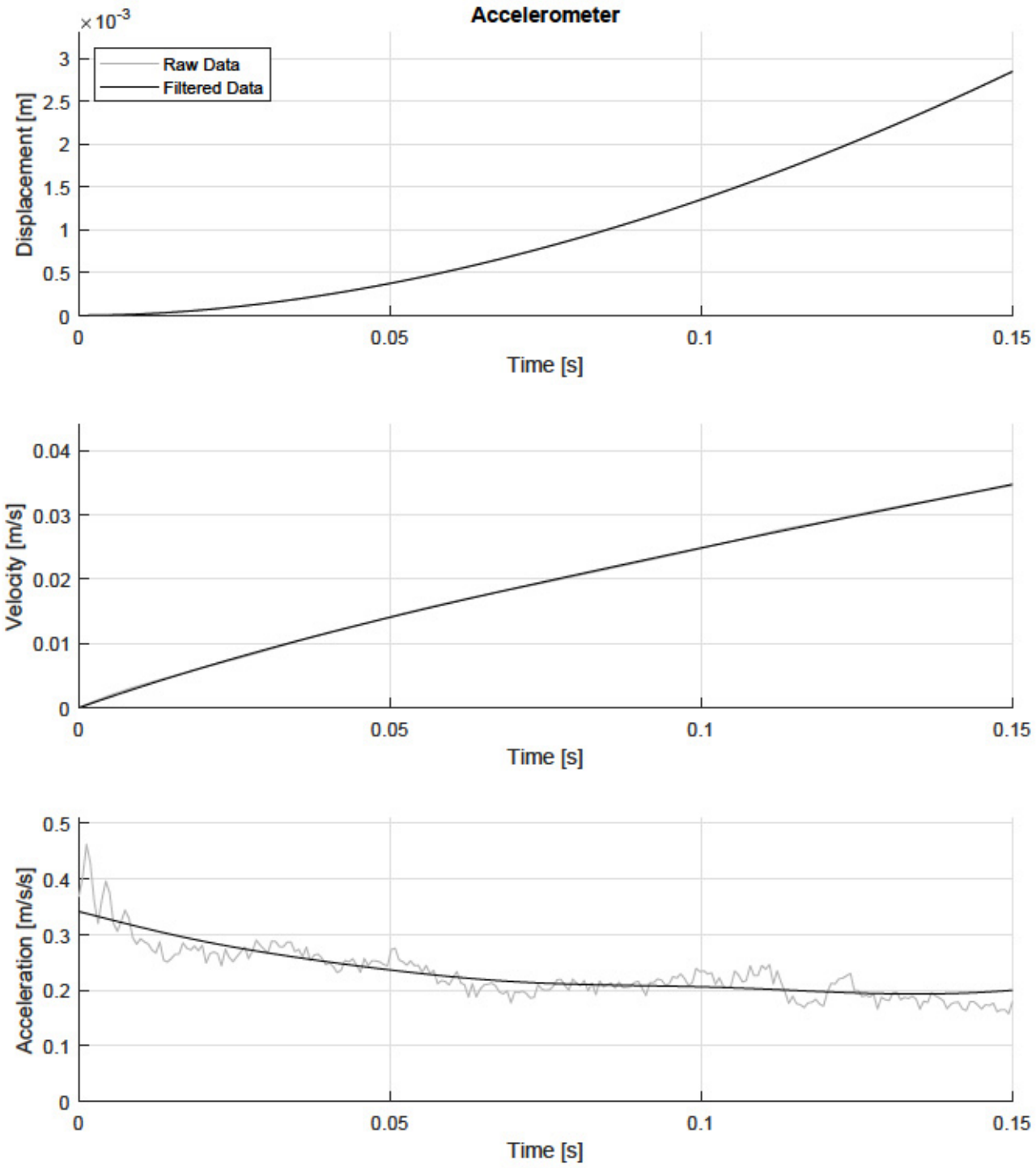

Figure C.55: Step-Force Kinematics of a 3-Sided Polygon: 4% of Ice Mass (Run 3)

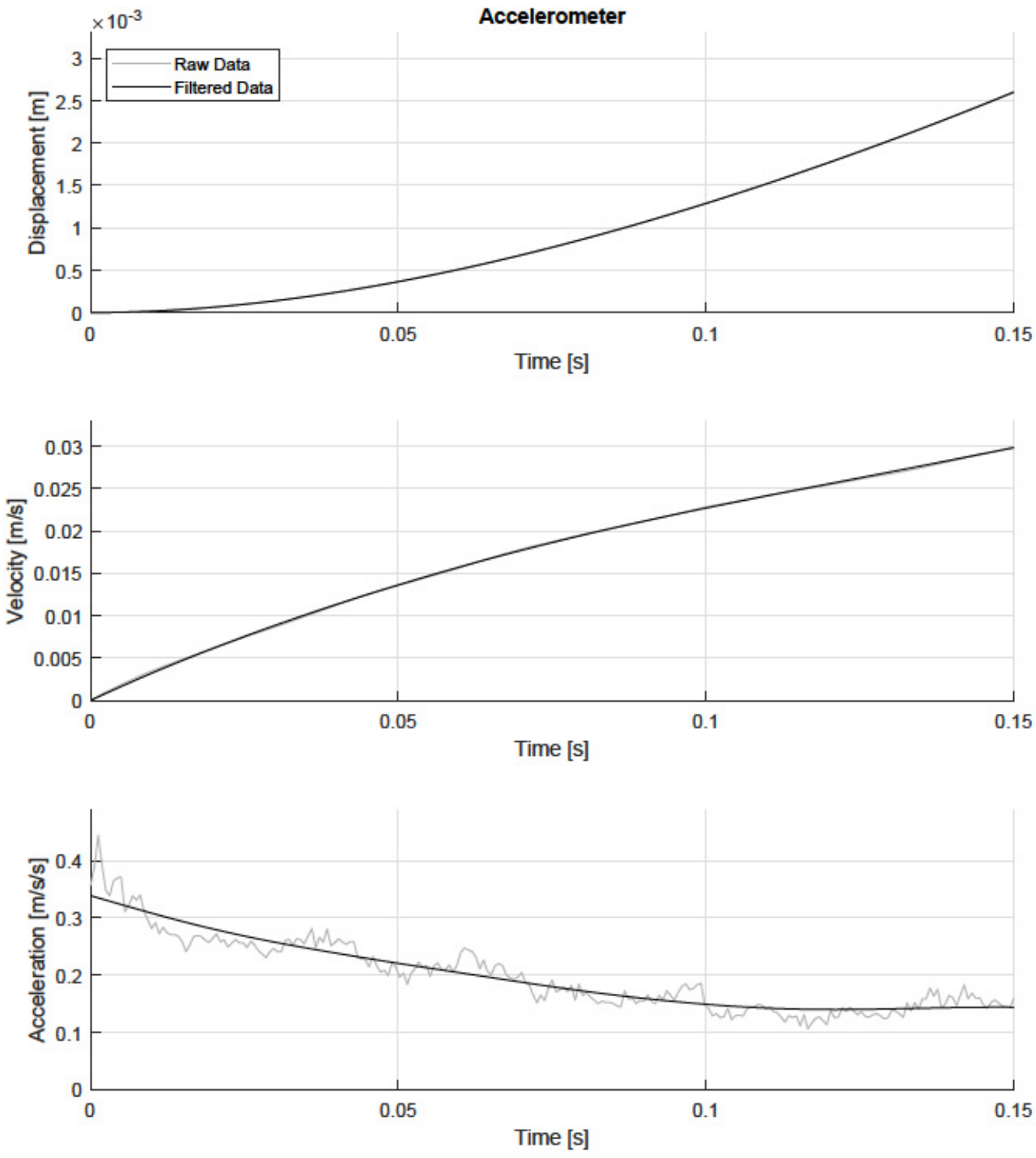

Figure C.56: Step-Force Kinematics of a 3-Sided Polygon: 4% of Ice Mass (Run 4)

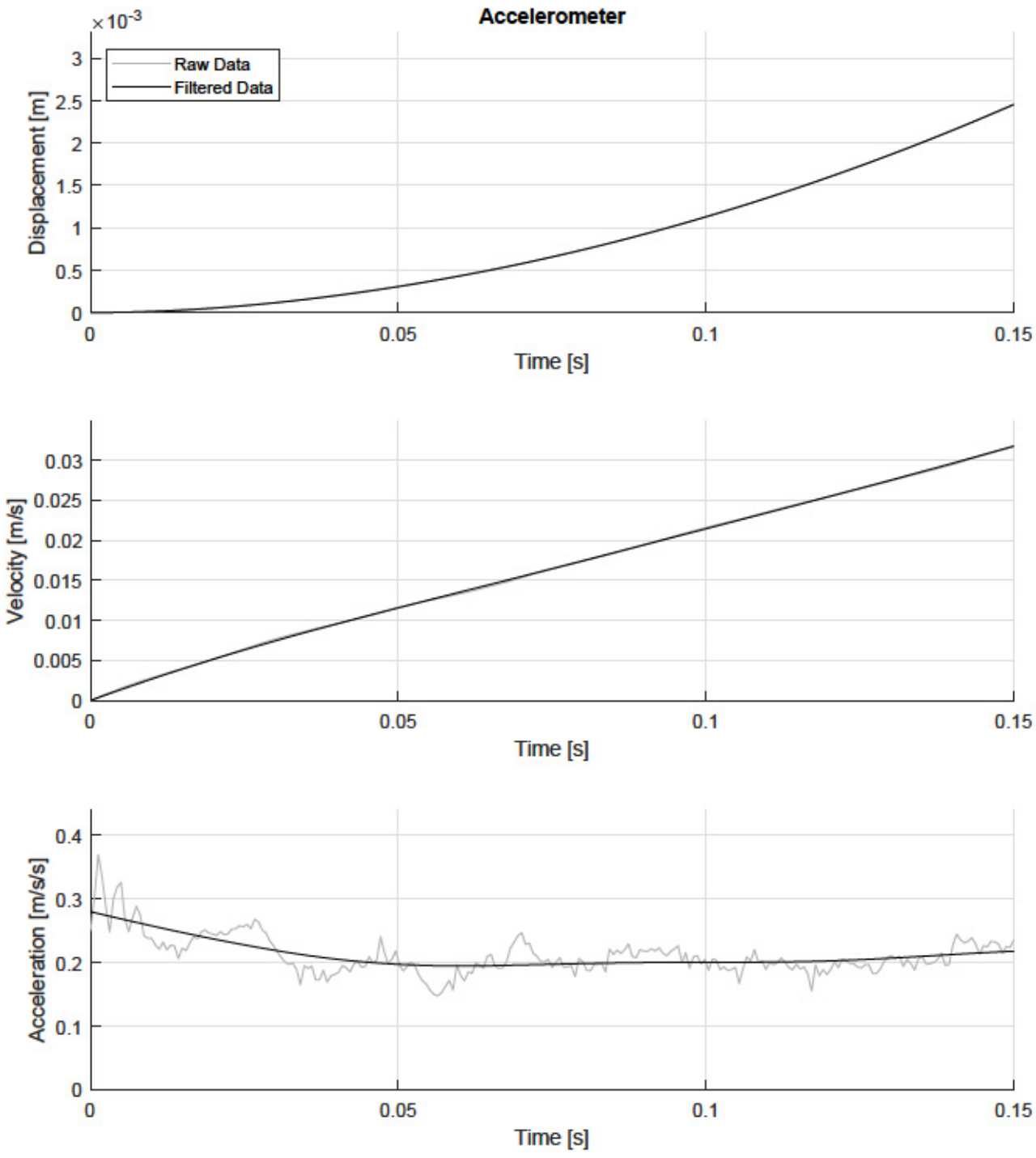

Figure C.57: Step-Force Kinematics of a 3-Sided Polygon: 4% of Ice Mass (Run 5)

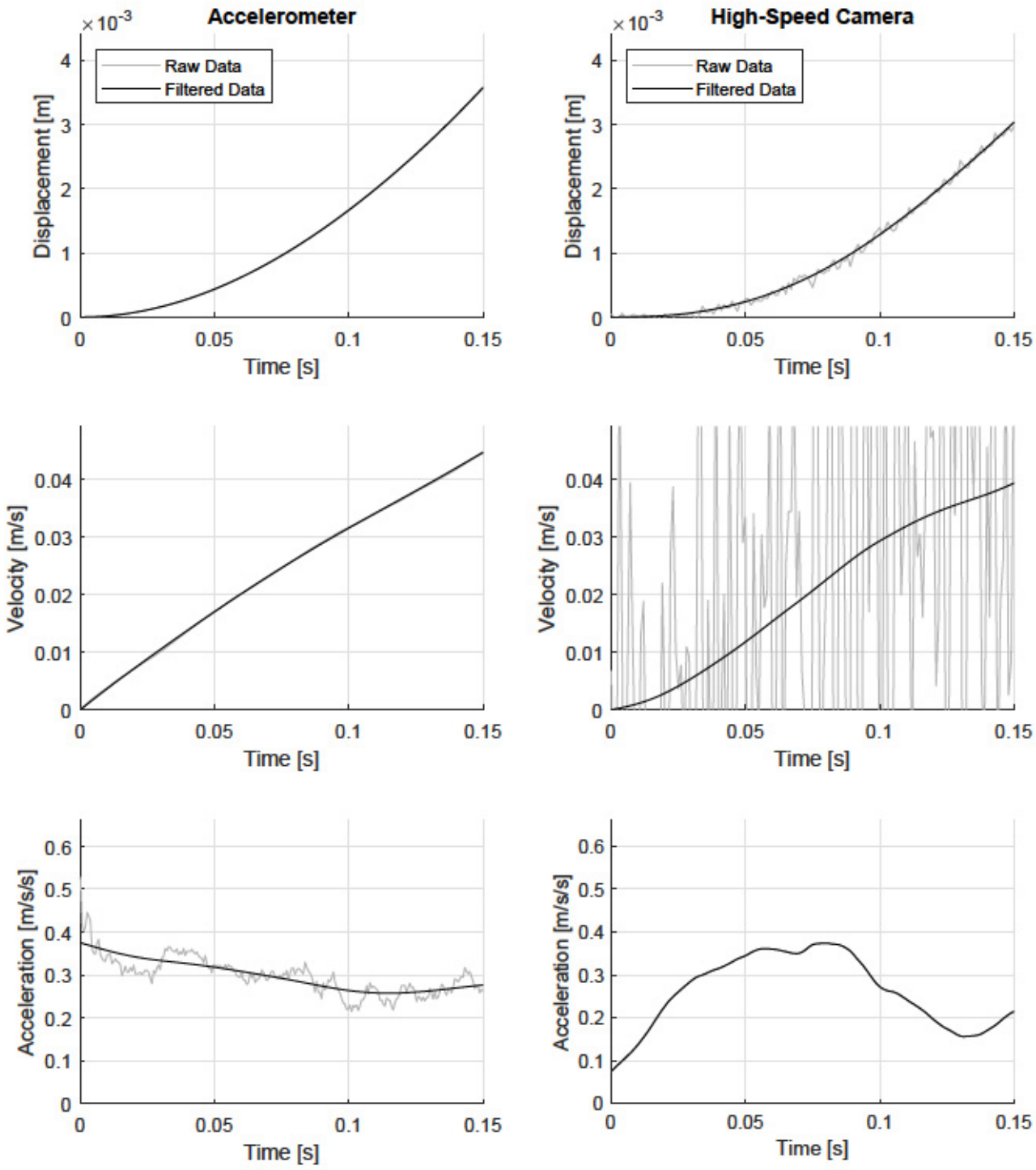

Figure C.58: Step-Force Kinematics of a 3-Sided Polygon: 5% of Ice Mass (Run 1)

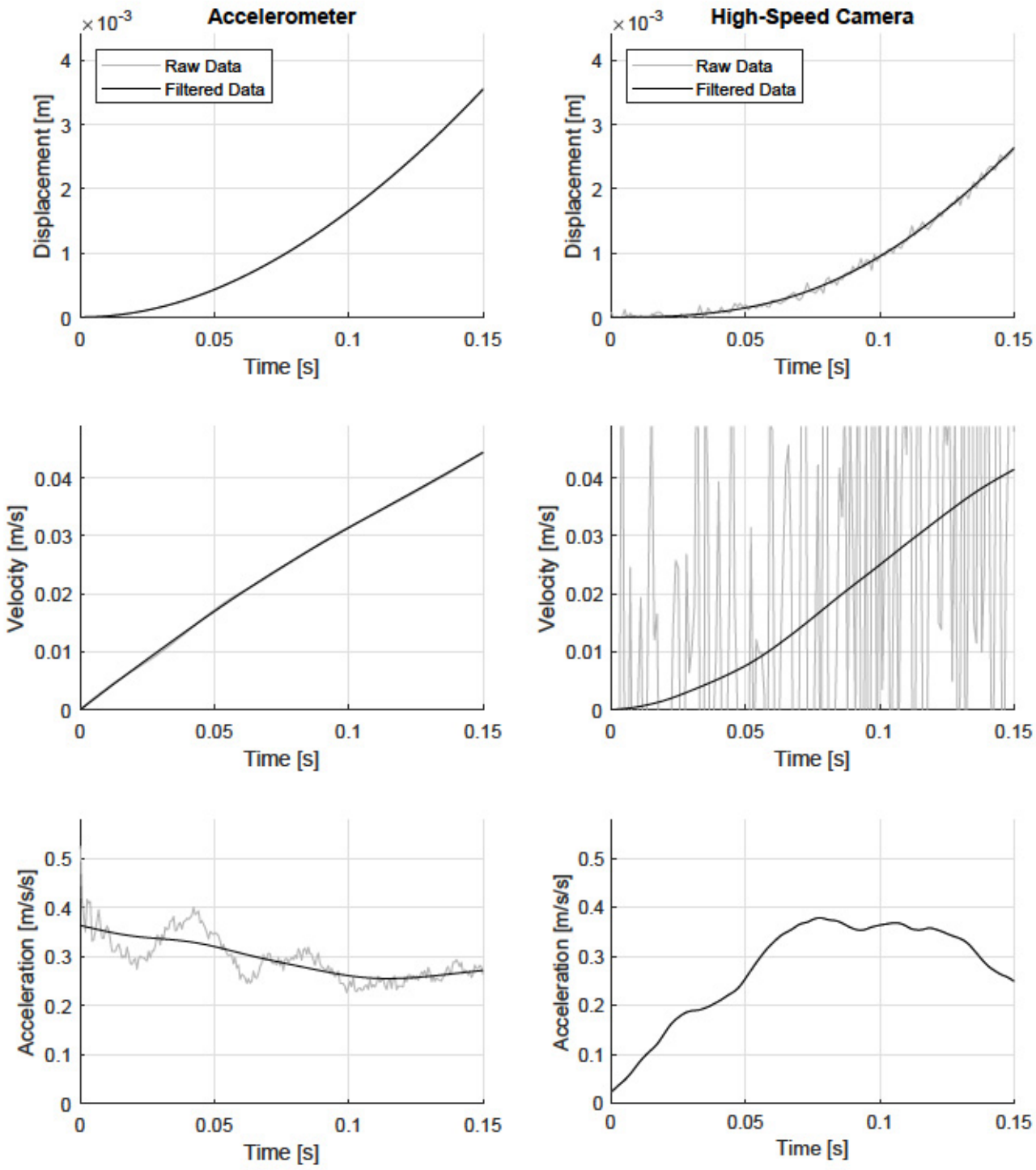

Figure C.59: Step-Force Kinematics of a 3-Sided Polygon: 5% of Ice Mass (Run 2)

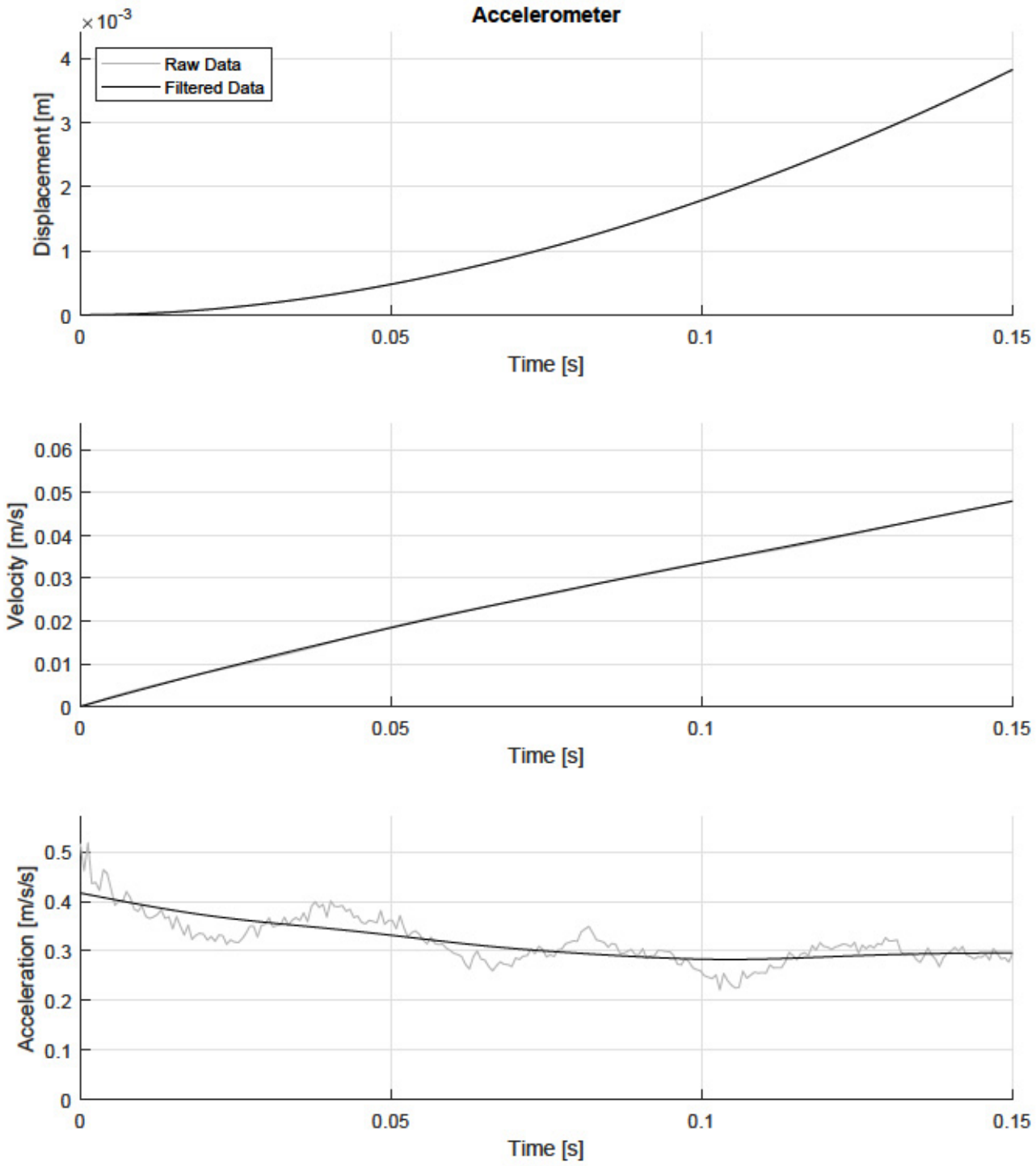

Figure C.60: Step-Force Kinematics of a 3-Sided Polygon: 5% of Ice Mass (Run 3)

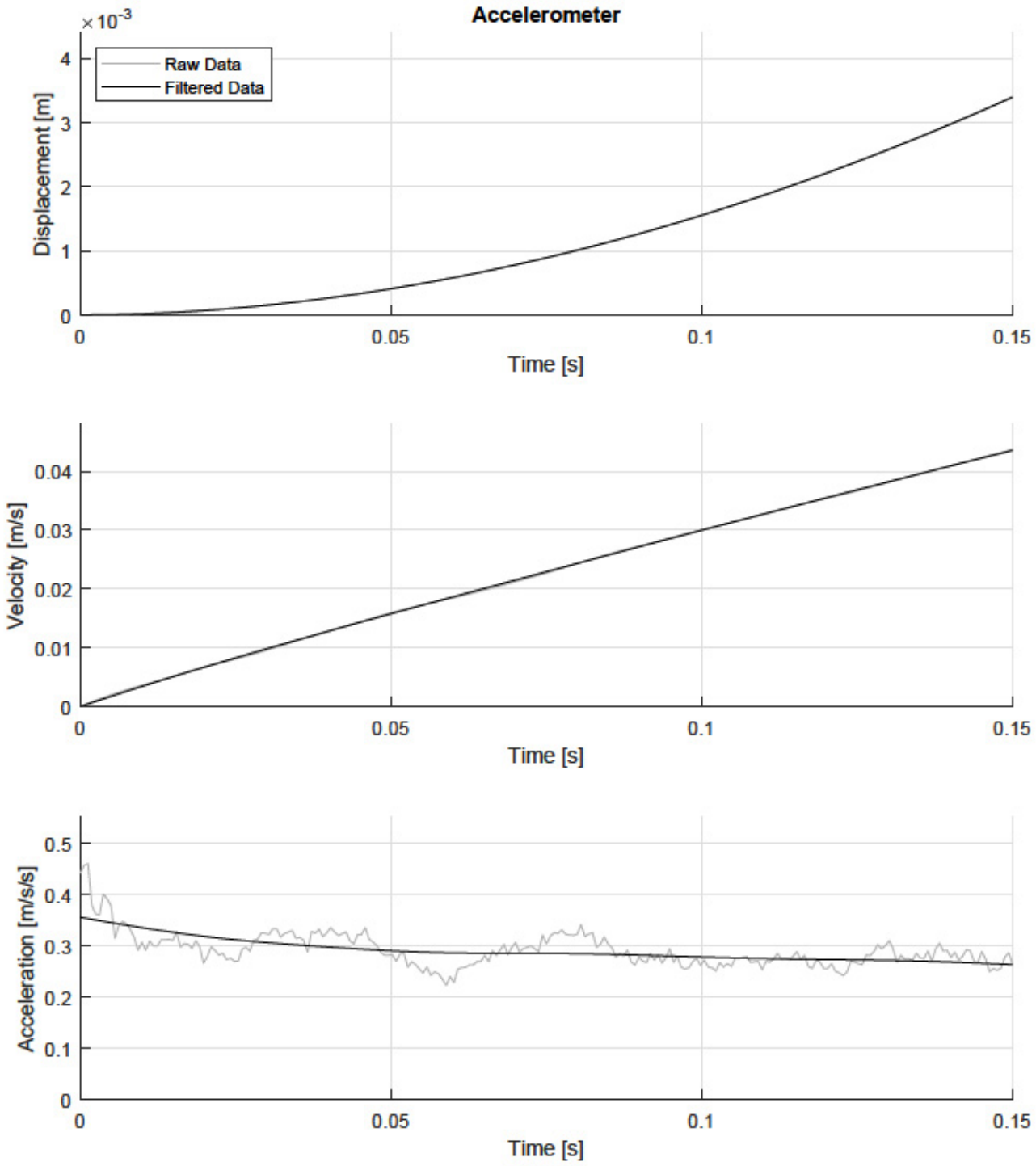

Figure C.61: Step-Force Kinematics of a 3-Sided Polygon: 5% of Ice Mass (Run 4)

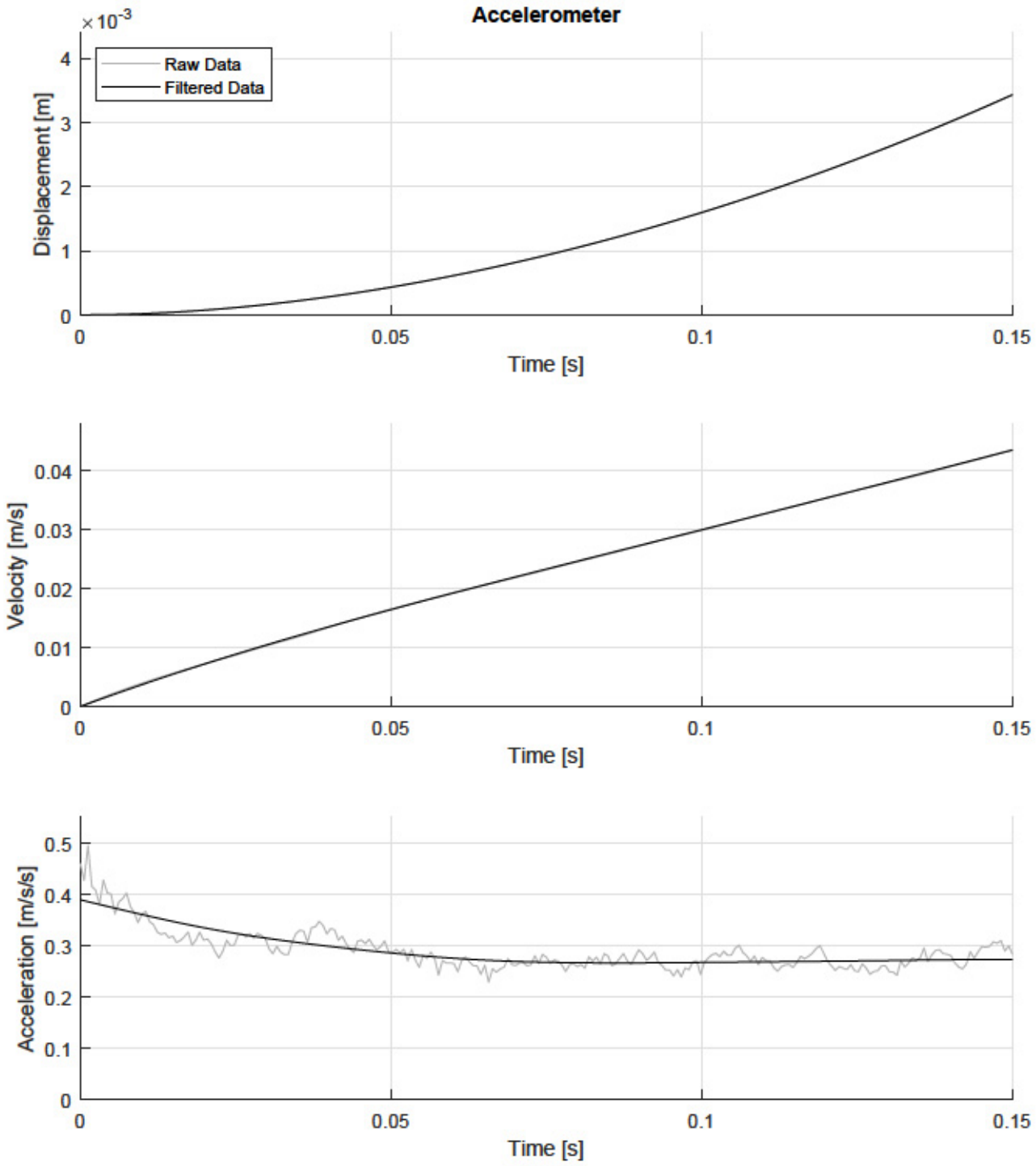

Figure C.62: Step-Force Kinematics of a 3-Sided Polygon: 5% of Ice Mass (Run 5)

Appendix D

Acceleration Measurments

Table D.1: Acceleration Measurements of the Disk

Percent	Block	Iteration	Mass Weight [kg]	Max. Acceleration (Camera) [m/s/s]	Max. Acceleration (Accelerometer) [m/s/s]	Average Acceleration (Accelerometer) [m/s/s]	Average Acceleration (Camera) [m/s/s]
3%	Block 1	1	0.0248	0.2606	0.3104	0.2020	0.1965
3%	Block 1	2	0.0248	0.2766	0.3048	0.2049	0.1972
3%	Block 2	3	0.0248		0.3304	0.2306	
3%	Block 2	4	0.0248		0.3086	0.2186	
3%	Block 2	5	0.0248		0.3309	0.2260	
4%	Block 1	1	0.0330	0.4100	0.4645	0.2795	0.2991
4%	Block 1	2	0.0330	0.3079	0.3809	0.2703	0.2640
4%	Block 2	3	0.0330		0.4115	0.2976	
4%	Block 2	4	0.0330		0.3868	0.2920	
4%	Block 2	5	0.0330		0.4142	0.2944	
5%	Block 1	1	0.0413	0.5080	0.5348	0.3506	0.4454
5%	Block 1	2	0.0413	0.5900	0.5842	0.3270	0.4679
5%	Block 2	3	0.0413		0.4573	0.3423	
5%	Block 2	4	0.0413		0.3756	0.3471	
5%	Block 2	5	0.0413		0.4702	0.3504	

Table D.2: Acceleration Measurements of the 5-Sided Polygon

Percent	Block	Iteration	Mass Weight [kg]	Max. Acceleration (Camera) [m/s/s]	Max. Acceleration (Accelerometer) [m/s/s]	Average Acceleration (Accelerometer) [m/s/s]	Average Acceleration (Camera) [m/s/s]
3%	Block 1	1	0.0185	0.2369	0.3466	0.2021	0.1780
3%	Block 1	2	0.0185	0.2483	0.4147	0.1976	0.1563
3%	Block 2	3	0.0185		0.2928	0.2140	
3%	Block 2	4	0.0185		0.3439	0.2047	
3%	Block 2	5	0.0185		0.3839	0.2133	
4%	Block 1	1	0.0247	0.3617	0.4978	0.2531	0.2512
4%	Block 1	2	0.0247	0.3368	0.4255	0.2574	0.2562
4%	Block 2	3	0.0247		0.3927	0.2558	
4%	Block 2	4	0.0247		0.3272	0.2481	
4%	Block 2	5	0.0247		0.4136	0.2608	
5%	Block 1	1	0.0309	0.4633	0.5677	0.3303	0.3154
5%	Block 1	2	0.0309	0.4252	0.5500	0.3364	0.3302
5%	Block 2	3	0.0309		0.4867	0.3246	
5%	Block 2	4	0.0309		0.5230	0.3312	
5%	Block 2	5	0.0309		0.5589	0.3261	

Table D.3: Acceleration Measurements of the 4-Sided Polygon

Percent	Block	Iteration	Mass Weight [kg]	Max. Acceleration (Camera) [m/s/s]	Max. Acceleration (Accelerometer) [m/s/s]	Average Acceleration (Accelerometer) [m/s/s]	Average Acceleration (Camera) [m/s/s]
3%	Block 1	1	0.0151	0.2730	0.3251	0.1865	0.1863
3%	Block 1	2	0.0151	0.3345	0.2832	0.1802	0.2070
3%	Block 2	3	0.0151		0.2771	0.1796	
3%	Block 2	4	0.0151		0.3403	0.1677	
3%	Block 2	5	0.0151		0.2860	0.1816	
4%	Block 1	1	0.0201	0.3294	0.3819	0.2435	0.2348
4%	Block 1	2	0.0201	0.3809	0.4047	0.2578	0.2577
4%	Block 2	3	0.0201		0.4033	0.2379	
4%	Block 2	4	0.0201		0.3871	0.2651	
4%	Block 2	5	0.0201		0.4247	0.2478	
5%	Block 1	1	0.0252	0.3990	0.4570	0.3106	0.3123
5%	Block 1	2	0.0252	0.3965	0.4957	0.3349	0.3159
5%	Block 2	3	0.0252		0.5360	0.3139	
5%	Block 2	4	0.0252		0.5641	0.3263	
5%	Block 2	5	0.0252		0.4012	0.3248	

Table D.4: Acceleration Measurements of the 3-Sided Polygon

Percent	Block	Iteration	Mass Weight [kg]	Max. Acceleration (Camera) [m/s/s]	Max. Acceleration (Accelerometer) [m/s/s]	Average Acceleration (Accelerometer) [m/s/s]	Average Acceleration (Camera) [m/s/s]
3%	Block 1	1	0.0102	0.2286	0.2206	0.1439	0.1421
3%	Block 1	2	0.0102	0.2278	0.2692	0.1419	0.1376
3%	Block 2	3	0.0102		0.2353	0.1477	
3%	Block 2	4	0.0102		0.1683	0.1502	
3%	Block 2	5	0.0102		0.2244	0.1474	
3%	Block 2	6	0.0102		0.2161	0.1449	
3%	Block 2	7	0.0102		0.1788	0.1677	
4%	Block 1	1	0.0136	0.3587	0.3715	0.1941	0.2164
4%	Block 1	2	0.0136	0.2520	0.3855	0.2190	0.2172
4%	Block 2	3	0.0136		0.3678	0.2234	
4%	Block 2	4	0.0136		0.3563	0.1886	
4%	Block 2	5	0.0136		0.2499	0.2047	
5%	Block 1	1	0.0170	0.3740	0.5288	0.2930	0.2582
5%	Block 1	2	0.0170	0.3782	0.5244	0.2909	0.2844
5%	Block 2	3	0.0170		0.5167	0.3116	
5%	Block 2	4	0.0170		0.4408	0.2863	
5%	Block 2	5	0.0170		0.4599	0.2809	

Appendix E

Kinematic Plots for Impulsive Impact Experiment

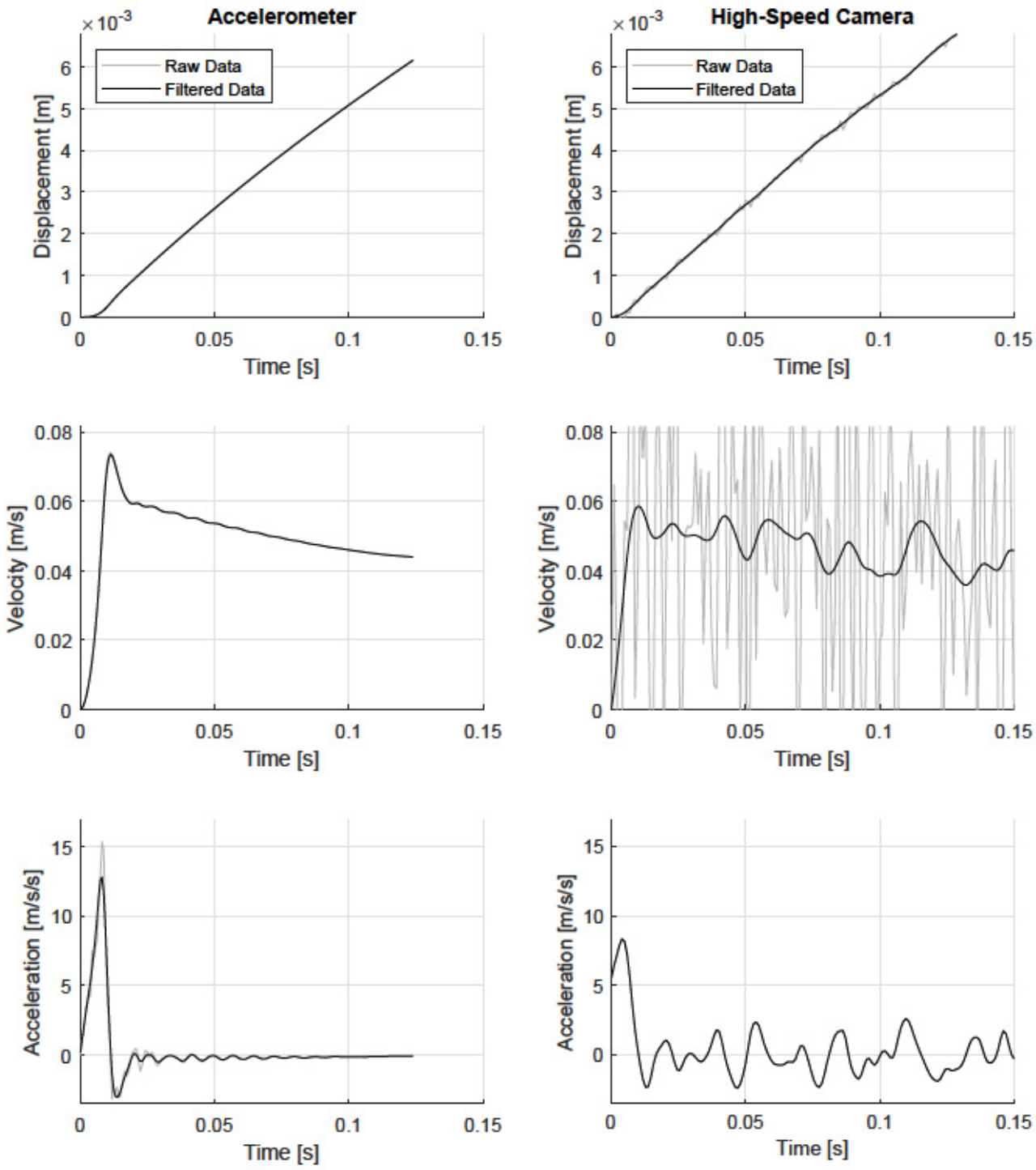

Figure E.1: Impusle-Momentum Kinematics of a Disk: 1 click (Run 1)

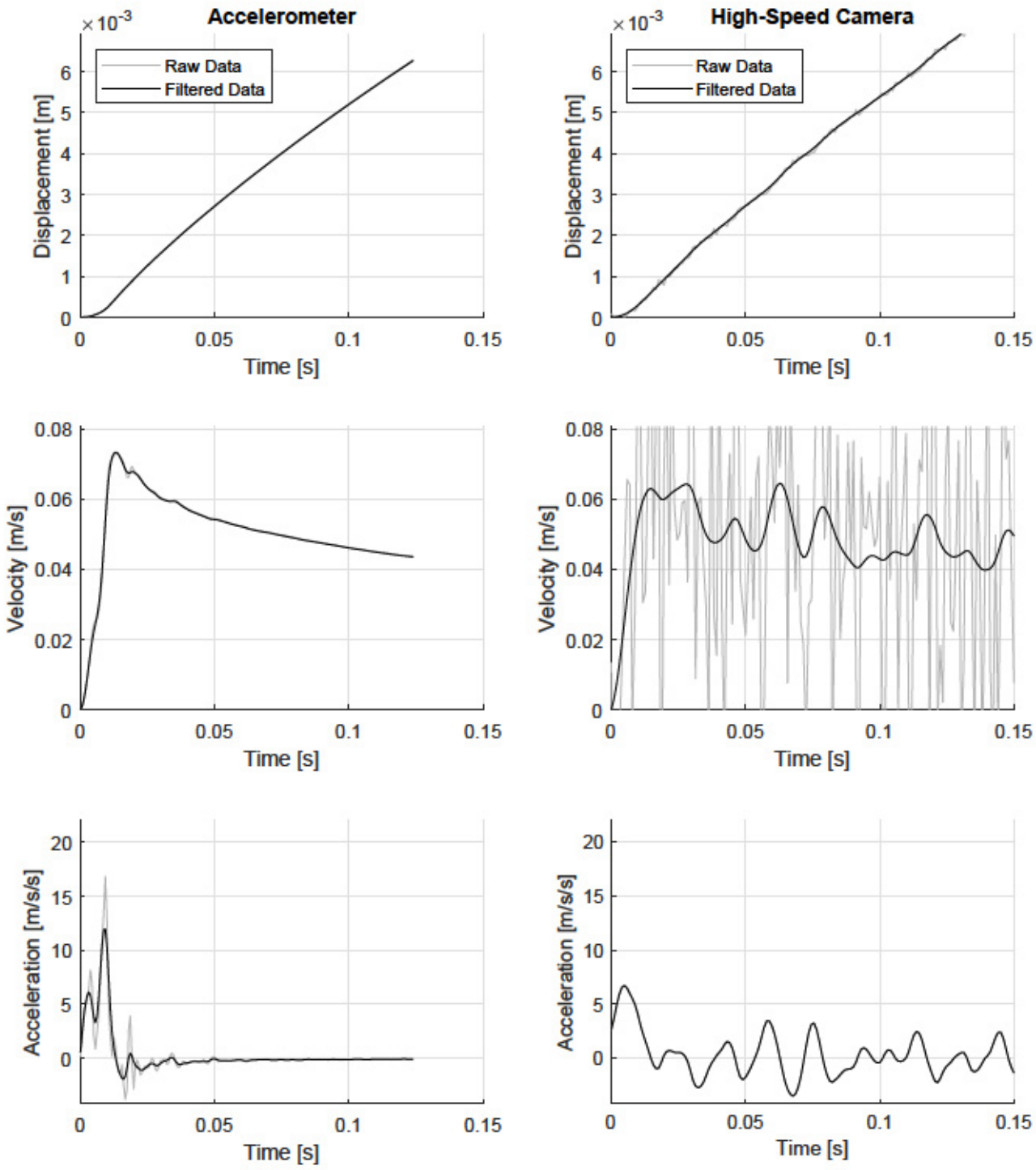

Figure E.2: Impusle-Momentum Kinematics of a Disk: 1 click (Run 2)

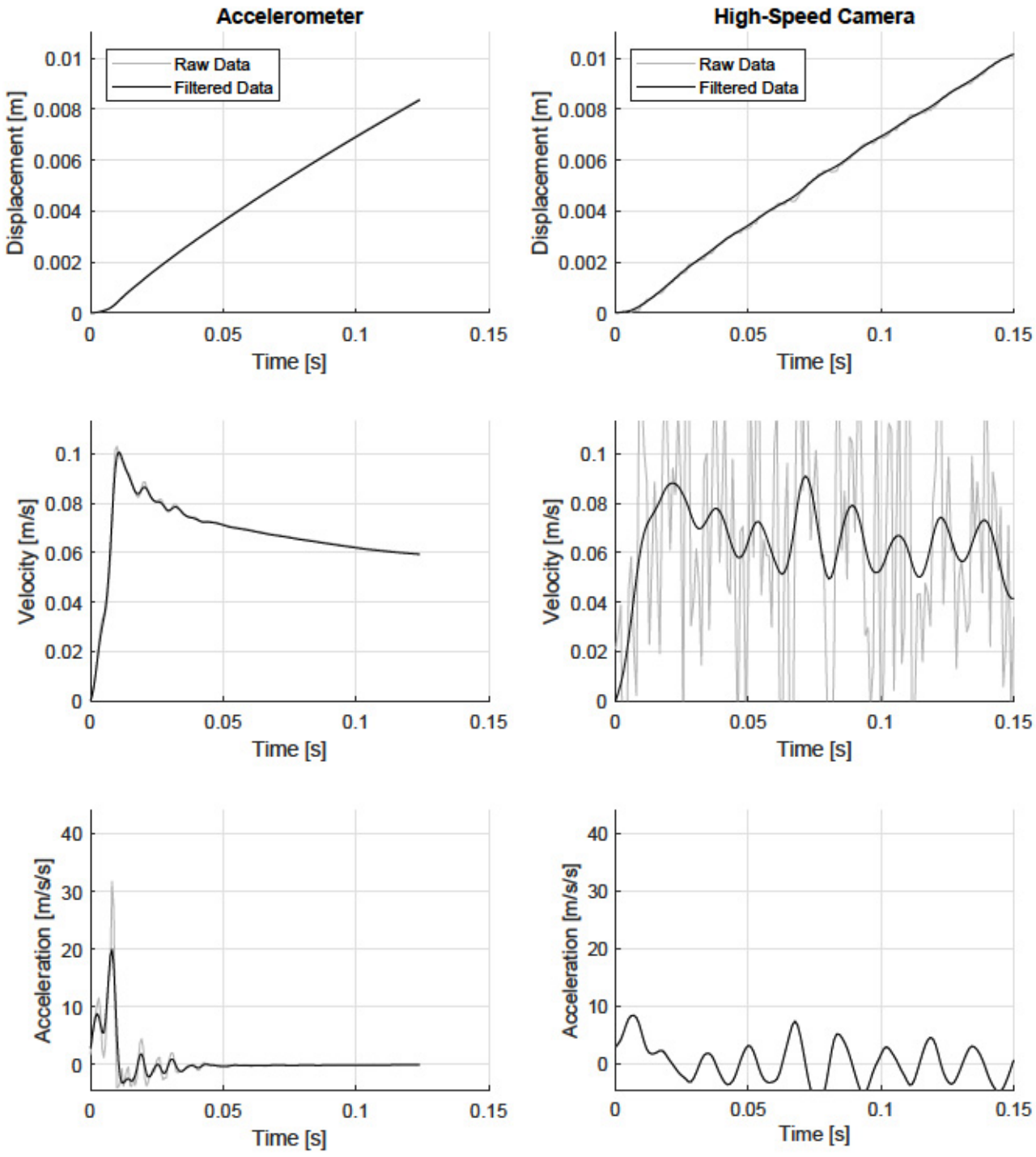

Figure E.3: Impusle-Momentum Kinematics of a Disk: 2 clicks (Run 1)

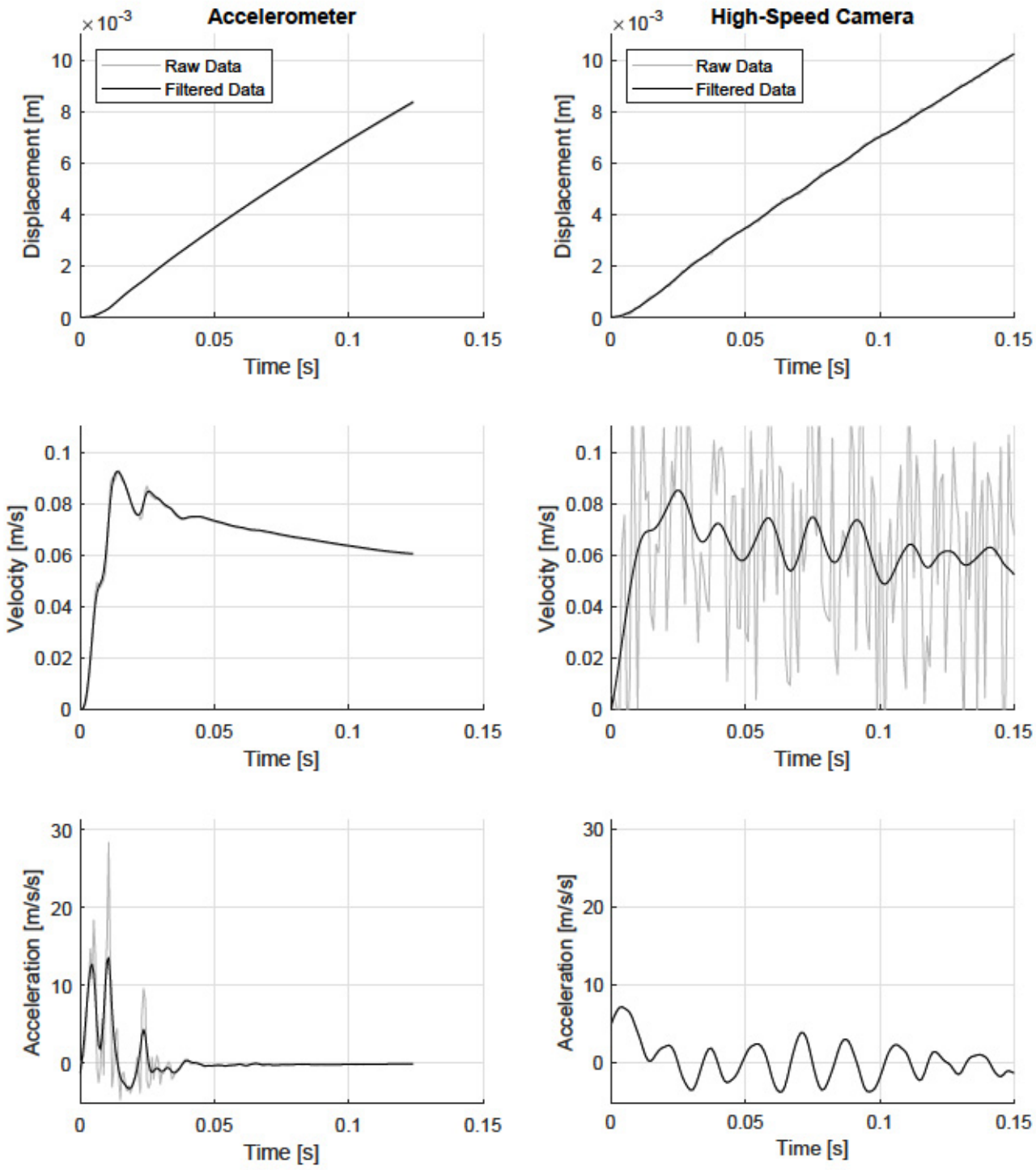

Figure E.4: Impusle-Momentum Kinematics of a Disk: 2 clicks (Run 2)

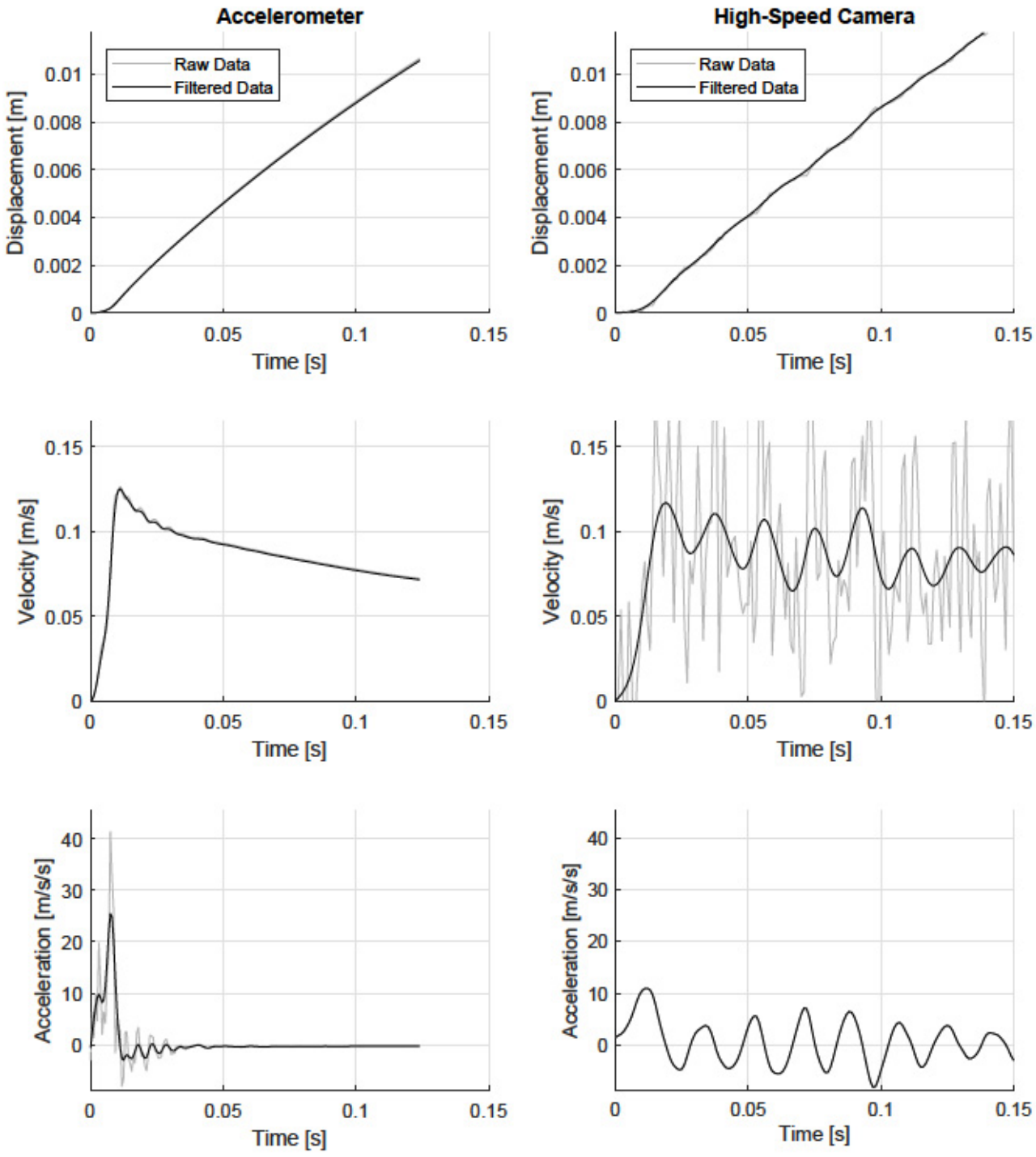

Figure E.5: Impusle-Momentum Kinematics of a Disk: 3 clicks (Run 1)

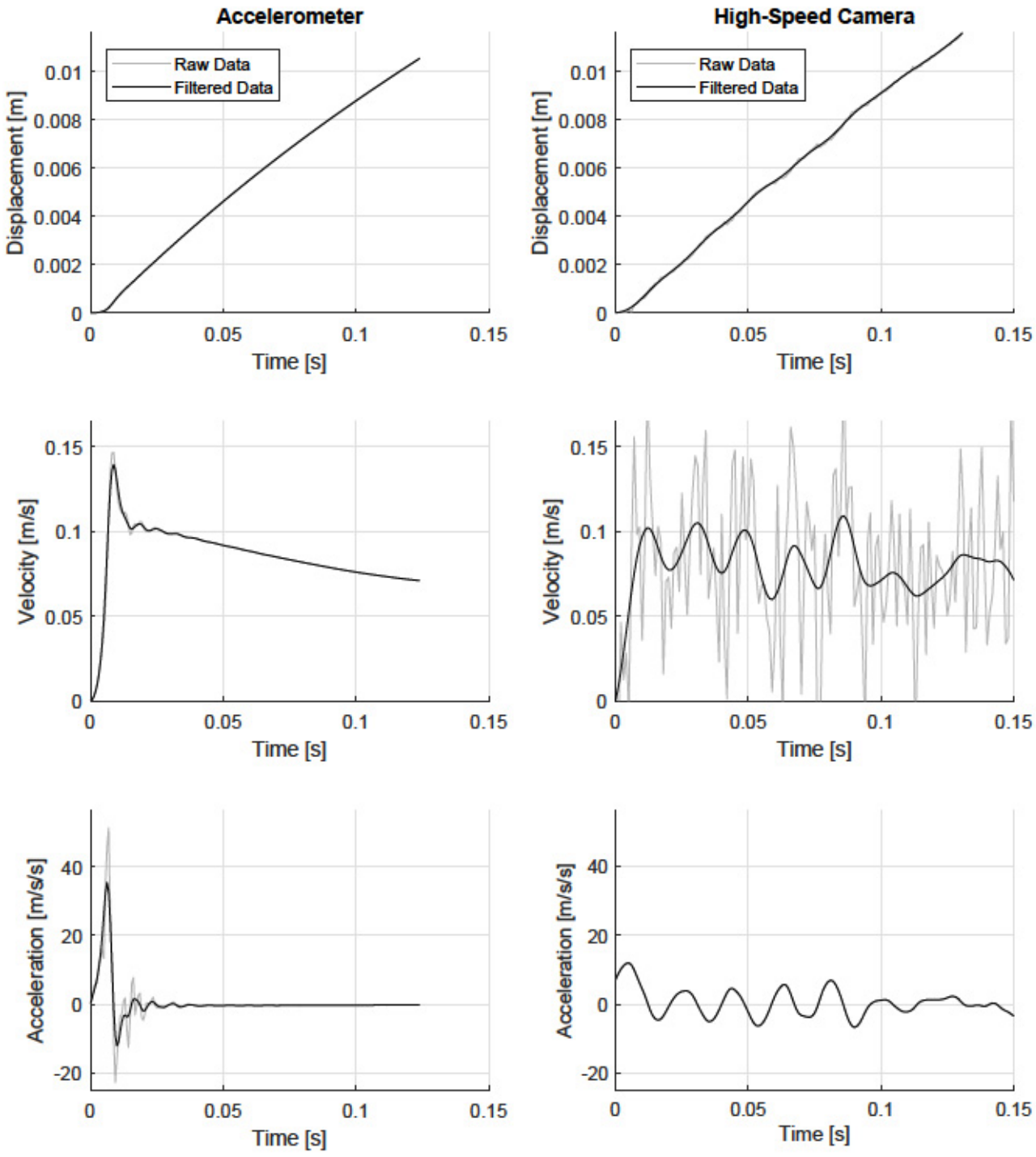

Figure E.6: Impusle-Momentum Kinematics of a Disk: 3 clicks (Run 2)